Institut für Physikalische und Theoretische Chemie,
Lehrstuhl für Theoretische Chemie
der Technischen Universität München

Theory of time- and frequency-gated spontaneous emission from systems with nonadiabatic coupling and dissipation

Andrei Pisliakov

Vollständiger Abdruck der von der Fakultät für Chemie der Technischen Universität München zur Erlangung des akademischen Grades eines

Doktors der Naturwissenschaften (Dr. rer. nat.)

genehmigten Dissertation.

Vorsitzender:	Univ.-Prof. Dr. A. Türler
Prüfer der Dissertation:	
	1. Univ.-Prof. Dr. W. Domcke
	2. Univ.-Prof. Dr. h.c. A. Lauberau

Die Dissertation wurde am 8.10.2003 bei der Technischen Universität München eingereicht und durch die Fakultät für Chemie am 4.11.2003 angenommen.

Contents

List of abbreviations

SE - spontaneous emission
TFG - time- and frequency-gated
CF - correlation function
RF - response function
TLS - two-level system
RWA - rotating-wave approximation
DW - doorway-window
WP- wave packet
DM - density matrix
SB - system-bath
RDM - reduced density matrix
ET - electron transfer
VC - vibrational coherence
EC - electronic coherence

To my wife and my daughter

Chapter 1

Introduction

Spectroscopic measurements are conventionally performed either in the time or in the frequency domain. The two kinds of experiments can however be successfully combined, thereby allowing us to follow the time evolution of spectra [1–3]. With nowadays available fs pulses [4, 5], various time-resolved spectroscopic techniques enable us to observe the evolution of spectra in "real time", and thus to monitor microscopic nuclear motion and the most elementary processes of chemical dynamics which take place on ultrafast time scales [6–10]. In particular, various time-resolved techniques have been applied to study directly the processes of ultrafast electron transfer, proton transfer, solvation dynamics of diverse material systems, ranging from diatomics to biomolecules [11].

The basic idea of time-resolved spectroscopy is to observe the evolution of the spectrum (and, therefore, the system under study) on the ultrafast timescale. In time-resolved spectroscopy, there exist a number of techniques (e.g., photon echo, pump-probe, time-resolved fluorescence, various four-wave mixing techniques), which mainly differ in the number of laser pulses used, the specific properties of the laser fields, and the way of detection of the spectroscopic signals. For a comprehensive theoretical overview of various techniques in ultrafast spectroscopy, see the book of Mukamel [1]. Some of these techniques provide an opportunity to study the evolution of "coherences". But in order to monitor the excited state dynamics, one should use the techniques dealing with "populations", namely, pump-probe spectroscopy and time-resolved fluorescence.

In pump-probe spectroscopy, the time resolution is provided by the dependence of the signal on the delay time between pump and probe pulses. Its common technical realization is the transient absorption technique [12–16]. This technique has been successfully used for a long time. Why is one interested in other techniques? The problem is in the interpretation of the results, because many processes contribute to the pump-probe signal, namely, stimulated emission, resonance Raman, and, possibly, excited-state absorption, and so-called bleaching. It is of importance that both stimulated emission (reflecting excited-state dynamics) and stimulated Raman (reflecting ground-state dynamics) processes contribute to the overall pump-probe signal, even in the case of sequential, non-overlapping pump and probe pulses. As a consequence, one cannot experimentally separate the ground and excited state contribution to the pump-probe signal (without using special technical tricks).

On the other hand, the femtosecond time-resolved fluorescence signal consists solely of the fluorescence (excited state) component. So this technique has an important advantage over diverse pump-probe techniques, since the signal is considerably easier to interpret.

The present thesis is devoted to the development of the theory of time and frequency gated (TFG) spontaneous emission (SE) spectroscopy (which is another name for the time-resolved fluorescence spectroscopy). The first experimental observation of coherent wave-packet (WP) dynamics via the TFG SE technique was reported in [17] for the sodium dimer (see also refs. [18–20]). Later on, coherent effects in TFG SE responses have been measured for diverse systems, ranging from diatomic molecules to polyatomic donor-acceptor complexes [1–3, 7, 17–22]. By monitoring the SE, one gets the opportunity to keep track of vibrational WP dynamics in the electronically excited state as well as decay of the excited state. The TFG SE has become an effective tool for the monitoring of the excited-state dynamics of various systems ranging from isolated diatomic molecules to rather complex systems (carotenoids, chromophore-solvent systems, porphyrins, or photoactive yellow protein) [7, 17, 23–28].

The technical realization of TFG SE spectroscopy is the fluorescence up-conversion technique [29–33], in which the SE and a short up-conversion (or time gate) pulse are mixed in a nonlinear crystal, and the integrated intensity of the sum frequency is monitored. The time resolution is achieved because the gate pulse creates a "time window" for SE and the signal depends on the time delay between the excitation pulse and a "time window", and the frequency resolution is achieved by dispersing the up-converted signal in a monochromator or "frequency filter".

The measured TFG SE signals depend, however, in a quite complicated manner on the laser pulse and system parameters. When interpreting ultrafast TFG SE experiments, a fundamental question therefore arises: how can one extract quantitative information on the dynamics of the material system from the measured signals? There is a certain gap between theoretical and experimental results. Theorists prefer to calculate quantities like the time-dependent electronic population probability or various correlation functions (CFs), while experimentalists measure certain time-dependent transients. Indeed, it is generally assumed that the measured TFG SE signal maps the excited-state population dynamics. But the question is, which population (diabatic or adiabatic) and to which extent? Clearly, the experimental transients are indirectly connected with the electronic population dynamics and are strongly influenced by the detection process. Thus, for systems with complicated and ultrafast dynamics, it is necessary to introduce explicitly the description of the TFG procedure into the theory and to establish rigorously the connection of the experimentally measured signals with the underlying microscopic dynamics. In the present thesis, we study this issue for several simple models (Chapter 3) and mainly for the case of ultrafast electron-transfer (ET) systems (Chapters 4 through 6).

We want to derive a theory of TFG SE which is not limited to a particular or simple material-system dynamics. Therefore, the ultimate goal of the present work is the development of a convenient, computationally oriented framework for the description of TFG SE of nontrivial systems, e.g., multi-mode systems with strong electronic interstate couplings which interact with a thermal bath. The specific tasks are as follows: (i) to develop a universal, eigenstate-free, description of the TFG SE, (ii) to clarify the

influence of the spectral filtering and temporal gating on the TFG SE spectra, and (iii) to connect the measured TFG SE spectra with the time evolution of the corresponding material systems.

In Chapter 2, the definitions of the TFG SE signals are introduced and the formal TFG SE theory is developed. We establish several generic properties of the TFG SE spectra and discuss the validity of two commonly employed assumptions (neglect of retardation effects and slowly-varying envelope approximation). This analysis provides insight into the information content of TFG SE spectra. The material-system dynamics is shown to enter the description in terms of two-time CFs of polarization. We show two approaches to calculate the polarization: perturbative (using time-dependent density matrix (DM) perturbation theory) and nonperturbative (including the system-field interaction into the system Hamiltonian). In the main text we concentrate on the perturbative theory since it gives a clear physical picture and allows one (i) to perform part of the calculations analytically and (ii) to uniformly classify various spectroscopic signals. The nonperturbative approach is briefly considered in Appendix B.

Employing the rotating-wave approximation [34], we derive an expression for the TFG SE in terms of third-order nonlinear response functions (RFs) [1]. These functions allow us to perturbatively calculate the nonlinear response of a material system to external time-dependent fields and, consequently, to calculate various spectroscopic signals.

If the problem under study can be treated in terms of quantum-mechanical basis-set methods, the computation of the RFs, in principle, presents no difficulties (see Chapter 2). For systems with a conical intersection, for example, time-dependent WP calculations have been reported which include up to seven nuclear degrees of freedom [2]. When the number of vibrational modes increases, a straightforward computational treatment of the quantum dynamics is no longer possible. It is a conventional practice to adopt a reduced density-matrix (RDM) description in such cases, where a few optically active vibrations are considered explicitly, while the rest of the inter- and intramolecular modes is treated as a heat bath. This leads to the problem of the evaluation of RFs in a dissipative environment, which complicates the computation considerably. It is therefore not surprising that the RFs have analytically been evaluated so far only for the harmonic oscillator bilinearly coupled to a heat bath [1] and for few-level systems [35, 36]. Recently, the damped harmonic oscillator model has been extended in several directions. For instance, the RFs have been calculated taking account of anharmonic effects [37–42], for nonequilibrium initial conditions [43], and for energy-transfer systems consisting of pairs of chromophores [44–47]. Nonlinear RFs for multidimensional systems (an I_2 molecule in a xenon fluid with up to 36 vibrational modes) have also been evaluated explicitly [48]. Instead of the standard RFs, one can also describe nonlinear spectroscopic signals in terms of so-called effective RFs [49].

For multi-mode systems with electronic couplings, the conventional treatment of dissipative effects is based on the Redfield [2, 50–64], the Fokker-Planck [65–67], and kinetic [68–74] equations, the implementation of which is very demanding numerically. For this reason, the nonlinear (third- and higher order) RFs have not explicitly been computed for such systems. The corresponding optical signals were evaluated either through the propagation of the DM in the ground and excited states [50–52,54,63,64,68, 69, 71–74], via calculation of the nonlinear polarization (which, in a sense, is equivalent

to the determination of certain conventional or effective RFs) [2, 65, 66, 75–77], by treating the problem in terms of the eigenvalues and eigenfunctions of the ground and excited state Hamiltonians [20,78,79], by invoking the Monte Carlo methods [2,80,81], and by nonperturbative methods [2,82].

In Chapters 2-4, 6 we present methods for the calculation of RFs and illustrate them by explicit calculations of TFG SE signals for different model systems. To simplify the presentation, we restrict ourselves to the system with a single optical transition between two separated electronic states (ground and excited) which are coupled only by the radiation field. Although this electronic two-level system (TLS) represents a restriction, it should be stressed that the theory still applies to many of the experimentally interesting systems [2]. In particular, H_e (the excited-state Hamiltonian) may represent several nonadiabatically coupled electronic states, e.g., the case of an optically bright excited state which is intramolecularly coupled to one or several optically dark states (in Section 4, e.g., H_e describes the dynamics of two coupled electronic states).

As we have already emphasized, the calculation of RFs for nontrivial multidimensional systems, in particular those exhibiting pronounced nonadiabatic couplings, is a difficult task: analytic solutions do not exist and a straightforward computational treatment of the quantum dynamics (computation of these functions) is not feasible. To solve this problem, we further develop in Chapter 2 the doorway-window (DW) picture of the TFG SE which will simplify the computation of RFs (and, consequently, the calculation of the signals) and is applicable in the most general cases. This has partially been done already in papers [3, 54] (for perfect spectral filters) and in [63, 64, 83–85] (for "bare" spectra, which are connected with "real" TFG SE spectra through the convolution with the joint time-frequency gate function). Our aim is to directly develop the DW description for "real" TFG SE spectra. This formulation reduces the computational effort considerably, since some of the integrals can be performed analytically. Concomitantly, this formulation allows us to obtain various forms of the explicit analytical expressions which can be useful in actual calculations.

To implement a developed formal DW-picture for nontrivial systems with electronic and vibrational relaxation, we adopt a system-bath (SB) approach (which leads to a RDM description), where a few optically active vibrations are considered explicitly, while the rest of the inter- and intramolecular modes is treated as a heat bath. We emphasize some important technical aspects in DW-formalism which arise due to the partitioning of the total system in a relevant part and an environment.

If the Born-Oppenheimer approximation is adequate, one can model the ground and excited state Hamiltonians via a collection of vibrational modes, which are usually assumed to be harmonic. In Chapter 3, we consider several standard benchmark systems for which RFs can be calculated analytically: free harmonic, Brownian (or damped harmonic), and Drude oscillators. These systems consist of displaced harmonic oscillators in the ground and excited states which are coupled to a bath in a different manner: the free harmonic oscillator is dissipation-free; the Brownian oscillator is coupled to a conventional (Markovian) thermal bath, while the Drude oscillator is coupled to a thermal bath with exponential memory kernel. We perform explicit calculations of TFG spectra for different values of the parameters of the models and for various qualities of the time and frequency filters. These systems with rather transparent dynamics will allow us to investigate separately the influence of different effects on TFG SE spectra: time and

frequency resolution effects, dissipation effects, and memory (or non-Markovian bath) effects. The conventional (Markovian) description is valid provided that the bath relaxation time is much shorter than all other relevant times of the problem. If one studies ultrafast relaxation dynamics, the Markovian assumption should be implemented with a certain caution, since it could be an unjustified oversimplification (see, e.g., recent references [86–92]). There exist also experimental evidences that non-Markovian effects could be important, e.g., for describing vibrational relaxation in hydrogen-bonded liquids (see Ref. [93] and references therein).

In order to describe the TFG SE spectra for *nontrivial multidimensional systems*, one has to employ the DW-representation. In Chapter 4, the DW-picture is applied for the calculation of TFG SE spectra of ultrafast ET systems which, due to a strong nonadiabatic coupling, exhibit ultrafast decay dynamics [2].

A number of papers have appeared in recent years, in which the problem of ultrafast ET has been treated at different levels of sophistication. Of particular relevance to the present consideration are the papers [51,52,54,63,64,71,94–98]. The theory presented in Chapter 4, in a sense, generalizes an earlier approach by Jean [52], extending the theory beyond bare time- and frequency-resolved spectra. A novel feature of the present work is the consideration of several carefully selected ET model systems exhibiting electronic coherence and/or vibrational coherence and the systematic exploration of the effects of the preparation and SE detection by pulses of finite duration.

One of the most fundamental questions, which is addressed when discussing ultrafast ET reactions, is the manifestation of various coherences in the population dynamics and measured responses. It has been shown theoretically that coherent effects in ultrafast ET can be either of vibrational or of electronic nature [51, 53, 56, 94, 99–105]. Therefore, it is necessary to distinguish between these two types of coherences when interpreting particular experiments. Recent ultrafast spectroscopic measurements have confirmed the persistence of pronounced coherent effects on a picosecond time scale in the ultrafast ET dynamics for various molecular systems, from diatomics to proteins [6–8, 28, 106–109]. However, when trying to interpret particular experiments, it is not entirely clear if the measured oscillatory patterns are to be attributed to vibrational or electronic coherences. So, it is of considerable importance to clarify this issue.

In Chapter 4, the ET model is introduced and "system" and "bath" parts are specified. We give the equations (Redfield theory) used for the calculation of the RDM- the primary quantity describing ET system dynamics. We present the results of calculations of TFG spectra for this ET model. To elucidate the effect of various coherences on SE signals, we have performed simulations for ET models in which either electronic or vibrational coherence effects are dominant. The effects of temporal resolution and pump-pulse duration are studied. The manifestation of various coherences in the signal is also discussed.

To show the performance of the developed approach, we demonstrate its application to real systems. The theory is implemented to describe the time-resolved fluorescence experiments on the electron donor-acceptor complex TCNE-HMB performed recently by Yoshihara and coworkers [7, 21, 110]. The results of our simulations are presented in Chapter 5. A theoretical model consisting of the ground and two nonadiabatically coupled excited electronic states which are strongly coupled to a single reaction mode is constructed. It is demonstrated that the developed model correctly reproduces general

behavior and trends in various experimentally measured responses. Possible generalizations of the model are proposed.

If the system under consideration possesses nonadiabatic electronic couplings within the excited-state vibronic manifold, the conventional displaced harmonic oscillator model no longer works, and other approaches have to be developed. One can use the DW-representation of the TFG SE spectra (Chapter 2). However, experimentalists often need to estimate quickly the expected signal, and the calculation of the quantum dissipative dynamics, i.e., RDM propagation, is expensive and not appropriate for this goal. In Chapter 6 we develop a simple reference model which allows the explicit calculation of RFs for electronically nonadiabatic systems coupled to a heat bath. The model is based on a phenomenological dissipation ansatz which describes the major bath-induced relaxation processes: excited-state population decay, optical dephasing, and vibrational relaxation. The model is constructed in such a way that it allows us to express the nonlinear RFs of a dissipative material system through those of the corresponding bath-free system. We derive explicit expressions for the TFG SE signal in the framework of this model. We illustrate the performance and validity of the theory by comparing the calculated TFG SE spectra with more accurate treatments for (i) the standard damped harmonic oscillator (Chapter 3) and (ii) a model nonadiabatic ET system (Chapter 4). This phenomenological model may prove useful as an efficient tool for the *qualitative* calculation of optical responses and, therefore, the interpretation of observed time-resolved spectra.

Chapter 2

Time- and frequency-gated spontaneous emission: general theory

2.1 Introduction

This chapter is devoted to the consideration of the theory of time- and frequency-gated (TFG) spontaneous emission (SE). This is not the first theoretical description of the TFG SE that has been proposed; however, our formalism and the derivation leading to it are not fraught with problems that arise due to several commonly used assumptions. Moreover, it generalizes previous theoretical considerations in several ways.

There exist two major approaches to the description of the TFG SE. In the first approach, the TFG SE spectrum is defined as the rate of emission of photons of a certain frequency within a definite time interval. The influence of the measuring device is not taken into account in this formulation [1, 52, 67, 71, 74, 75, 102, 103, 114–116]. Starting from this definition, one obtains an ideal (bare) TFG SE spectrum, which is not guaranteed to be positive, however. For instance, for certain parameters of the Brownian oscillator model, the spectrum can attain negative values [1,3]. Moreover, the time and frequency resolution of this ideal spectrum are not limited by the fundamental time-frequency uncertainty principle. This underlines the necessity to develop a more comprehensive theory, in which both a spectrometer and a time-gating device enter the description from the outset.

This is the characteristic feature of the second group of approaches, in which the TFG SE is taken to be proportional to the integrated intensity of the total emitted field which has passed through a spectrometer and a temporal gating device [117, 118]. Following the guidelines developed in [117], the TFG SE has been investigated by a number of authors [2, 18–20, 78, 79, 119]. The explicit consideration of the TFG process adds, however, additional complexity to the problem, and it is therefore not surprising that the papers [18–20, 78, 79, 119] deal with one-dimensional dissipation-free systems, which allows the description of the material dynamics in terms of the eigenvalues and eigenfunctions of the Hamiltonian. Cina and coworkers have formulated a theory which is intermediate between the two approaches [3, 54, 95]. These authors have investigated the influence of the time gate on the intensity [3,54] and anisotropy [95] of the SE, while the frequency resolution was tacitly assumed to be perfect. Mukamel and coworkers have developed a general description, which ensures a correct inclusion of the TFG

process for any material system under study [83–85]. The passage to an ideal gate also has been briefly discussed by these authors.

The formulations developed in [83–85] provide deep insight into the problem of the TFG SE. However, their implementation for the calculation of the TFG SE is difficult for complex material systems, due to the necessity to perform numerous time integrations and Fourier transforms involving multi-time RFs. Moreover, several other questions deserve further clarification and investigation. The articles [83–85], as well as the pivotal paper [117], are based on the assumption that the emitted field is proportional to the transition dipole moment. This is a good approximation for spectrally narrow bands, but, in a more general context, it may be necessary to go beyond this approximation [78]. In addition, the excitation pulse is treated perturbatively in [83–85], which may not be appropriate for typical experiments which employ a short, but not necessarily, weak laser pulse.

Explicit calculations of the TFG SE for dissipative systems have so far been performed only for the classical overdamped Brownian oscillator [83,84] and, very recently, for molecular aggregates within the Redfield theory [63, 64]. Important questions concerning the manifestation of different regimes of the bath-induced vibrational relaxation in the TFG SE have not yet been addressed. An important issue is to clearly separate the contributions due to the material system dynamics from those of the measuring device in the TFG SE signal. The two groups of approaches to the TFG SE, [1,52,71,74,75,102,103,114–116] and [2,18–20,63,64,78,79,83–85,119], have so far been developed separately from each other, so that their interrelationship is not obvious. It is also of importance to establish more rigorously the interconnection between the TFG SE signal and other spectroscopic signals, in particular transient absorption pump-probe signals.

This state of affairs indicates the necessity to cast the TFG spectrum in a form which is computationally convenient, but not limited to a particular or simple material-system dynamics. To achieve this goal, it seams promising to further develop the doorway-window (DW) picture of the TFG SE. This has partially been done already in papers [3, 54] (for perfect spectral filters) and in [63, 64, 83–85] (for "bare" spectra, which are connected with "real" TFG SE spectra through the convolution with the joint time-frequency gate function). The aim of the present contribution is to directly develop the DW description for "real" TFG SE spectra. This formulation reduces the computational effort considerably, since some of the integrals can be performed analytically. Concomitantly, this formulation allows us to make the interrelations between the approaches mentioned above more transparent and to obtain various forms of the expressions which can be useful in actual calculations. It is hoped that the proposed theory will simplify the computation of the TFG SE for nontrivial multidimensional systems, in particular those exhibiting pronounced nonadiabatic couplings and therefore ultrafast decay dynamics.

For notational convenience, we use units in which $\hbar = 1$.

2.2 Definition of the time-resolved spectrum

The total intensity of the temporally gated and spectrally filtered field at the position $\overrightarrow{r}$ in the far-field region is given by the general expression [117]

$$S_{st}(t_0,\omega_0) \sim \int_{-\infty}^{\infty} dt \int_{-\infty}^{\infty} dt' \int_{-\infty}^{\infty} dt''\, E_t(t';t_0)E_t^*(t'';t_0)\times \tag{2.1}$$

$$F_s(t-t',\omega_0)\, F_s^*(t-t'',\omega_0) \; < E(\overrightarrow{r},t')E(\overrightarrow{r},t'')^* > .$$

Here $E_t(t;t_0)$ is the time-gate function which is strongly peaked near the gating time $t \sim t_0$, the function $F(t-t',\omega_0)$ is responsible for the spectral filtering near the central frequency ω_0, and $< E(\overrightarrow{r},t')E(\overrightarrow{r},t'')^* >$ is the CF of the emitted field. It is clear from this definition that the TFG SE spectrum is always positive, in contrast to its bare counterpart [1,3].

For performing explicit calculations, we shall further use the standard approximations [18, 19, 78, 79, 83–85, 117–119]

$$E_t(t;t_0) = \exp(-[\Gamma(t-t_0)]^2) \tag{2.2}$$

or

$$E_t(t;t_0) = \exp(-\Gamma|t-t_0|) \tag{2.3}$$

for the time gate function and

$$F_s(\omega,\omega_0) = \frac{\gamma^2}{\gamma^2+(\omega_0-\omega)^2}$$

leading to

$$F_s(t,\omega_0) = \vartheta(t)\frac{\gamma}{2}\exp\left\{-(\gamma+i\omega_0)t\right\}, \tag{2.4}$$

for the frequency filter (which is a good approximation for the Fabry-Perot filter [117]). The constants Γ and γ determine the widths of the corresponding filters ($\Gamma=\infty$ and $\gamma=0$ correspond to an ideal time and frequency resolution, respectively). $\vartheta(t)$ is the Heaviside step function which ensures causality, and Fourier transforms are denoted as

$$f(\omega) \equiv \int_{-\infty}^{\infty} dt\, f(t)\, e^{i\omega t} \quad \forall\ f(t).$$

Following Ref. [117], we normalize the TFG spectrum according to the condition that the total energy passed through the TFG filter is equal to the emitted energy, namely

$$C\int_{-\infty}^{\infty}\frac{dt_0 d\omega_0}{2\pi}S_{st}(t_0,\omega_0) = \int_{-\infty}^{\infty} dt < |E(\overrightarrow{r},t)|^2 > . \tag{2.5}$$

The normalization constant C is readily obtainable for the TFG functions (2.2)-(2.4). One gets

$$C = 8\xi\Gamma/\gamma, \tag{2.6}$$

with $\xi = \sqrt{2/\pi}$ for Gaussian (2.2) and $\xi = 1$ for the exponential (2.3) time-gate.

It is straightforward to demonstrate that the light emitted by a collection of independent dipoles in the far-field region is proportional to the second derivative of the optically induced polarization [78, 84, 120]

$$\overrightarrow{E}(\overrightarrow{r}, t) = -\frac{2\pi}{c^2 r}\frac{d^2}{dt^2}\overrightarrow{P}(\overrightarrow{r}, t - \tau_r). \tag{2.7}$$

Here c is the speed of light, and $\tau_r \equiv r/c$ is the retardation time. Integrating the CF of the emitted light over a small solid angle on the sphere of radius r, one arrives at the expression

$$< E(\overrightarrow{r}, t')E(\overrightarrow{r}, t'')^* > \sim \frac{d^2}{dt'^2}\frac{d^2}{dt''^2} < P(t' - \tau_r)P(t'' - \tau_r) > . \tag{2.8}$$

In order to derive the TFG SE signal from this definition, it is standard practice in the literature **(a)** to neglect by the retardation effects ($\tau_r \equiv 0$) and **(b)** to invoke the slowly-varying-envelope approximation, i.e. $\partial_t^2 \overrightarrow{P}(t) \approx -\omega^2 \overrightarrow{P}(t)$, where ω is the carrier frequency. That is tantamount to the assumption

$$< E(\overrightarrow{r}, t')E(\overrightarrow{r}, t'')^* > \sim < P(t')P(t'') > . \tag{2.9}$$

Here we would like to analyze the above assumptions in some detail.

(a) Starting from the definition (2.1), it is elementary to demonstrate that one obtains the signal $S_{st}(t_0 - \tau_r, \omega_0)$ from the retarded CF $< P(t' - \tau_r)P(t'' - \tau_r) >$, if the unretarded CF $< P(t')P(t'') >$ gives the signal $S_{st}(t_0, \omega_0)$. (In the derivation of this result, it has been assumed that $E_t(t; t_0) = E_t(t_0 - t)$, which is a natural approximation for a time gate). The retardation thus merely gives rise to a shifted time origin of the TFG spectrum. Keeping this in mind, we put $\tau_r \equiv 0$ in all subsequent calculations. It should be pointed out, however, that for $r = 1$ cm, for example, one gets $\tau_r = 100$ ps, so that it is necessary to decide in a particular ultrafast experiment if the consideration of retardation effects is important or not, and to define correctly the time $t = 0$.

(b) By expressing the frequency-gate functions through their Fourier transforms and inserting the corresponding formulas into (2.1), one gets

$$S_{st}(t_0, \omega_0) = \int_{-\infty}^{\infty} d\omega_1 |F_s(\omega_1, \omega_0)|^2 \, S_t(t_0, \omega_1), \tag{2.10}$$

where

$$S_t(t_0, \omega_1) \sim \int_{-\infty}^{\infty} dt' \int_{-\infty}^{\infty} dt'' \, \exp(-i\omega_1(t' - t'')) \times \tag{2.11}$$

$$E_t(t'; t_0)E_t^*(t''; t_0)\frac{d^2}{dt'^2}\frac{d^2}{dt''^2} < P(t')P(t'') >$$

is the TFG spectrum obtained with ideal spectral resolution ($|F_s(\omega, \omega_0)|^2 = \delta(\omega - \omega_0)$). The spectral filtering is seen to be independent of the time gating and material system dynamics, so that its effect on the TFG SE can always be removed by deconvolution [83–85]. Proceeding in the spirit of papers [83–85], one can use Eq. (2.11) to develop generalized Wigner spectrograms for the description of the TFG SE (see Appendix A).

For the purposes of the further presentation, we prefer to stay in the time domain. Integrating Eq. (2.11) by parts, one transfers the action of the time derivatives from the polarization CF to the time gate functions, so that

$$S_t(t_0,\omega_0) \sim \int_{-\infty}^{\infty} dt \int_{-\infty}^{\infty} dt' \, \overline{E}_t(t;t_0)\overline{E}_t^*(t';t_0) \exp(-i\omega_0(t-t')) < P(t)P(t') >, \quad (2.12)$$

where

$$\overline{E}_t(t;t_0) = (\frac{d^2}{dt^2} - 2i\omega_0\frac{d}{dt} - \omega_0^2)E_t(t;t_0). \quad (2.13)$$

The explicit inclusion of the time derivatives in the definition of the TFG SE results in a redetermination of the time gate functions. For instance, starting from Eq. (2.2), one gets:

$$\overline{E}_t(t;t_0) = [(\Gamma^2(t-t_0) + i\omega_0)^2 - \Gamma^2]E_t(t;t_0). \quad (2.14)$$

Formally speaking, these generalized gate functions become complex and frequency dependent. The inspection of the above equations allows one to estimate a criterion for the validity of Eq. (2.9). In an experiment with ultrafast time resolution, one normally has $\Gamma \gg \gamma$ (a good filter), Γ being the inverse of the gating-pulse duration. If the material system under study possesses a narrow spectrum in the vicinity of the relatively well defined frequency $\omega_{eg} \gg \Gamma$ of an electronic transition, then $\overline{E}_t(t;t_0) \approx -\omega_0^2 E_t(t;t_0)$. When the system under study exhibits a broad or multi-peaked spectrum, one should use the more general expressions (2.12) and (2.13). Keeping in mind the above restrictions, we shall use formula (2.9) as the basic equation for the analysis of the TFG SE.

Adopting the standard Fabry-Perot-like form (2.4) of the frequency filter, one can immediately perform the integration over t in Eq. (2.1) analytically. This yields:

$$S_{st}(t_0,\omega_0) = C' \int_{-\infty}^{\infty} dt \int_{-\infty}^{t} dt' \, E_t(t;t_0)E_t^*(t';t_0)\times \quad (2.15)$$

$$(\exp\{-(\gamma + i\omega_0)(t-t')\} < E(\overrightarrow{r},t)E(\overrightarrow{r},t')^* > + c.c.)$$

Here a new normalization constant, $C' = C\gamma/4$, has been introduced. According to Eq. (2.6), it is independent of the frequency filter resolution γ. We shall further accept the assumption (2.9), so that

$$S_{st}(t_0,\omega_0) \sim Re \int_{-\infty}^{\infty} dt \int_{-\infty}^{t} dt' \, E_t(t;t_0)E_t^*(t';t_0)\times$$

$$\exp\{-(\gamma + i\omega_0)(t-t')\} < P(t)P(t') > . \quad (2.16)$$

2.3 Polarization

2.3.1 Definition

The material-system dynamics is shown to enter the description in terms of two-time CF of polarization. The optically-induced polarization $P(t)$ is the key quantity of

the theoretical consideration. It is the only material quantity that appears in the equations. Consequently, a complete knowledge of the optical polarization is sufficient for the interpretation of any time-resolved spectroscopic experiment. Electronic and nuclear motions and relaxation processes will show up in optical measurements only through their effect on the polarization. The calculation of the polarization is therefore the primary goal of any theory of optical spectroscopy, and is a key for interpreting spectroscopic measurements [1].

Polarization is, by a definition, a quantum-mechanical expectation value of the transition dipole moment operator $\widehat{\overrightarrow{V}}$:

$$\overrightarrow{P}(t) =< \widehat{\overrightarrow{V}} >\equiv Tr\left\{\widehat{\overrightarrow{V}}\,\rho(t)\right\}. \tag{2.17}$$

It describes the system response to the external field. We further adopt the semiclassical level of theoretical description, treating the material system quantum mechanically and the external field classically.

To calculate the polarization, we assume that initially (at $t=-\infty$, before "switching on" the external field) the system was in thermal equilibrium with respect to its Hamiltonian H. Therefore, its density operator is given by

$$\rho(-\infty) = Z^{-1}e^{-H/kT}, \tag{2.18}$$

where Z is the partition function and T is the temperature.

As we have mentioned, the interaction with the external field is given by

$$H_{SF}(t) = \overrightarrow{\varepsilon}\cdot\overrightarrow{\mu}\,E(t)e^{-i\omega t}\,\widehat{V} + H.c., \tag{2.19}$$

where $E(t)$ and ω are the envelope (slow function) and carrier frequency of the external field, $\overrightarrow{\varepsilon}$ is the field polarization, and $\overrightarrow{\mu}$ is the optical dipole moment ($\widehat{\overrightarrow{V}} = \overrightarrow{\mu}\,\widehat{V}$). Since we are not interested in orientational effects, we let $\overrightarrow{\varepsilon}\cdot\overrightarrow{\mu} = 1$.

The total Hamiltonian of the system is $H_{tot} = H + H_{SF}(t)$, and the Liouville equation is

$$\frac{\partial\rho(t)}{\partial t} = -i\,[H + H_{SF}(t),\,\rho(t)]. \tag{2.20}$$

In order to calculate the polarization of the material system according to Eq. (2.17), we have to solve this Liouville equation for the DM.

There are two ways to proceed further: perturbatively (with respect to H_{SF}), using time-dependent DM perturbation theory [1, 121, 122], or nonperturbatively, incorporating the system-field interaction into the system Hamiltonian and performing a numerical propagation of the density matrix of the driven system.

The perturbative treatment is well justified in time-resolved spectroscopy, because in virtually all experiments discussed here the laser fields are much weaker than the internal electric fields. A nonperturbative treatment, on the other hand, naturally allows the consideration of strong-field effects. This approach is straightforward for the implementation and often is advantageous (however expensive computationally).

Throughout the text we will confine ourselves to the perturbative approach, since it provides a clear physical picture and allows one to uniformly classify and to distinguish various physical processes contributing to a given spectroscopic experiment [1, 2].

This aspect is crucial for the interpretation of the spectroscopic signals in terms of the system dynamics. Even if one adopts a nonperturbative approach, it still requires a perturbative analysis of the calculated signals in order to distinguish various contributions to the signal [123,124]. Another reason for employing a perturbative treatment is the possibility to perform part of the calculations analytically, which reduces the subsequent computational effort considerably. The implementation of the nonperturbative approach for the calculation of TFG SE signals is outlined in Appendix B.

2.3.2 Calculation of the polarization: perturbative approach

Using time-dependent DM perturbation theory, we can expand the density operator in powers of the external field:

$$\rho(t) = \rho^{(0)}(t) + \rho^{(1)}(t) + \rho^{(2)}(t) + \dots . \tag{2.21}$$

Here $\rho^{(n)}(t)$ denotes the nth order contribution in the electric field and $\rho^{(0)}(t) = \rho(-\infty)$. Substituting this expression into Eq. (2.17), we obtain the corresponding expansion for the polarization:

$$P(t) = P^{(1)}(t) + P^{(2)}(t) + P^{(3)}(t) + ..., \tag{2.22}$$

where $P^{(n)}(t)$ denotes the polarization to the nth order in the electric field (we assume that polarization vanishes at thermal equilibrium, $P^{(0)} = 0$).

As we have mentioned, the perturbative approach is an elegant theory which allows one to classify various signals and to distinguish different contributions. Each order in this expansion corresponds to a certain class of optical measurements. The first-order polarization $P^{(1)}$ is responsible, e.g., for linear absorption. $P^{(2)}$ (and all higher order even contributions to the polarization) vanish for isotropic systems, in particular, for the electronic two-level system (TLS) which contains no permanent dipoles. Therefore, the third-order polarization $P^{(3)}$ is the first non-vanishing nonlinear contribution. It enters into all nonlinear spectroscopic techniques of the third order, e.g., pump-probe spectroscopy, time-resolved fluorescence, and four-wave mixing.

Expanding the polarization to the first order in the field, we obtain [1]

$$P^{(1)}(t) = i \int_0^\infty dt_1 \, E(t - t_1) \, \{J(t_1) - J^*(t_1)\} , \tag{2.23}$$

where $J(t) =< V(t)V(0)\rho(-\infty) >$ is a linear (2-time) dipole CF ($V(t)$ is the Heisenberg operator).

For the third-order polarization, on gets the formula

$$P^{(3)}(t) = i^3 \int_0^\infty dt_3 \int_0^\infty dt_2 \int_0^\infty dt_1 \, E(t - t_3)E(t - t_3 - t_2)\times \tag{2.24}$$

$$E(t - t_3 - t_2 - t_1) \sum_{i=1}^{4} \{R_i(t_3, t_2, t_1) - R_i^*(t_3, t_2, t_1)\},$$

where $R_i(t_3, t_2, t_1)$ are the third-order nonlinear RFs [1]:

$$R_1(t_3, t_2, t_1) =< V(t_1)V(t_1 + t_2)V(t_1 + t_2 + t_3)V(0)\rho(-\infty) >, \tag{2.25}$$

$$R_2(t_3,t_2,t_1) =< V(0)V(t_1+t_2)V(t_1+t_2+t_3)V(t_1)\rho(-\infty) >, \tag{2.26}$$

$$R_3(t_3,t_2,t_1) =< V(0)V(t_1)V(t_1+t_2+t_3)V(t_1+t_2)\rho(-\infty) >, \tag{2.27}$$

$$R_4(t_3,t_2,t_1) =< V(t_1+t_2+t_3)V(t_1+t_2)V(t_1)V(0)\rho(-\infty) > . \tag{2.28}$$

Time variables t_i represent the time intervals between successive interactions with a field.

The RFs (2.25)-(2.28) provide us with the standard and universal description of various nonlinear (third-order) spectroscopic techniques [1]. Eqs. (2.25)-(2.28) are very general. They are not limited to any specific model for the system dynamics. For the purposes of further consideration, we restrict ourselves to the system consisting of two electronic states (ground and excited) treated in the adiabatic approximation (electronic TLS). Furthermore, we assume that the two separated electronic states are coupled only by the radiation field. Therefore, we write the Hamiltonian as

$$H = \begin{pmatrix} H_g & 0 \\ 0 & H_e \end{pmatrix}. \tag{2.29}$$

Here H_α are the vibrational Hamiltonians in the ground state ($\alpha = g$) and the excited electronic state ($\alpha = e$). While this form of the Hamiltonian excludes intramolecular nonadiabatic coupling of the excited electronic state with the ground state, it should be stressed that H_e may represent several nonadiabatically coupled electronic states. The ensuing formulation includes, in particular, the case of an optically bright excited state which is intramolecularly coupled to one or several optically dark states. Even more generally, it allows for an arbitrary oscillator strength for all of the nonadiabatically coupled states. Although the form (2.29) of the molecular Hamiltonian represents a restriction, the theory still applies to many of the experimentally interesting systems [2] (in Section 4, e.g., H_e describes the dynamics of two coupled electronic states representing ET model).

Substituting $V(t) = e^{iHt}Ve^{-iHt}$ with the Hamiltonian (2.29) into Eqs. (2.25)-(2.28), one can rewrite the RFs in the explicit form:

$$R_1(t_3,t_2,t_1) = \left\langle \exp\left\{\frac{i}{\hbar}H_g t_1\right\} V_{ge} \exp\left\{\frac{i}{\hbar}H_e t_2\right\} V_{eg} \exp\left\{\frac{i}{\hbar}H_g t_3\right\} V_{ge} \times \right. \tag{2.30}$$

$$\left. \exp\left\{\frac{-i}{\hbar}H_e(t_1+t_2+t_3)\right\} V_{eg}\rho_g \right\rangle ,$$

$$R_2(t_3,t_2,t_1) = \left\langle V_{ge} \exp\left\{\frac{i}{\hbar}H_e(t_1+t_2)\right\} V_{eg} \exp\left\{\frac{i}{\hbar}H_g t_3\right\} V_{ge} \times \right. \tag{2.31}$$

$$\left. \exp\left\{\frac{-i}{\hbar}H_e(t_2+t_3)\right\} V_{eg} \exp\left\{\frac{-i}{\hbar}H_g t_1\right\} \rho_g \right\rangle ,$$

$$R_3(t_3,t_2,t_1) = \left\langle V_{ge} \exp\left\{\frac{i}{\hbar}H_e t_1\right\} V_{eg} \exp\left\{\frac{i}{\hbar}H_g(t_2+t_3)\right\} V_{ge} \times \right. \tag{2.32}$$

$$\left. \exp\left\{\frac{-i}{\hbar}H_e t_3\right\} V_{eg} \exp\left\{\frac{-i}{\hbar}H_g(t_1+t_2)\right\} \rho_g \right\rangle ,$$

$$R_4(t_3,t_2,t_1) = \left\langle \exp\left\{\frac{i}{\hbar}H_g(t_1+t_2+t_3)\right\} V_{ge} \exp\left\{\frac{-i}{\hbar}H_e t_3\right\} V_{eg} \times \right. \tag{2.33}$$

$$\left. \exp\left\{\frac{-i}{\hbar}H_g t_2\right\} V_{ge} \exp\left\{\frac{-i}{\hbar}H_e t_1\right\} V_{eg}\rho_g \right\rangle ,$$

where V_{ge} , V_{eg} are the (coordinate-dependent) electronic matrix elements of the transition dipole operator coupling these states ($\widehat{V} = V_{eg}(q)\,|e\rangle\langle g| + V_{ge}(q)\,|g\rangle\langle e|$).

To get a clear physical interpretation, one can switch from the ordinary Hilbert space to an equivalent expression in the Liouville space (see a book of Mukamel [1]). For example, the RFs R_1 and R_2 (only these functions will appear in the expressions for TFG SE) can be written as (Eq. (7.11) in [1]):

$$R_1 = \left\langle \left\langle V_{eg}|G_{eg}(t_3)\widetilde{V}_{eg,ee}G_{ee}(t_2)\widetilde{V}_{ee,eg}G_{eg}(t_1)\widetilde{V}_{eg,gg}|\rho_g\right\rangle \right\rangle , \tag{2.34}$$

$$R_2 = \left\langle \left\langle V_{eg}|G_{eg}(t_3)\widetilde{V}_{eg,ee}G_{ee}(t_2)\widetilde{V}_{ee,ge}G_{ge}(t_1)\widetilde{V}_{ge,gg}|\rho_g\right\rangle \right\rangle , \tag{2.35}$$

where $G(t)$ is the Liouville space Green function and $\widetilde{V}$ is the dipole operator in Liouville space, which are defined by its action on an ordinary nuclear operator A : $G_{nm}(t)A = e^{-iH_n t}Ae^{iH_m t}$; $\widetilde{V}A = [V,\, A]$.

The nonlinear RFs have the following physical interpretation in Liouville space: the system is initially at equilibrium in the ground electronic state and its nuclear density operator is ρ_g. The *first interaction* with the external field (pump pulse) [which takes place at time $t - t_1 - t_2 - t_3$] sets up an *optical coherence* in the system; $G_{eg}(t_1)$ [or $G_{ge}(t_1)$] represents the evolution and dephasing of this coherence. The *second interaction* (at time $t - t_2 - t_3$) converts the coherence into the *population* of the excited electronic state ($|e\rangle$). During the time t_2 between the second and third interactions, the system's evolution is given by $G_{ee}(t_2)$. This represents a propagation in the excited electronic state. Subsequently, the *third interaction* (at time $t - t_3$) creates again an electronic coherence that evolves during t_3 [$G_{eg}(t_3)$]. Finally, at time t the polarization is calculated by acting with V from left and performing the trace.

2.3.3 Time- and frequency-resolved signal in terms of response functions

Now we are in a position to develop further the theory of TFG SE. We restrict ourselves to the simplest (but important) case when the excitation and emission processes are well separated temporally (non-overlapping pulses assumption). Under these conditions, the SE consists primarily of the fluorescence component; the Raman contribution

can be neglected due to fast optical dephasing [1–3]. We proceed further in a standard way. Employing the rotating-wave approximation (RWA) [34] (only completely resonant interactions are considered), retaining only sequential contributions (excitation precedes gating) and performing some standard manipulations (see, e.g., [1, 83–85]), one can recast Eq. (16) in the following form:

$$S_{st}(t_0,\omega_0) \sim Re \int_{-\infty}^{\infty} dt \int_0^{\infty} dt_3 \int_0^{\infty} dt_2 \int_0^{\infty} dt_1 \times \tag{2.36}$$

$$E_t(t-t_0)E_t(t-t_3-t_0)E_L(t-t_3-t_2)E_L(t-t_3-t_2-t_1)\times$$

$$e^{-(\gamma-i\omega_0)t_3}\left\{R_1(t_3,t_2,t_1)e^{i\omega_L t_1}+R_2(t_3,t_2,t_1)e^{-i\omega_L t_1}\right\},$$

Here ω_L and $E_L(t)$ are the frequency and the envelope of the excitation pulse; and $E_t(t)$ is the envelope of the gate pulse which was introduced in Eqs. (2.2), (2.3).

Before proceeding further, let us analyze this equation. Clearly, if there is no time gating ($\Gamma = 0$, $E_t = 1$), then the TFG spectrum reduces to the frequency-domain fluorescence spectrum (see Eq. (9.10b) in [1]). On the other hand, by comparing Eq. (2.36) with Eq. (11.8) in [1], one immediately realizes that the TFG SE is nothing else than the excited-state (stimulated-emission) contribution to the integrated pump-probe spectrum for non-overlapping pulses. The filter thus defines an effective carrier frequency ω_0 of the probe, and the temporal gate function represents the probe envelope centered at t_0. The only difference stems from the imperfection of the frequency filter γ, which controls the spectral resolution of the TFG SE. For an ideal filter ($\gamma = 0$) the analogy is complete, and one recovers the equations derived in [3, 54].

A close similarity between the TFG SE and pump-probe spectra has repeatedly been emphasized in the literature [1–3, 67, 75, 114]. It should be noted, however, that the equivalence between the TFG SE signal and stimulated-emission contribution to the sequential integral pump-probe signal holds only in the leading (second) order in the pump and probe pulses. In this case also the "bare" TFG SE spectrum coincides with the stimulated-emission contribution to the dispersed pump-probe spectrum [75, 114]. It is of importance that both stimulated emission (from the electronically excited state) and stimulated Raman (from the ground state) processes contribute to the overall pump-probe signal, even in the case of sequential, nonoverlapping pump and probe pulses. On the other hand, if the excitation and gate pulses do not overlap, the SE consists solely of the fluorescence (excited state) component. As a consequence, one cannot experimentally separate the ground and excited state contribution to the pump-probe signal. The SE signal from the excited state is, however, background free. So, in general, the TFG SE is not simply related to the pump-probe signal.

2.3.4 Calculation of response functions

The system dynamics enters into TFG SE signal via nonlinear RFs, which become the key quantities of our consideration. However, the calculation of these nonlinear RFs for most of the systems is a difficult task. In Chapters 2-4 and 6 we present different methods for the calculation of RFs and illustrate them by explicit calculations of

TFG SE signals for different model systems. In Chapter 3 we consider the situation when *explicit expressions* for RFs are available (simple model systems). For electronically nonadiabatic systems, an alternative simple model for the calculation of RFs is developed in Chapter 6. This model produces qualitatively correct RFs.

The main goal of this thesis is the development of the tool for the interpretation of the TFG SE spectra of *nontrivial*, i.e., multidimensional, dissipative and/or nonadiabatic systems. For such systems, analytic solutions do not exist and a straightforward computational treatment of the quantum dynamics (computation of RFs) is not feasible. To solve this problem, we further develop in this chapter the doorway-window (DW) picture of the TFG SE which will simplify the computation of RFs (and, consequently, the calculation of the signals). This formulation reduces the computational effort considerably, since some of the integrals can be performed analytically. Concomitantly, this formulation allows us to obtain various forms of the explicit analytical expressions (if the problem is treated in terms of the eigenvalues and eigenfunctions of the ground and excited state Hamiltonians) which can be useful in actual calculations.

2.4 Doorway-window representation of time-resolved spectra

To achieve our goals, it is convenient to develop the DW representation of the TFG spectrum. This has already been done partially in papers [3, 54] (for perfect spectral filters) and in [63,64,83–85] (for "bare" spectra, which are connected with "real" TFG SE spectra through the convolution with the joint time-frequency gate function). The aim of the present consideration is to directly develop the DW description for "real" TFG SE spectra. The idea of this representation is to separate the four-time integral in the expression for the TFG SE spectrum (2.36) into two independent two-time integrals, which have clear physical interpretations.

2.4.1 Doorway-window picture: operator form

Keeping in mind the above-mentioned analogy between TFG SE and stimulated emission, the desired DW representation can directly be taken over from the corresponding representation for the pump-probe spectrum (see, e.g., [1, 3, 84]). The result reads:

$$S_{st}(t_0,\omega_0) \sim Tr[W(\omega_0)G(t_0)D(\omega_L)]. \tag{2.37}$$

Here

$$D(\omega_L) = \int_{-\infty}^{\infty} dt' \int_0^{\infty} dt_1\, E_L(t')E_L(t'-t_1)e^{i\omega_L t_1}\times \tag{2.38}$$

$$e^{iH_e t'}\, e^{-iH_e t_1}\, V_{eg}\rho_g\, e^{iH_g t_1}\, V_{ge}\, e^{-iH_e t'} + H.C.$$

is the doorway operator,

$$W(\omega_0) = \int_{-\infty}^{\infty} dt \int_0^{\infty} dt_3\, E_t(t+t_3)E_t(t)e^{(i\omega_0-\gamma)t_3}\times \tag{2.39}$$

$$e^{iH_e t}\, V_{eg}\, e^{iH_g t_3}\, V_{ge}\, e^{-iH_e t_3} e^{-iH_e t} \; + H.C.$$

is the window operator,

$$G(t)X = e^{-iH_e t} X e^{iH_e t} \quad \forall\; X \tag{2.40}$$

is the excited-state propagator, V_{eg} and V_{ge} are the transition dipole moments (these are constants in the Condon approximation),

$$\rho_\alpha \equiv Z_\alpha^{-1} e^{-H_\alpha / kT} \tag{2.41}$$

are the equilibrium vibrational distributions in the ground ($\alpha = g$) and excited ($\alpha = e$) states, and Z_α are the corresponding partition functions.

The DW representation is seen to provide a very simple and intuitive picture of the TFG SE measurement. We can think of the fluorescence emission as a stepwise process, which proceeds via optical creation of population in the excited state by the pump pulse (which is defined by the D operator), its subsequent evolution (which is described by the excited-state propagator e^{-iLt_0}), and fluorescence emission (the W operator describes the TFG detection). Evidently, the entire information about the TFG process is contained in the window operator (2.39). When $\gamma = 0$, one recovers the standard window operator for pump-probe spectroscopy (see, e.g., Eq. (13.4a) in [1]). In the opposite limit, $\gamma \to \infty$, the frequency resolution disappears entirely, $W_0(\omega_0) \approx 1/\gamma$, so that the TFG SE reflects the time-dependent excited-state population:

$$S_{st}(t_0, \omega_0) \sim \; Tr[G(t_0) D(\omega_L)] =< \rho_e(t_0) > .$$

Starting from the DW representation, we can immediately establish several general properties of TFG spectra. If $t_0 = 0$, the TFG spectrum is just the trace of the product of the doorway and window WPs. Since the doorway function represents the initial population of the electronically excited state, the corresponding TFG spectrum can be interpreted as SE from this nonequilibrium excited state. In the opposite extreme case, $t_0 \to \infty$, there are two possibilities. First, if our system is coupled to a dissipative bath, then eventually

$$G(t_0 \to \infty) D(\omega_L) \to \rho_e.$$

If, in addition, the time-gate function is short enough at the time scale of nuclear motion, but long enough compared with the optical coherence dephasing time, one arrives at the so-called snapshot limit for the window function [1], in which

$$W_0(\omega_0) = \int_0^\infty dt_3\, e^{(i\omega_0 - \gamma)t_3}\, V_{eg}\, e^{iH_g t_3}\, V_{ge}\, e^{-iH_e t_3} \; + H.C., \tag{2.42}$$

so that

$$S_{st}(t_0 \to \infty, \omega_0) \to Tr[W_0(\omega_0)\rho_e].$$

This is nothing else than the relaxed fluorescence spectrum, in which γ plays the role of the inverse fluorescence lifetime. To put it differently, the TFG SE spectrum tends to

a certain asymptotic spectrum, which reflects emission from the equilibrated excited-state distribution ρ_e.

If one considers non-dissipative system dynamics, then the limit $G(t_0 \to \infty)D(\omega_L)$ does not exist, and the TFG spectrum mirrors the oscillatory WP motion in the excited state. Generally, if the dissipation is not very strong, the processes of fluorescence and intramolecular dissipation are in competition, resulting in a time-dependent fluorescence shift and an oscillatory approach to the asymptotic relaxed fluorescence spectrum (see Chapter 3).

Note also that the doorway function (2.38) is nothing else than the asymptotic (at times much greater than the excitation-pulse duration) value of the DM, evaluated to the leading (second-order) contribution in the perturbation expansion. Alternatively (and more accurately), it can be computed nonperturbatively in the pump field, by including the field-matter interaction during the excitation into the system Hamiltonian [67,82] (see Appendix B for the further details).

2.4.2 Doorway-window picture: computational aspects

To evaluate the D and W functions (2.38), (2.39), we introduce the eigenstates:

$$H_g|n>=E_n|n>,\ H_e|\alpha>=E_\alpha|\alpha> \tag{2.43}$$

(hereafter, the eigenvalues and eigenfunctions of H_g and H_e are denoted by Latin and Greek letters, respectively). The corresponding frequencies read:

$$\omega_{\alpha n}=E_\alpha-E_n,\ \omega_{\alpha\beta}=E_\alpha-E_\beta. \tag{2.44}$$

The D and W functions can then be expressed in terms of the eigenvalues and eigenfunctions of the system Hamiltonians. It should be remarked that for electronically nonadiabatic systems the use of the eigenstate representation is computationally feasible for system Hamiltonians containing several vibrational modes (up to 7 in favorable cases [2, 55–57]), so that the use of Eqs. (2.43) is not very restrictive.

One can additionally assume that the time-gate functions and the excitation pulses are exponential and described by equations like (2.3). It may seam somewhat unrealistic to model the envelopes of laser pulses by exponentials, but, at the qualitative level at least, it is justified. It has been shown that the substitution of "actual" Gaussian pulse envelopes by their exponential counterparts does not give rise to substantial quantitative differences in the pump-probe signals [78, 79]. This approximation makes it possible to analytically perform all the time integrations in (2.38) and (2.39), with the result:

$$S_{st}(t_0,\omega_0)\sim\sum_{\alpha,\beta,\alpha_1,\beta_1}W_{\alpha\beta}(\omega_0)G^{\alpha\beta}_{\alpha_1\beta_1}(t_0)D_{\alpha_1\beta_1}(\omega_L) \tag{2.45}$$

where

$$D_{\alpha\beta}(\omega_L)=\sum_n V_{\alpha n}V_{n\beta}\rho_g(n)\left\{\frac{1}{\Gamma_L-i(\omega_L-\omega_{\alpha n})}\frac{1}{\Gamma_L-i(\omega_L-\omega_{\beta n})}\right. \tag{2.46}$$

$$\left.+\frac{1}{2\Gamma_L-i\omega_{\alpha\beta}}\frac{1}{\Gamma_L-i(\omega_L-\omega_{\beta n})}+\frac{1}{2\Gamma_L+i\omega_{\alpha\beta}}\frac{1}{\Gamma_L-i(\omega_L-\omega_{\alpha n})}\right\}+C.C.$$

$$W_{\alpha\beta}(\omega_0) = \sum_n V_{\alpha n} V_{n\beta} \left\{ \frac{1}{\Gamma - i(\omega_0 - \omega_{\alpha n})} \frac{1}{\Gamma + \gamma - i(\omega_0 - \omega_{\beta n})} \right. \tag{2.47}$$

$$\left. + \frac{1}{2\Gamma + \gamma - i\omega_{\alpha\beta}} \frac{1}{\Gamma + \gamma - i(\omega_0 - \omega_{\beta n})} + \frac{1}{2\Gamma + \gamma + i\omega_{\alpha\beta}} \frac{1}{\Gamma - i(\omega_0 - \omega_{\alpha n})} \right\} + C.C.$$

Here $V_{\alpha n}$, $V_{n\beta}$ are the matrix elements of the transition dipole moments between the eigenstates $|\alpha>$ and $|\beta>$ (belonging to the excited electronic state) and $|n>$ (belonging to the ground electronic state). These are the final expressions for the TFG SE spectrum which are used in most of the subsequent calculations.

If one wishes to develop the DW description beyond the slowly varying envelope approximation, it is possible to start from the definition (2.39) for the window function, but with the gate function $E_t(t; t_0)$ substituted by its generalized counterpart $\overline{E}_t(t; t_0)$ (2.13). One can then analytically obtain the analogue of Eq. (2.47), but we avoid doing this here in order not to overburden the presentation with technical details.

2.4.3 Connection between the two theoretical approaches

If one considers a bath-free material system, then

$$G^{\alpha\beta}_{\alpha_1\beta_1}(t_0) = e^{-i\omega_{\alpha\beta}t_0}\delta_{\alpha\alpha_1}\delta_{\beta\beta_1} \tag{2.48}$$

so that

$$S_{st}(t_0, \omega_0) \sim \sum_{\alpha,\beta} W_{\alpha\beta}(\omega_0) e^{-i\omega_{\alpha\beta}t_0} D_{\alpha\beta}(\omega_L). \tag{2.49}$$

This is nothing else than a compact form of the formula obtained by Kowalczyk et al. (Ref. [79], Eq. (17)) and subsequently rederived by Santoro et al. (Ref. [78], Eq. (11)). The formula in Ref. [78] additionally contains contributions due to the time derivatives of the dipole moments (cf. the discussion in Sec. 2.2). If the frequency filter is good enough ($\Gamma \gg \gamma$) and if $1/\Gamma$ is much shorter than the characteristic vibrational relaxation time and much longer than the optical coherence dephasing time, one arrives at an ideal (snapshot) TFG spectrum [85]. In that case

$$W_{\alpha\beta}(\omega_0) \approx \frac{1}{2\Gamma} \sum_n V_{\alpha n} V_{n\beta} \left\{ \frac{1}{\Gamma - i(\omega_0 - \omega_{\beta n})} + \frac{1}{\Gamma - i(\omega_0 - \omega_{\alpha n})} \right\} + C.C. \tag{2.50}$$

As has been explained above (see Eq. (2.12)-(2.14)), the ideal spectrum $S_0(t_0, \omega_0) \sim \omega_0^4$. Therefore, to find the number of photons passed through the detector, one must divide $S_0(t_0, \omega_0)$ by ω_0, which gives rise to a ω_0^3 dependence of the signal. Keeping this in mind, one immediately notes that Eq. (2.45) with the window function (2.50) recovers the result by Jean [52] and Lin et al. [102, 103] obtained for an ideal time and frequency resolved SE spectrum. The present analysis therefore bridges the gap between the different formulations of the TFG SE signal [1, 52, 71, 75, 102, 103, 115, 116], [2, 18, 19, 78, 79, 83–85, 119], and [3, 54], and also provides the criterion of the validity of passing from "real" to "bare" SE spectra.

2.4.4 Transient effects

Up to now, the theory relied significantly upon the assumption that the excitation pulse and the temporal gating were well separated, so that all transient effects can be neglected. These effects manifest themselves through exponentially small contributions to the TFG SE spectra, which are proportional to the terms like $\exp(-\Gamma t_0)$ and disappear for $t_0 \gg 1/\Gamma$. There exists, however, an important particular case, which allows one to explicitly incorporate the transient terms into the DW picture. Namely, let us consider the so-called impulsive excitation, when the pump pulse can be regarded as truly instantaneous on the time scale of both nuclear dynamics and electronic dephasing. By inserting the expression $E_L(t) = \delta(t)$ into Eq. (2.36) and making no further approximations, one also arrives at the DW formula (2.37), but with modified doorway $D^{imp}(\omega_L)$ and window $W^{imp}(\omega_0)$ operators. Evidently, Eq. (2.38) simplifies to $D^{imp}(\omega_L) = \rho_g$. On the other hand, $W^{imp}(\omega_0)$ is also given by Eq. (2.39) in which, however, the lower limit of integration over t changes from $-\infty$ to $-t_0$. Clearly, for $t_0 \gg 1/\Gamma$ (that is tantamount to saying that the pump and gating processes are well separated) $W^{imp}(\omega_0) \to W(\omega_0)$. Moreover, following the argumentation outlined above for the standard DW operators, it is natural to invoke the eigenvalue representation (2.43), (2.44) for obtaining the explicit form of $W^{imp}(\omega_0)$. The result reads:

$$W^{imp}_{\alpha\beta}(\omega_0) = W_{\alpha\beta}(\omega_0) - W^{tr}_{\alpha\beta}(\omega_0), \tag{2.51}$$

where $W_{\alpha\beta}(\omega_0)$ is given by Eq. (2.47) and

$$W^{tr}_{\alpha\beta}(\omega_0) = \sum_n V_{\alpha n} V_{n\beta} \left\{ \frac{\exp\{-(2\Gamma + \gamma + i\omega_{\alpha\beta})t_0\}}{2\Gamma + \gamma + i\omega_{\alpha\beta}} \frac{1}{\Gamma + \gamma + i(\omega_0 - \omega_{\beta n})} + \right. \tag{2.52}$$

$$\left. \frac{\exp\{-(\Gamma - i(\omega_0 - \omega_{\alpha n}))t_0\}}{\Gamma - i(\omega_0 - \omega_{\alpha n})} \left[\frac{1}{\Gamma + \gamma - i(\omega_0 - \omega_{\beta n})} + \frac{1}{\Gamma + \gamma + i(\omega_0 - \omega_{\beta n})} \right] \right\} + c.c.$$

As is expected, the transient terms influence the TFG SE at times $t_0 \sim 1/\Gamma$ (see also Chapter 3) but vanish for $t_0 \gg 1/\Gamma$. The above results show that, if one intends to extract information about the system dynamics from the TFG SE spectra, there is no intrinsic limitation to the duration of the pump pulse, since its variation just modifies the doorway function, i.e. the initial vibrational distribution in the excited state. In that sense, the δ-excitation pulse creates the most natural distribution, by merely transferring ρ_g into the excited state without distortions. On the other hand, if one wishes to monitor the SE with time and frequency resolution, the gating time should not be too small. Otherwise ($\Gamma \gg 1$), the spectral resolution is completely lost.

2.5 Doorway-window picture for dissipative systems

Up to this moment, the precise meaning of the Hamiltonians H_g and H_e in Eqs. (2.37)-(2.40) has not been specified yet. The explicit expressions for the TFG SE signal within DW-picture have been obtained in terms of the system eigenstates. As we have already emphasized, an eigenvalue representation is computationally feasible for Hamiltonians

containing *several* vibrational modes with electronic inter-state couplings [2, 55–57]. However, the objects of interest for experimentalists (and for us) are nontrivial systems, i.e., *polyatomic* molecules with the excited-state dynamics characterized by ultrafast electronic and vibrational relaxation processes. When the number of vibrational modes increases, a straightforward computational treatment of the quantum dynamics is no longer possible. For this reason, it is conventional practice to adopt a system-bath (SB) approach, which leads to a reduced density matrix (RDM) description. In this section, we extend the DW formalism to TFG SE of dissipative systems.

In the system-bath approach only a few optically active vibrational modes, which are directly coupled to the electronic transition, constitute the relevant system, while the bath represents the manifold of inactive vibrational modes of the molecule and/or the degrees of freedom of the solvent. For example, this naturally allows one to study the relaxation behavior of molecules letting a system (the chromophore) to be coupled to an environment. Thus, the total Hamiltonian is expressed as a sum of system (S), bath (B) and a system-bath interaction (SB) contributions:

$$H_g = H_g^S + H_g^B + H_g^{SB},\ H_e = H_e^S + H_e^B + H_e^{SB}. \tag{2.53}$$

In order to propagate $D(\omega_L)$ for a time t_0 in Eq. (2.45), we can then switch from the entire (system plus bath) phase space to that of the system only. This is a standard procedure in problems of this kind [1]. It is believed that, in doing so, we do not introduce significant errors into the description. By integrating out the bath degrees of freedom (see Chapter 4), one arrives at the dissipative kinetic equation for the RDM in the excited electronic state

$$\frac{\partial \sigma(t)}{\partial t} = -iL\sigma(t), \tag{2.54}$$

where, in a general form, L is the excited-state Liouvillian. The RDM $\sigma(t)$ is the primary quantity describing the *system* dynamics.

One thus can regard $D(\omega_L)$ as the initial value of the reduced (system) DM in the excited state, which subsequently evolves according to the appropriate kinetic equation of motion. For multimode systems with electronic couplings, one can invoke different methods for the treatment of dissipative effects: (i) certain phenomenological dissipative equations (see, e.g., [2, 3, 75, 122] and a more general model in Chapter 6), (ii) Redfield formalism in various approximations [2, 50–64] (see Chapter 4), (iii) semiclassical and quantum Fokker-Planck equations [65–67], or (iv) kinetic equations [68–74].

We have to emphasize some important technical aspects in DW-formalism which arise due to the partitioning of the total system. We invoke a standard assumption that the excitation and the gate pulses are short enough at the time scale of the system-bath relaxation [1, 3]. In this case, no bath-induced excited-state population relaxation occurs during the pump and probe processes, and one can substitute the corresponding total Hamiltonians by their system parts in the doorway (2.38) and window (2.39) operators , i.e.

$$H_g \to H_g^S,\ H_e \to H_e^S. \tag{2.55}$$

This justifies the evaluation of the DW functions in terms of the eigenvalues and eigenfunctions of these system Hamiltonians: for $|\alpha>$ and $|n>$ in Eqs. (2.45)-(2.47) one

should take the *system* eigenstates. Therefore, for the calculation of the TFG SE spectra for dissipative systems one can use the general DW equations in an operator form (2.37)-(2.39), or explicit expressions in the eigenstate representation (2.45)-(2.47) *having first substituted* the Hamiltonians and eigenstates of the total (S plus B) system by the corresponding operators and values of the relevant system only.

Summarizing, a general scheme for the calculation of TFG SE within DW representation is the following: The first step is to evaluate the eigenstates of the *system* Hamiltonians H_g^S and H_e^S (Eq. (2.43)). One then calculates the D function (2.46) which describes the optically prepared initial state of the system (the initial value of the RDM in the excited state):

$$\sigma_{\alpha\beta}(0) = D_{\alpha\beta}(\omega_L). \tag{2.56}$$

After that one performs a propagation over a time interval t_0 according to the appropriate kinetic equations of motion describing system dynamics with the initial condition (2.56), yielding the RDM $\sigma_{\alpha\beta}(t_0)$. For nontrivial systems, this is the computationally most expensive part. The final step is the contraction of the RDM $\sigma_{\alpha\beta}(t_0)$ with the W function (2.47) which describes the detection process. This yields the desired TFG SE spectrum:

$$S_{st}(t_0, \omega_0) = \sum_{\alpha,\beta} W_{\alpha\beta}(\omega_0)\sigma_{\alpha\beta}(t_0). \tag{2.57}$$

Note that this method requires the D and W operators to be calculated only once.

2.6 Summary

The ultimate goal of the present work is the development of a computationally oriented framework for the description of TFG SE of nontrivial systems, that is, multi-mode systems with strong electronic inter-state couplings which interact with a thermal bath. The specific tasks are as follows: (i) to develop a universal description of the TFG SE, (ii) to clarify the influence of the spectral filtering and temporal gating on the TFG SE spectra, and (iii) to connect the measured TFG SE spectra with the time evolution of the corresponding material systems.

The material-system dynamics has been shown to enter the description in terms of the two-time CF of the second derivatives of the transition dipole moment (Eqs. (2.1) and (2.8)). In the evaluation of the CF, retardation effects due to the finiteness of the speed of light should be taken into account. The CF, convoluted appropriately with the corresponding time-gate and filter functions, yields the experimentally measured TFG SE spectra. The convolution requires three consecutive time integrations to be performed. It has been demonstrated that, by taking the standard Fabry-Perot-like frequency-filter function (2.4), one of these integrations can be performed analytically (Eq. (2.15)), irrespective of a particular form of the CF (2.8) and the time-gate function. The validity of the commonly employed approximation (2.9) has been discussed and generalized expressions have been derived for the TFG SE in terms of Wigner spectrograms beyond this approximation. The retardation effects are demonstrated to give rise to a redefinition (back shift) of the time origin of the TFG SE spectrum.

We have further developed the DW picture of the TFG SE, under the assumption that the excitation and gating processes are well temporally separated. This casts the description of the TFG SE into an intuitively appealing form in terms of WP dynamics in the excited state. This method requires the doorway and window operators to be calculated only once, so that subsequent propagation of the doorway operator over a time interval t_0 and its averaging together with the window operator according to Eq. (2.37) yield the TFG SE spectrum $S_{st}(t_0, \omega_0)$. It has been shown that the TFG SE is equivalent to the stimulated-emission contribution to the integral pump-probe spectrum. In this case the time-gate function plays the role of the envelope of the probe pulse, and the spectral filter function determines its carrier frequency. The only subtle difference stems from the imperfection of the spectral filter ($\gamma \neq 0$), but this is negligibly small for good filters.

It should be noted, however, that the equivalence between the TFG SE signal and stimulated-emission contribution to the sequential integral pump-probe signal holds only in the leading (second) order in the pump and probe pulses. In this case also the "bare" TFG SE spectrum coincides with the stimulated-emission contribution to the dispersed pump-probe spectrum [75,77]. It is of importance that both stimulated emission (from the electronically excited state) and stimulated Raman (from the ground state) processes contribute to the overall pump-probe signal, even in the case of sequential, nonoverlapping pump and probe pulses. On the other hand, if the excitation and gate pulses do not overlap, the SE consists solely of the fluorescence (excited state) component. As a consequence, one cannot experimentally separate the ground and excited state contribution to the pump-probe signal. The SE signal from the excited state is, however, background free. So, in general, the TFG SE is not simply related to the pump-probe signal.

If the DW operators are expanded over the complete set of eigenfunctions of the bath-free Hamiltonian and if one assumes the exponential time-gate function (2.3), the DW functions can be evaluated analytically beyond the snapshot limit. The theory developed in the present work (i) allows one to establish some model-independent properties of TFG spectra, (ii) bridges the gap between the different kinds of descriptions introduced previously, (iii) helps in determining their limitations, and (iv) clarifies interconnections between "real" and "bare" spectra.

Chapter 3

Time-resolved fluorescence of simple model systems

3.1 Introduction

As we have already emphasized, all third-order nonlinear spectroscopic signals can be expressed in terms of response functions $R_i(t_3, t_2, t_1)$ [1]. In this chapter, we consider systems for which the third-order nonlinear RFs can be calculated analytically, i.e., *explicit expressions* for RFs are available. We perform explicit calculations of TFG spectra for several standard benchmark systems (namely, free, Brownian, and Drude oscillators). These systems are modeled by displaced harmonic oscillators in the ground and excited electronic states which are coupled to a bath in a different manner: the free harmonic oscillator is dissipation-free, the Brownian oscillator is coupled to a conventional (Markovian) thermal bath, while the Drude oscillator is coupled to a thermal bath with the exponential memory kernel. These systems with rather transparent dynamics allow us to illustrate the material of the preceding chapter and to investigate separately different effects on the TFG SE spectra:

- By considering the TFG SE of harmonic oscillators (Sec. 3.2), we will (i) study the influence of the quality of the spectral and temporal filtering on the measured spectra and (ii) show to what extent the measurable signals reflect the intrinsic WP motion.
- The Brownian oscillator model (Sec. 3.3) is adopted to illustrate the manifestation of different regimes of the bath-induced relaxation in the time-frequency evolution of the SE spectra. The analysis focuses on the strength of the system-bath coupling.
- The effect of the finite bath correlation time (non-Markovian bath) on the TFG spectra is addressed within a Drude oscillator model (Sec. 3.4).

Nonlinear RFs are uniquely determined by the lineshape function [1]

$$g(t) = \int_0^t dt' \int_0^{t'} dt'' \, C(t''), \tag{3.1}$$

where

$$C(t) =< e^{iH_g t} U\, e^{-iH_g t} U \rho_g > \tag{3.2}$$

is the energy-gap CF, $U \equiv H_e - H_g - \hbar\omega_{eg}$ is a collective energy gap coordinate with ω_{eg} being a parameter (usually, it is chosen to be equal to the thermally averaged electronic energy gap: $\omega_{eg} \equiv \langle H_e - H_g \rangle$).

Nonlinear RFs $R_{1,2}(t_3, t_2, t_1)$ can be written explicitly in terms of $g(t)$ [1]:

$$R_1(t_3, t_2, t_1) = exp(-i\omega_{eg} t_1 - i\omega_{eg} t_3) \times exp\{-g^*(t_3) - g(t_1) - f(t_3, t_2, t_1)\}, \tag{3.3}$$

$$R_2(t_3, t_2, t_1) = exp(i\omega_{eg} t_1 - i\omega_{eg} t_3) \times exp\{-g^*(t_3) - g^*(t_1) + f^*(t_3, t_2, t_1)\}, \tag{3.4}$$

with

$$f(t_3, t_2, t_1) = g(t_2) - g(t_2 + t_3) - g(t_1 + t_2) + g(t_1 + t_2 + t_3). \tag{3.5}$$

For a specific model system, one defines the energy gap coordinate U, then calculates $g(t)$ according to Eq. (3.1), and finally obtains $R_{1,2}(t_3, t_2, t_1)$ from Eqs. (3.3), (3.4).

To render the presentation more transparent and to visualize the dynamic and transient effects, we invoke the Condon approximation (V_{eg} is independent of nuclear coordinates) and restrict ourselves to the case of impulsive excitation (cf. the discussion in Section 2.4.4). After separating $g(t)$ into real and imaginary parts [$g(t) = g'(t) + ig''(t)$] and inserting $E_L(t) = \delta(t)$ into Eq. (2.36), this equation reduces to

$$S_{st}(t_0, \omega_0) \sim Re \int_0^\infty dt \int_0^\infty dt_3\, E_t(t - t_0) E_t(t - t_3 - t_0) \times \tag{3.6}$$

$$\left\{ e^{-g^*(t_3) - 2i[g''(t) - g''(t - t_3)]}\, e^{[-\gamma + i(\omega_0 - \omega_{eg})]t_3} \right\}.$$

The formula (3.6) allows us to calculate TFG spectra for different values of the parameters of the models and for various qualities of the time and frequency filters (see Figs. 3.1-3.4).

3.2 Harmonic oscillator

The simplest system for which the RFs can be calculated analytically is a free harmonic oscillator. It represents an electronic TLS coupled to a number of independent harmonic modes (representing, e.g., intramolecular vibrations, local intermolecular modes, and collective solvent modes) whose equilibrium position is displaced between the two electronic states. In this model, the vibrational Hamiltonians assume the form (we consider a case of a single vibrational mode):

$$H_g = \frac{\Omega}{2}(p^2 + q^2), \tag{3.7}$$

$$H_e = \omega_{eg}^0 + \frac{\Omega}{2}(p^2 + (q+d)^2), \tag{3.8}$$

where Ω is the oscillator frequency, and p, q and d are the (dimensionless) momentum, coordinate and the horizontal displacement (between the minima of the two electronic states), representing this mode.

3.2.1 Analytic response functions

Nonlinear RFs for harmonic oscillators can be obtained in several ways:

1) via thermally averaged linear RF (using the Feynman disentangling technique) which provides an interpretation and evaluation in terms of vibrational WPs ([125]);

2) using time-dependent DM perturbation theory and decomposing the nonlinear RF in a product of two CFs ([122, 126]);

3) using the cumulant expansion which provides an exact solution for systems with Gaussian statistics, e.g., when the electronic system is coupled to a harmonic bath ([1]).

We will adopt the notation introduced by Mukamel, since this is the generally accepted one in the field of nonlinear spectroscopy.

The electronic energy gap in the harmonic oscillator model is

$$\omega_{eg} = \omega_{eg}^0 + \Omega d^2/2 = \omega_{eg}^0 + \lambda. \tag{3.9}$$

Here ω_{eg}^0 is the frequency of the 0-0 transition, and $\lambda = \Omega d^2/2$ is Stokes shift. For the energy gap coordinate we obtain:

$$U = \Omega dq. \tag{3.10}$$

Substituting this into Eq. (3.2), and using creation [$a^+ = \frac{1}{\sqrt{2\Omega}}(\Omega q - ip)$] and annihilation [$a = \frac{1}{\sqrt{2\Omega}}(\Omega q + ip)$] operators, one arrives at the following expression for the CF:

$$C(t) = \Omega^2 S\{(\langle n\rangle + 1)e^{-i\Omega t} + \langle n\rangle\, e^{+i\Omega t}\}, \tag{3.11}$$

where $S = d^2/2$ is the Huang-Rhys factor (which is a dimensionless parameter representing the coupling strength of the vibrational mode to the electronic coupling), $\langle n\rangle = 1/(e^{2\varepsilon} - 1)$ is the thermally averaged occupation number of the harmonic mode, and $\epsilon = \hbar\Omega/2kT$ is the ratio of zero-point energy and thermal energy of the oscillator.

As a result, the model leads to the following expression for the line shape function [1]:

$$g(t) = S\{coth(\varepsilon)[1 - cos(\Omega t)] + i[sin(\Omega t) - \Omega t]\}. \tag{3.12}$$

We see that the parameters which determine the system dynamics are the oscillator frequency Ω, the horizontal shift d (or, equivalently, Stokes shift λ) and "temperature" ε.

Note that in this chapter we use dimensionless variables, in which time is measured in units of Ω^{-1} and frequencies in units of Ω, and the frequency origin is chosen as ω_{eg}.

3.2.2 Time and frequency resolution effects

The consideration of the TFG SE of harmonic oscillators allow us to investigate in detail the influence of the quality of temporal and spectral filtering (to get a feeling how the TFG procedure works). We consider the case of a large Stokes shift ($\lambda = 5$) and low temperature ($\varepsilon = 10$). Fig. 3.1a corresponds to the case of good spectral resolution ($\gamma = 0.3$) but poor temporal resolution ($\Gamma = 0.2$). The TFG spectrum changes only slightly with time. It looks almost static, since the fundamental vibrational period τ_Ω (which equals 2π in our dimensionless units) is of the order of the characteristic gating time $1/\Gamma$. The spectrum exhibits a double ridge structure, which reflects the locations of the WP on the excited-state potential surface in the vicinity of the classical turning points. That is why the local maxima of the right (left) ridge occur at $t_0 = 0,\ 2\pi,\ 4\pi, ...$ ($t_0 = \pi,\ 3\pi, ...$). Since quantum effects are pronounced ($\epsilon = 10$) and the frequency resolution is high, the spectrum possesses vibrational structure.

If one improves the temporal resolution ($\Gamma = 1$), the following qualitatively new properties emerge (Fig. 3.1b). First, the formerly static spectrum acquires pronounced dynamic features and exhibits an oscillatory behavior, which mirrors the motion of the WP in the excited state. Evidently, the frequency of these oscillations coincides with the free oscillator frequency $\Omega = 1$. Second, the vibrational structure completely disappears, despite the fact that the frequency resolution is kept unchanged. The maxima of the TFG SE signal correspond to the classical turning points of the WP in the excited state as discussed above. So, in the vicinity of these points ($t_0 = \pi,\ 2\pi,\ 3\pi, ...$), the WP rephases and becomes narrow. On the contrary, it develops the maximal speed near the potential minimum ($t_0 = \pi/2,\ 3\pi/2,\ 5\pi/2, ...$) and, therefore, broadens. The signal thus monitors not only the position of the WP, but also the speed of the WP motion. By comparing Fig. 3.1b with those from, e.g., the reviews [2, 125], one sees that the overall behavior of the TFG SE signal and the stimulated-emission contribution to the integral pump-probe signal is essentially the same. In general, $S_{st}(t_0, \omega_0)$ can be regarded as a progression of instantaneous (at a particular t_0) spectra, which exhibit a time-dependent shift. Since there is no dissipation, $S_{st}(t_0, \omega_0)$ is τ_Ω-periodic, but the widths and heights of the maxima of these instantaneous spectra are t_0-dependent.

This kind of behavior should be contrasted with that depicted in Fig. 3.1c, in which $S_{st}(t_0, \omega_0)$ is shown for the case of high temporal resolution ($\Gamma = 5,\ 1/\Gamma \ll \tau_\Omega$), the other parameters being unchanged. This situation corresponds, in fact, to the ideal (snapshot) TFG SE spectrum. As in the previous figure, $S_{st}(t_0, \omega_0)$ is τ_Ω-periodic, but the widths and heights of the maxima of the instantaneous spectra are almost t_0-independent. The explanation of these qualitative changes is provided by Eqs. (2.47)-(2.50). To calculate the ideal TFG spectrum for a dissipation-free system, one may use Eqs. (2.49) and (2.50). The inspection of these formulas reveals that $S_0(t_0, \omega_0)$ consists of a sum of Lorentzians which are multiplied by time-dependent factors $e^{-i\omega_{\alpha\beta}t_0}$. Note that these factors are determined by the transition frequencies in the excited state. For a particular t_0, these factors just single out the maximal contributions to $S_0(t_0, \omega_0)$, corresponding to $\omega_{\alpha\beta}\, t_0 = 2\pi n\, (n = 0,\ 1,\ 2,\ ...)$. On the other hand, the widths and heights of the Lorentzians are time-independent and specified by the $e \to g$ transition frequencies $\omega_{\alpha n}$. If one considers the TFG SE beyond the snapshot limit, one should

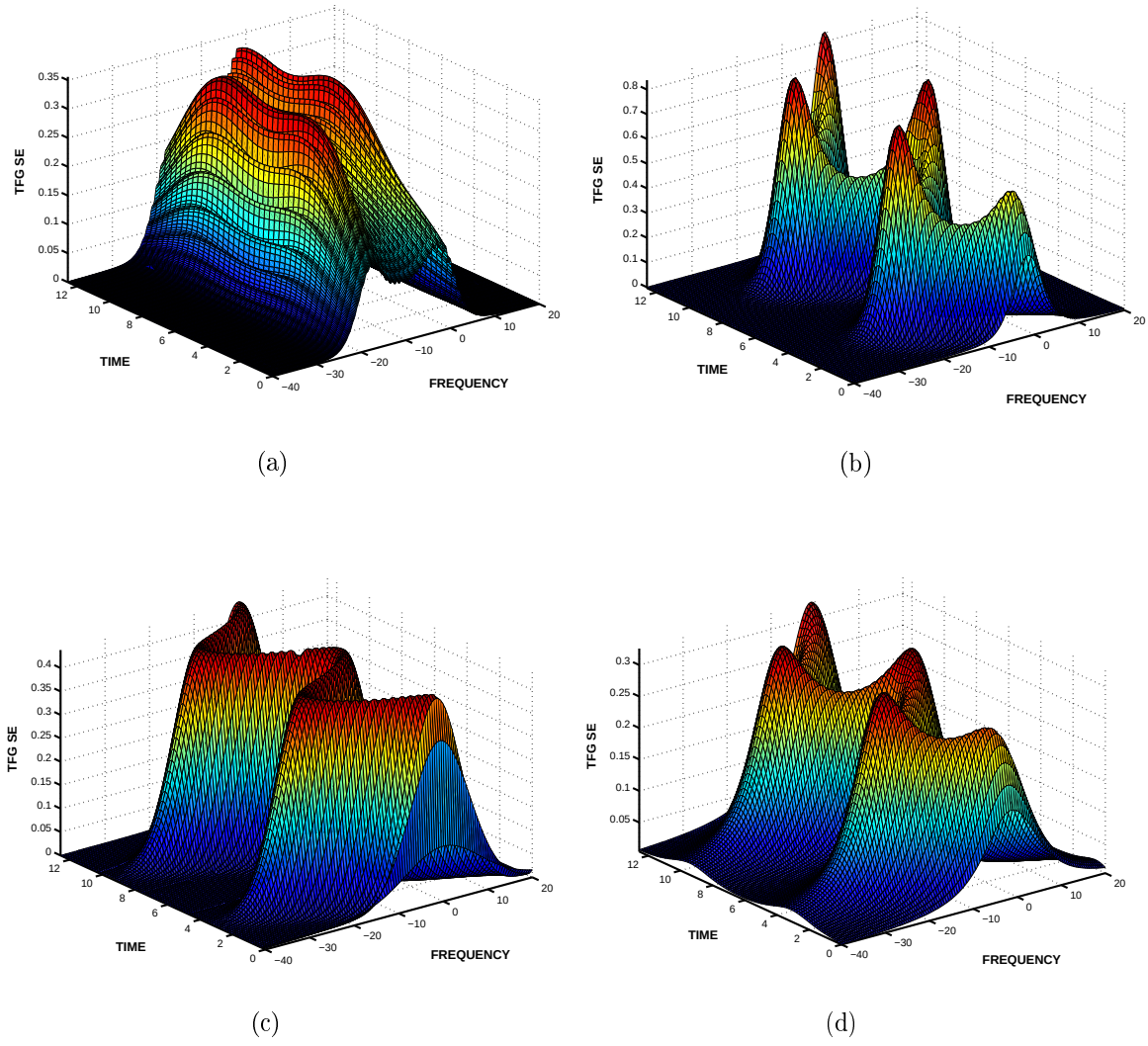

Figure 3.1: Influence of temporal and spectral resolution on the SE spectrum of a bath-free ($\Lambda = 0$) displaced ($\lambda = 5$) harmonic oscillator in the low-temperature limit ($\epsilon = 10$) with **(a)** $\gamma = 0.3$ (good spectral resolution) and $\Gamma = 0.2$ (poor time resolution); **(b)** $\gamma = 0.3$ and $\Gamma = 1$ (satisfactory time resolution); **(c)** $\gamma = 0.3$ and $\Gamma = 5$ (high time resolution); **(d)** $\gamma = 5$ (poor frequency resolution) and $\Gamma = 1$. The TFG SE intensity is given in arbitrary units. All the other parameters are dimensionless, the free oscillator frequency Ω is taken as the frequency unit and its inverse $1/\Omega$ as the time unit.

employ the more general Eq. (2.47) for the window function. It also can approximately be regarded as a sum of certain "spectral functions", multiplied by the same time-dependent factors $e^{-i\omega_{\alpha\beta}t_0}$. In contrast to the snapshot case, the "spectral functions" are the products of two Lorentzians, which are both $\omega_{\alpha n}$ and $\omega_{\alpha\beta}$ dependent. So, in general, the excited-state frequencies $\omega_{\alpha\beta}$ affect the widths and maxima of $S_{st}(t_0,\omega_0)$ and, therefore, make these t_0-dependent. When Γ is further increased, the spectral features of $S_{st}(t_0,\omega_0)$ are smeared out. In principle, any frequency resolution disappears in the limit $\Gamma \gg 1$, in which one merely measures the time-dependent population in the excited state, since $S_{st}(t_0,\omega_0) \to Tr[G(t_0)D(\omega_L)]$. Similarly, if the spectral resolution decreases ($\gamma = 5$), the TFG SE broadens and tends to become more featureless (Fig. 3.1d). In this sense, poor spectral resolution ($\gamma \gg 1$) is equivalent to high temporal resolution ($\Gamma \gg 1$).

By inspecting Figs. 3.1a-d, as well as the subsequent Figs. 3.2 and 3.3, one clearly observes the signature of the transient effects. These manifest themselves through the increase of the area under the instantaneous spectra $S_{st}(t_0,\omega_0)$ at short times. In other words, the TFG SE spectra "flare up" on a time scale of $1/\Gamma$. The origin of this phenomenon has been discussed at the end of Sec. 2.4 (see Eqs. (2.51) and (2.52)). Here we present the corresponding quantitative estimates. Integrating Eq. (3.6) over ω_0 one finds that, irrespective of the particular form of $g(t)$,

$$\int_{-\infty}^{\infty} d\omega_0\, S_{st}(t_0,\omega_0) \sim \int_{-t_0}^{\infty} dt\, E_t^2(t) = \frac{1}{2\Gamma}\left[\begin{array}{ll} \sqrt{\frac{\pi}{2}}(1+\Phi(t_0)) & for\ Eq.(2) \\ 2-e^{-2\Gamma t_0} & for\ Eq.(3) \end{array}\right. \tag{3.13}$$

where Φ is the error function. This result shows that the initial ($t_0 = 0$) area under the TFG SE spectrum is smaller by a factor of two than the asymptotic ($t_0 \to \infty$) area. Evidently, the better the temporal resolution, the less visible are the transient effects.

3.3 Brownian oscillator

The free harmonic oscillator model considered above misses an important aspect of real systems, namely, dissipation. This model is incapable of describing the phenomenon of excited-state vibrational relaxation. The Brownian oscillator (or damped harmonic oscillator) model [1, 115, 127–130] introduces dissipation into the harmonic oscillator by coupling the primary oscillator to a *harmonic bath*. Thus the model explicitly introduces vibrational damping and solvent friction into the spectral line shapes.

3.3.1 Analytic response functions

The Brownian oscillator model leads to the following expressions for the lineshape functions [127, 128]

$$g(t) = g'(t) + ig''(t),\ C(t) = C'(t) + iC''(t), \tag{3.14}$$

$$C'(t) = \lambda\left\{\frac{1}{z_- - z_+}\left[e^{-z_+ t}\cot(\epsilon z_+/\Omega) - e^{-z_- t}\cot(\epsilon z_-/\Omega)\right] - \Gamma(t)\right\}, \tag{3.15}$$

$$C''(t) = \frac{\lambda}{z_- - z_+}\left[e^{-z_+ t} - e^{-z_- t}\right]. \tag{3.16}$$

Here

$$\Gamma(t) = \frac{2\Lambda}{\epsilon} \sum_{n=1}^{\infty} \frac{\nu_n e^{-\nu_n t}}{(1+\nu_n^2)^2 - \Lambda^2 \nu_n^2}, \ \nu_n = \pi n/\epsilon, \tag{3.17}$$

$$z_{\pm} = (-\Lambda \pm i\sqrt{4-\Lambda^2})/2, \tag{3.18}$$

Comparing with the harmonic oscillator model, the new parameter Λ appears here which describes the coupling to a bath. When $\Lambda = 0$, one recovers the case of the free oscillator, $\Lambda \gg 1$ corresponds to the overdamped oscillator limit.

3.3.2 Dissipation effects

To investigate the influence of a dissipative environment on the TFG SE, we consider different kinds of dissipation mechanisms within a Brownian oscillator model. (Here we assume the standard Markovian bath, so the analysis focuses on the strength of the system-bath coupling.) Fig. 3.2a-c show the TFG SE spectra obtained for increasing strength of the system-bath coupling. A large Stokes shift ($\lambda = 5$) and high temperature ($\varepsilon = 0.1$) are assumed, as well as good time and frequency resolution ($\gamma = \Gamma = 1$). The evolution of the TFG SE spectra reflects the strength of system-bath coupling, as expected. The initial spectrum, $S_{st}(0, \omega_0)$, eventually develops into the asymptotic one, $S_{st}(\infty, \omega_0)$, which exhibits the Stokes shift of 2λ. When the damping effects are not strong, the system dynamics is underdamped and the signal exhibits weakly damped oscillations (Fig. 3.2a). When the dissipation strength is further increased, the WP oscillations are rapidly damped (Fig. 3.2b). In the overdamped limit, $S_{st}(0, \omega_0)$ tends to $S_{st}(\infty, \omega_0)$ monotonously (Fig. 3.2c).

To get a better understanding of the TFG SE of the overdamped oscillator, it is useful to calculate the spectrum analytically. Moreover, one can surmount the restriction of impulsive excitation and assume that the pump and gate pulses have a Gaussian shape (Eq. (2.2)). The spectral filter is assumed to be "ideal" ($\gamma = 0$). To arrive at the desired result, one can start either from the general Eq. (2.36), or from the DW description (2.37)-(2.39). Let us assume, in addition, that the oscillator motion is much slower than the optical dephasing time. This allows us to neglect the system dynamics during t_3 and t_1, when the system is in the coherence state. We can thus retain only the leading contributions to the g-functions, up to quadratic terms in t_3 and t_1. The corresponding expression has been derived and discussed in [1, 129, 131, 132] for the sequential pump-probe spectrum, but we can further generalize it by invoking the modified gate function (2.14). The result reads

$$S_t(t_0, \omega_0) = \frac{2\pi(3A^2 + 6AB^2 + B^4)}{\sqrt{(\Delta^2 + \Gamma_L^2)\alpha^2(t_0)}} \exp\left\{-\frac{\overline{\omega_L}^2}{2(\Delta^2 + \Gamma_L^2)}\right\} \exp\left\{-\frac{(\overline{\omega_0} - \overline{\omega}(t_0))^2}{2\alpha^2(t_0)}\right\} \tag{3.19}$$

Here

$$\overline{\omega}_L = \omega_L - \omega_{eg}, \ \overline{\omega}_0 = \omega_0 - \omega_{eg}, \ \widetilde{\omega} = \overline{\omega}_L \frac{\Delta^2}{\Delta^2 + \Gamma_L^2}, \ \Delta^2 \equiv 2\lambda kT/\hbar, \tag{3.20}$$

$$\overline{\omega}(t) = -2\lambda + e^{-\Lambda t}(\widetilde{\omega} + 2\lambda), \tag{3.21}$$

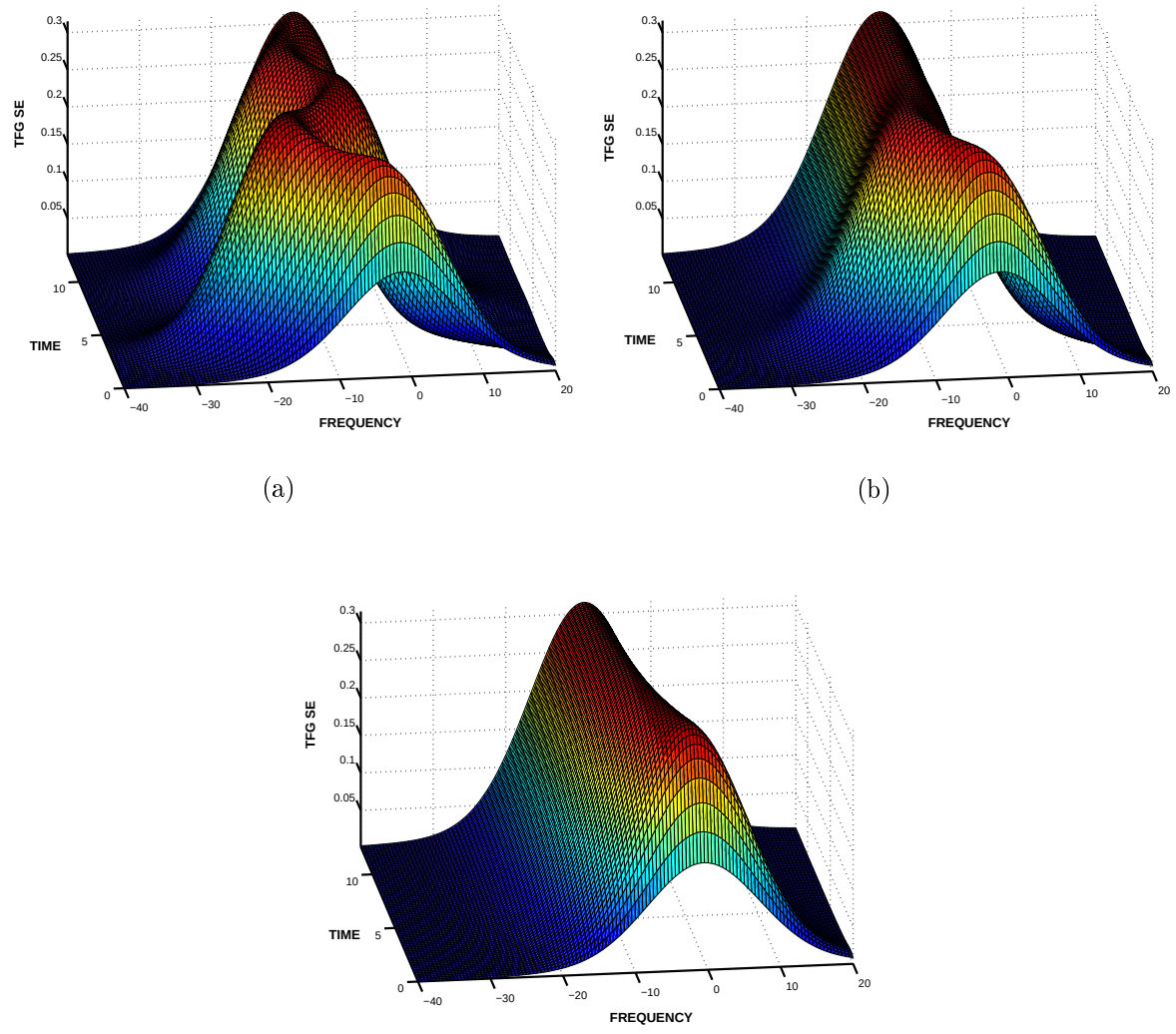

(a) (b)

(c)

Figure 3.2: Manifestation of the dissipation strength in the TFG SE spectrum in the case of satisfactory time and frequency resolution ($\gamma = \Gamma = 1$) for a classical ($\epsilon = 0.1$) displaced ($\lambda = 5$) harmonic oscillator coupled to a Markovian bath. **(a)** $\Lambda = 0.3$ (underdamped oscillator); **(b)** $\Lambda = 1$ (moderately damped oscillator); **(c)** $\Lambda = 5$ (overdamped oscillator).

$$\alpha^2(t) = \Delta^2[1 - \frac{\Delta^2}{\Delta^2 + \Gamma_L^2} e^{-2\Lambda t}] + \Gamma^2; \tag{3.22}$$

$$A = \frac{\Gamma^2\Delta^2(1 - e^{-2\Lambda t})}{\Gamma^2 + \Delta^2(1 - e^{-2\Lambda t})},\ B = \frac{(\overline{\omega}(t) + \omega_{eg})\Gamma^2 + \omega_0\Delta^2(1 - e^{-2\Lambda t})}{\Gamma^2 + \Delta^2(1 - e^{-2\Lambda t})}, \tag{3.23}$$

Eq. (3.21) allows us to visualize the origin of the time-dependent Stokes shift, which is seen to reflect the relaxation of the system towards its equilibrium in the excited state. One should also note the factor $3A^2 + 6AB^2 + B^4$, which ensures a correct description beyond the slowly-varying-envelope approximation (see the pertinent discussion in Sec. 2.2). Evidently, when ω_{eg} exceeds substantially all relevant frequencies of the problem, then $\omega_0 \sim \omega_{eg}$, so that $3A^2 + 6AB^2 + B^4 \approx B^4$, where

$$B \approx \frac{\omega_{eg}\Gamma^2 + \omega_0\Delta^2(1 - e^{-2\Lambda t})}{\Gamma^2 + \Delta^2(1 - e^{-2\Lambda t})}.$$

Therefore, $B \approx \omega_0$, and the standard approximation (2.9) is justified. When the temporal resolution is high compared to the time scale of the inhomogeneous broadening ($\Gamma \gg \Delta$), the additional term also reduces to a constant factor. If this is not the case, the additional contribution depends in a complicated manner on t_0, ω_0 and also on the parameters determining the excitation, the system dynamics and temporal gating. It is important that Eq. (3.19) allows one to determine the influence of the duration of the excitation pulse on the TFG SE signal (see also [1,3,129,131,132]). When the pulse is short ($\Gamma_L \gg 1$), the spectral width $\alpha^2(t) \approx \Delta^2 + \Gamma^2$ is time-independent, so that the TFG SE spectrum experiences no time-dependent broadening. In the opposite case ($\Gamma_L \ll 1$), $\alpha^2(0) < \alpha^2(\infty)$, so that the spectrum broadens. To put it differently, the finiteness of the pump duration results in a time-dependent broadening of $S_t(t_0, \omega_0)$, which is governed by the parameter $\alpha^2(t)$. When the gate pulse is truly instantaneous ($\Gamma \gg 1$), then $\alpha^2(t) \to \infty$ and the TFG spectrum looses any frequency resolution. This is an additional confirmation of the fact that an ideal time gate should be a δ-function on the time scale of the system relaxation, but a constant on the time scale of the optical coherence dephasing.

3.4 Drude oscillator

Now we turn to the study of the impact of memory (or non-Markovian bath) effects on the TFG spectra. To evaluate the importance of these effects, we perform explicit calculations of TFG spectra by invoking the so-called Drude model for $C(t)$ [1,115,127–130], i.e., we consider again a system, consisting of displaced harmonic oscillators in the ground and excited states, which are bilinearly coupled to a thermal *bath with exponential memory kernel*. *Inter alia*, this allows us to explore the influence of non-Markovian effects on the vibrational relaxation. The conventional (Markovian) description is valid provided that the bath relaxation time is much shorter than all other relevant times of the problem. If one studies ultrafast relaxation dynamics, the Markovian assumption should be implemented with caution, since it could be an unjustified oversimplification (see, e.g., recent references [86–92]). There exist also experimental evidences that

non-Markovian effects could be important, e.g., for describing vibrational relaxation in hydrogen-bonded liquids (see Ref. [93] and references therein). These effects manifest themselves through the multi-exponentiality of the energy-gap CF. The Drude model is not limited to weak system-bath coupling. This allows one to continuously follow the transformation of the TFG spectra from the bath-free to the overdamped limit.

3.4.1 Analytic response functions

The Drude model leads to the following expressions for the lineshape functions [127,128]

$$g(t) = g'(t) + ig''(t),\ C(t) = C'(t) + iC''(t), \tag{3.24}$$

$$C'(t) = \lambda(C'_1 e^{-z_1 t} + C'_2 e^{-z_2 t} + C'_3 e^{-z_3 t} - \Gamma(t)), \tag{3.25}$$

$$C''(t) = \lambda(C''_1 e^{-z_1 t} + C''_2 e^{-z_2 t} + C''_3 e^{-z_3 t}). \tag{3.26}$$

Here

$$z_1 = \alpha + i\eta,\ z_2 = \alpha - i\eta,\ z_3 = \delta \tag{3.27}$$

are the roots of the cubic equation

$$z^3 - \omega_D z^2 + (1 + \Lambda\omega_D)z - \omega_D = 0, \tag{3.28}$$

and the other parameters are given by the expressions

$$C''_1 = -\frac{i}{2\eta}\frac{\alpha - i\eta + \delta}{\alpha + i\eta - \delta},\ C''_2 = \frac{i}{2\eta}\frac{\alpha + i\eta + \delta}{\alpha - i\eta - \delta}, \tag{3.29}$$

$$C''_3 = \frac{2\alpha}{(\alpha - i\eta - \delta)(\alpha + i\eta - \delta)},\ C'_i = C''_i \cot(\epsilon z_i), \tag{3.30}$$

$$\Gamma(t) = \frac{2\Lambda\omega_D^2}{\epsilon}\sum_{n=1}^{\infty}\frac{\nu_n e^{-\nu_n t}}{(z_1^2 - \nu_n^2)(z_2^2 - \nu_n^2)(z_3^2 - \nu_n^2)},\ \nu_n = \pi n/\epsilon. \tag{3.31}$$

A new parameter ω_D is responsible for the memory effects: $1/\omega_D$ can be regarded as the bath relaxation time, so that $\omega_D \exp(-\omega_D t)$ is the memory kernel in the corresponding semiclassical generalized Langevin equation for the energy-gap coordinate (see [1,115, 127–130]). When $\omega_D \to \infty$, one recovers the standard Markovian description.

3.4.2 Memory effects

To evaluate the impact of memory effects on the TFG spectra, let us compare Fig. 3.2b and Fig. 3.3, in which $S_{st}(t_0, \omega_0)$ is presented for the Markovian ($\omega_D \to \infty$) and the Brownian (or non-Markovian, $\omega_D = 1$) oscillator, respectively, in the case of moderate coupling with the bath ($\Lambda = 1$). In both situations, $S_{st}(t_0, \omega_0)$ eventually arrives at the relaxed spectrum. However, the manner in which this asymptotic spectrum is approached is very different in the Markovian and non-Markovian cases, respectively. Indeed, after the elapse of a characteristic time of the order of $1/\Lambda$ (this time scale is determined by the strength of the system-bath coupling), the "centers of gravity" of both Markovian and non-Markovian TFG spectra exhibit the same Stokes shift. In the Markovian case, the subsequent relaxation of the spectrum occurs more or less

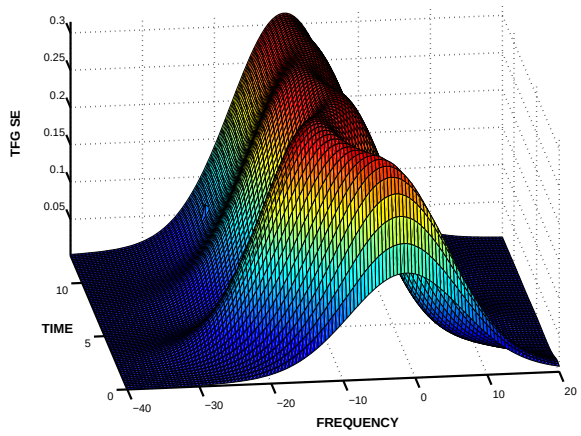

Figure 3.3: TFG SE spectrum in the case of satisfactory time and frequency resolution ($\gamma = \Gamma = 1$) for a classical ($\epsilon = 0.1$) displaced ($\lambda = 5$) harmonic oscillator moderately ($\Lambda = 1$) coupled to a highly non-Markovian bath ($\omega_D = 1$).

monotonically (Fig. 3.2b). When memory effects come into play, the TFG SE signal tends to the relaxed spectrum non-monotonically, its "center of gravity" exhibiting pronounced oscillatory behavior (Fig. 3.3). The TFG SE spectrum of the underdamped Markovian oscillator (Fig. 3.2a) looks qualitatively similar to the spectrum of the moderately damped non-Markovian oscillator (Fig. 3.3). The question therefore arises: is it possible to distinguish between these two situations?

It is Eq. (3.28) which allows one to answer this question. Evidently, the two roots z_1 and z_2 of this equation can be either real and positive (if η in Eq. (3.27) is imaginary), or complex conjugate to each other, with a positive real part (if η is real). The third root z_3 is always real and positive. Clearly, if all roots are positive, the system relaxes to its equilibrium distribution monotonically. This is so, e.g., in the overdamped Markovian case (Fig. 3.2c). If Eq. (3.28) possesses two complex conjugated roots, it is the magnitude of η which determines the fundamental oscillation frequency of the problem. It is possible to derive an analytical expression for η, but it turns out to be cumbersome and difficult to analyze. For our purposes it is sufficient to realize that, in the Markovian limit ($\omega_D \to \infty$), the cubic equation (3.28) reduces to a quadratic equation, yielding $\eta = \sqrt{1 - \Lambda^2/4}$ (recall that the unperturbed oscillator frequency is $\Omega = 1$). On the other hand, one gets a simple solution of Eq. (3.28) in the overdamped ($\Lambda \gg 1$), but strongly non-Markovian ($\omega_D \sim 1$) case: $\eta \approx \sqrt{\Lambda \omega_D}$. So, one arrives at the remarkable conclusion that in the Markovian limit the oscillation frequency η cannot exceed the free oscillator frequency $\Omega = 1$, while in the non-Markovian case it can. To put it differently, the period of the WP oscillations in the Markovian limit can be 2π (free oscillator) or larger (underdamped oscillator), while in the non-Markovian case that period can be less than 2π. This observation allows one to distinguish between the damped non-Markovian and underdamped Markovian oscillators, if one knows the unperturbed oscillator frequency Ω.

These qualitative considerations are illustrated by Fig. 3.4 which shows the comparable top view of the TFG SE spectra of the systems just discussed above: Markovian

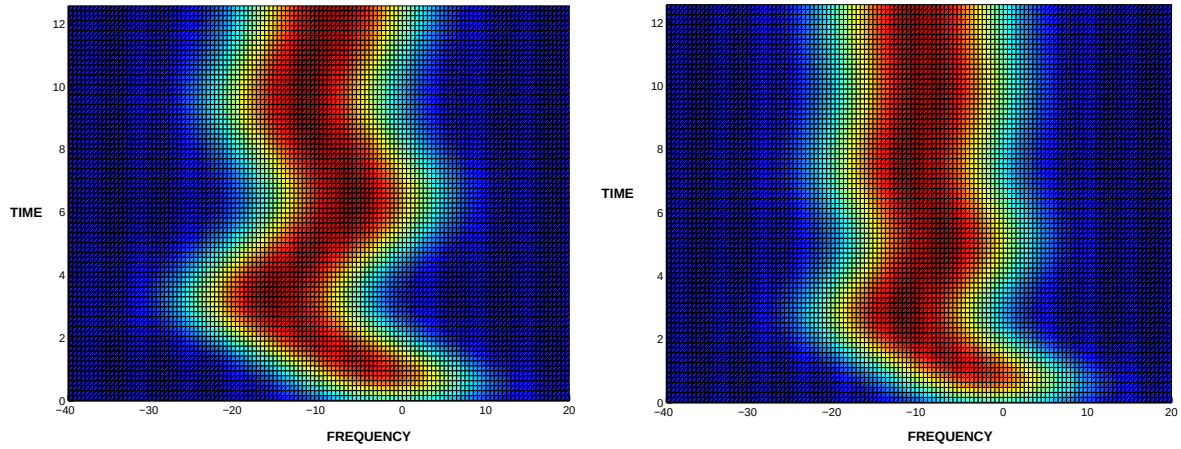

(a) (b)

Figure 3.4: Top view of TFG SE spectrum in the case of satisfactory time and frequency resolution ($\gamma = \Gamma = 1$) for a classical displaced harmonic oscillator ($\epsilon = 0.1$, $\lambda = 5$) moderately ($\Lambda = 1$) coupled to **(a)** Markovian ($\omega_D \to \infty$) and **(b)** highly non-Markovian ($\omega_D = 1$) bath.

(Fig. 3.2b) vs. non-Markovian (Fig. 3.3) oscillators. One can observe the positions of the SE spectra maxima as a function of the gating time t_0. It is seen that the TFG spectra exhibit 7.1 (damped Markovian oscillator) and 4.8 (damped non-Markovian oscillator) periodic oscillations. These are larger and smaller, respectively, than the oscillation period of the corresponding free oscillator (6.3). The message is that the TFG SE signal of a system coupled to a non-Markovian bath can exhibit pronounced oscillations with a period which is less than that of the bath-free system. This qualitative effect can be helpful for the estimation of the importance of memory effects in dissipative systems.

3.5 Summary

Nonlinear response functions have been calculated analytically for the standard benchmark systems: free harmonic, Brownian, and Drude oscillators. These model systems have been adopted to illustrate the time-frequency evolution of the SE spectra for different regimes of dissipation. The TFG SE spectra have been found to be quite sensitive not only to the overall strength of the system-bath coupling, but also to finer features, like memory effects. The influence of the quality of the spectral and temporal filtering on the measured TFG SE spectra also has been studied in some detail.

We have established that the specific features of the WP dynamics in the excited state survive the TFG mapping procedure, and manifest themselves in the SE spectra. Recent TFG SE measurements [7, 21, 22] have confirmed the persistence of pronounced vibrational coherence effects in the spectra. This underlines that the TFG SE clearly reflects the WP dynamics in the excited state, provided a good compromise is found be-

tween temporal and spectral resolution. The information about the material dynamics can be extracted from the TFG SE spectra by an appropriate theoretical analysis.

Additionally, the interpretation of the TFG SE spectra can provide us with a certain knowledge not only on the strength of the system-bath coupling, but also on the bath correlation functions.

Chapter 4

Time-resolved fluorescence of ultrafast electron transfer systems

4.1 Introduction

The doorway-window picture developed in Chapter 2 introduces explicitly the description of the time- and frequency-gating procedure into the theory. Our goal is to establish rigorously the connection of the experimentally measured signals with the underlying microscopic dynamics. In this chapter we study this issue for the case of ultrafast electron transfer systems which, due to a strong nonadiabatic coupling, exhibit ultrafast decay dynamics [2]. The DW-picture is employed here for direct calculations of TFG SE spectra of ultrafast ET systems.

One of the most fundamental questions, which arises when discussing ultrafast ET reactions, is the manifestation of various coherences in the population dynamics and measured responses. It has been shown theoretically that coherent effects in ultrafast ET can be either of vibrational or of electronic nature [51,53,56,94,99–105]. Therefore, it is necessary to distinguish between these two types of coherences when interpreting particular experiments. Excitation of vibrational modes by a short pump pulse with a broad bandwidth results in a coherent superposition of vibrational levels, i.e. in the creation of a vibrational WP in the excited electronic state. Vibrational coherence (VC) effects in ultrafast ET have been studied theoretically with time-dependent WP and RDM techniques (see, e.g., [51,53,56,94,99–101]). These calculations have shown that the WP motion in the excited state manifests itself in the time-dependent population dynamics through characteristic step-like structures. Another conclusion of the theoretical analysis [56,102–105] is that, under certain circumstances, another type of coherence, i.e., electronic coherence (EC), also plays an important role in ultrafast ET. Sufficiently large values of the electronic coupling may result in a coherent electronic motion ("coherent ET") between donor and acceptor states. The effect of EC, if it is present in the system, can be observed as large-amplitude quantum beatings in the population dynamics [56,102–105], which are analogous to the well-known Rabi oscillations in optical physics [133]. Naturally, both EC and VC contribute to the population evolution in the excited state for systems with sufficiently strong electronic coupling and nonstationary preparation. This leads to a complex dynamics with peculiar features, ranging from step-like structures (due to VC) to electronic quantum beats (due

to EC). Recent ultrafast spectroscopic measurements have confirmed the persistence of pronounced coherent effects on a picosecond time scale in the ultrafast ET dynamics for various molecular systems, from diatomics to proteins [6–8, 106–109]. However, when trying to interpret particular experiments, it is not entirely clear if the measured oscillatory patterns are to be attributed to vibrational or electronic coherences. So, it is of considerable importance to clarify (i) which types of coherences are responsible for the excited state dynamics and can, therefore, be observed through TFG SE responses for real systems, and (ii) how to separate the two types of coherences.

A number of papers has appeared in recent years, in which the problem of ultrafast ET has been treated at different levels of sophistication. Of particular relevance to the present consideration are the papers [51, 52, 54, 63, 64, 71, 94–98]. The present work is, in a sense, a generalization of an earlier paper by Jean [52], extending the theory beyond bare time- and frequency-resolved spectra. A limitation of the formulation of the TFG SE signal by Jean is the fact that the influence of the measuring device was not taken into account, which results in "idealized" time- and frequency-resolved spectra. The ideal (or bare) signal is not guaranteed to be positive, however [1, 3]. Moreover, the time and frequency resolution of this ideal spectrum are not limited by the fundamental time-frequency uncertainty principle, as they should be. Our theory shares the general methodology with recent papers by Matro and Cina [95] and Mukamel and collaborators [63, 64] (preparation by a pump pulse of finite duration, explicit consideration of the TFG procedure, RDM description of the nonadiabatic excited-state dynamics within the Redfield theory, the doorway-window formalism). A novel feature of the present work is the consideration of several carefully-selected ET model systems exhibiting electronic coherence and/or vibrational coherence and the systematic exploration of the effects of the preparation and SE detection by pulses of finite duration. In particular, we want to answer the following fundamental question: to which extent is the intrinsic system dynamics reflected by TFG SE spectra?

4.2 Electron transfer model

4.2.1 Hamiltonians

The standard model of an ET system consists of a ground state and two electronically coupled excited donor and acceptor states [134]. The excited states are linearly coupled to a reaction mode (Fig. 4.1), which in turn is weakly coupled to a harmonic bath. In the present context, the general formula (2.53) is specialized as follows: the electronic states and vibrational modes, which are directly involved in the reaction, constitute the relevant system and are described by H^S. The bath degrees of freedom (described by H^B) are only indirectly involved via the system-bath coupling H^{SB}, which is assumed to be weaker than the primary interactions contained in the system Hamiltonian.

We shall restrict ourselves to the consideration of a single-vibrational-mode system Hamiltonian:

$$H_g^S = |g > H_0 < g|, \tag{4.1}$$

$$H_0 = \Omega \left\{ b^\dagger b + 1/2 \right\}, \tag{4.2}$$

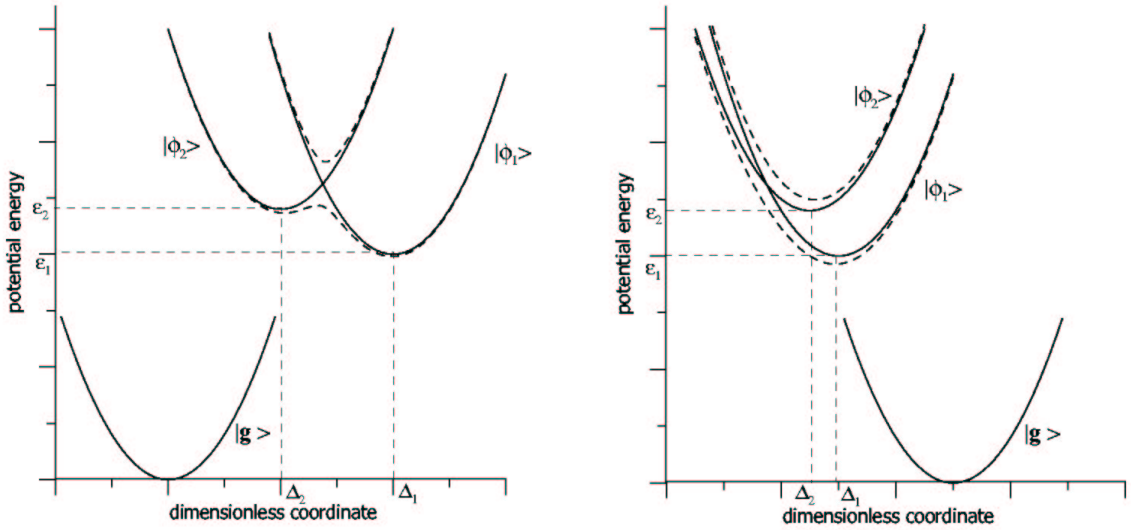

(a) (b)

Figure 4.1: Diabatic (solid) and adiabatic (dashed) potential-energy surfaces for the normal **(a)** and inverted **(b)** regime.

$$H_e^S = \sum_{i=1,2} |\phi_i > (H_i + \varepsilon_i) < \phi_i| + \{|\phi_1 > V_{12} < \phi_2| + H.c.\}, \tag{4.3}$$

$$H_i = \Omega \left\{ b^\dagger b + 1/2 + \frac{\Delta_i}{\sqrt{2}}(b^\dagger + b) \right\}. \tag{4.4}$$

Here $|\phi_2>$ and $|\phi_1>$ label the diabatic donor and acceptor excited electronic states, ε_i are the vertical electronic excitation energies, and V_{12} is the electronic coupling matrix element. The vibrational Hamiltonians, which are written in the second quantization representation, are taken to be harmonic. Ω is the vibrational frequency of this reaction mode (it is assumed to be the same for both electronic states) and Δ_i are the horizontal displacements of the excited-state potentials from the energy minimum of the electronic ground state. It is assumed that the ET takes place between the two excited electronic states, one of which (the donor state $|\phi_2>$) is optically bright, while the second (the acceptor state $|\phi_1>$) is optically dark, so that the transition-dipole operator is $\widehat{V} = V_{eg}\,|g><\phi_2| + H.c.$

A standard assumption is to model the bath by a collection of harmonic oscillators:

$$H^B = \sum_q \omega_q (a_q^\dagger a_q + 1/2). \tag{4.5}$$

We further introduce the simplest approximation for the system-bath interaction, a bilinear system-bath coupling in the RWA [130, 135]:

$$H^{SB} = \sum_q g_q (b^\dagger a_q + b a_q^\dagger). \tag{4.6}$$

The system-bath coupling is assumed to be the same for both electronic states. It is entirely described by the so-called bath spectral function $J(\omega)$. The latter has been taken in the Ohmic form with exponential cutoff [136], viz.,

$$J(\omega) = \eta\omega exp\{-\omega/\omega_c\}. \tag{4.7}$$

Here η is a dimensionless system-bath coupling strength and ω_c is a cutoff frequency.

4.2.2 Equations of motion (Redfield theory)

As has been mentioned earlier, the key quantity describing the relevant system dynamics is the RDM (2.54), which is defined as the trace over all bath variables of the full DM. In this chapter, the RDM $\sigma(t_0)$ is calculated in the framework of Redfield theory, as has been described in detail elsewhere [62]. Assuming sufficiently weak system-bath coupling, the bath degrees of freedom are traced out in the Born and Markov approximations, yielding the Redfield equation of motion for the RDM in the system eigenstate representation [137, 138], so that Eq. (2.54) is written explicitly as follows

$$\frac{\partial\sigma_{\mu\nu}(t)}{\partial t} = -i\omega_{\mu\nu}\sigma_{\mu\nu}(t) + \sum_{\kappa\lambda} R_{\mu\nu\kappa\lambda}\sigma_{\kappa\lambda}(t). \tag{4.8}$$

Here $R_{\kappa\lambda\mu\nu}$ is the relaxation or Redfield tensor. The first term on the right-hand side describes the isolated system evolution, while the second one represents its interaction with the dissipative environment. The Redfield tensor which is responsible for the system relaxation can be expressed as

$$R_{\mu\nu\kappa\lambda} = \Gamma^{+}_{\lambda\nu\mu\kappa} + \Gamma^{-}_{\lambda\nu\mu\kappa} - \delta_{\nu\lambda}\sum_{\alpha}\Gamma^{+}_{\mu\alpha\alpha\kappa} - \delta_{\mu\kappa}\sum_{\alpha}\Gamma^{-}_{\lambda\alpha\alpha\nu} \tag{4.9}$$

where

$$\Gamma^{+}_{\lambda\nu\mu\kappa} = \int_0^\infty dt \left\langle \langle\lambda| H^{SB}(t) |\nu\rangle \langle\mu| H^{SB} |\kappa\rangle \right\rangle_B e^{-i\omega_{\mu\kappa}t}, \tag{4.10}$$

$$\Gamma^{-}_{\lambda\nu\mu\kappa} = \int_0^\infty dt \left\langle \langle\lambda| H^{SB} |\nu\rangle \langle\mu| H^{SB}(t) |\kappa\rangle \right\rangle_B e^{-i\omega_{\lambda\nu}t}, \tag{4.11}$$

$$H^{SB}(t) = e^{iH^B t} H^{SB} e^{-iH^B t}, \tag{4.12}$$

and $\langle ... \rangle_B$ denotes the thermal average over the bath. For the Hamiltonians defined above, the Redfield tensor components can be expressed in closed form [56, 62].

Eqs. (4.8)-(4.12) [Redfield equations of motion] together with Eqs. (2.45)-(2.47) [TFG SE spectrum] are utilized to calculate TFG SE signals for the ET system according to a general scheme given in Section 2.5. We remark that in the present chapter, a fourth-order Runge-Kutta scheme [139] has been employed for the numerical time propagation over a time interval t_0 according to the Redfield equations (4.8)-(4.12).

4.3 Specific examples and discussion

4.3.1 Integral signal

To reveal the connection between the electronic population dynamics and spectroscopic measurements, we consider the frequency-integrated signal

$$I(t_0) = \int_{-\infty}^{\infty} d\omega_0 \, S_{st}(t_0, \omega_0) = Tr\{\widetilde{W}\sigma(t_0)\}, \tag{4.13}$$

where

$$\widetilde{W} = \int_{-\infty}^{\infty} d\omega_0 \, W(\omega_0) \tag{4.14}$$

is the frequency-integrated W operator. Evidently, the integral signal is equivalent to the TFG SE signal in the limit of poor frequency resolution ($\gamma \to \infty$) [111]. In terms of the system eigenstates [78]:

$$\widetilde{W}_{\alpha\beta} \sim < \alpha|\phi_2 >< \phi_2|\beta > \frac{4\Gamma^2}{4\Gamma^2 + \omega_{\alpha\beta}^2} = \sum_n V_{\alpha n} V_{n\beta} \frac{4\Gamma^2}{4\Gamma^2 + \omega_{\alpha\beta}^2}. \tag{4.15}$$

It is further useful to consider separately the limiting cases of good ($\Gamma \to \infty$) and poor ($\Gamma \to 0$) temporal resolution. If the gate pulses are short enough ($\Gamma \to \infty$), then $\widetilde{W} = |\phi_2\rangle \langle\phi_2|$ and

$$I(t_0) = \sum_{\alpha,\beta} \sigma_{\alpha\beta}(t_0) \; < \alpha|\phi_2 >< \phi_2|\beta >= Tr[|\phi_2 >< \phi_2| \, \sigma(t_0)] = P_2(t_0). \tag{4.16}$$

The integral signal is thus nothing else than the time-dependent population $P_2(t_0)$ of the diabatic donor state $|\phi_2>$. The fact that in the ideal limit of ultrashort pulses the integral fluorescence signal is equivalent to the diabatic population of the optically bright electronic state has been established earlier by Meyer and Koeppel [140] and for the integral pump-probe signal by Domcke and Stock [114, 141].

If the gate pulses are longer than any relevant timescale of the system dynamics ($\Gamma \to 0$), then

$$\frac{4\Gamma^2}{4\Gamma^2 + \omega_{\alpha\beta}^2} = \delta_{\alpha\beta}, \tag{4.17}$$

so that

$$I(t_0) = \sum_{\alpha} \sigma_{\alpha\alpha}(t_0) \; < \alpha|\phi_2 >^2 . \tag{4.18}$$

In the system-eigenstate representation, the difference between these two limits becomes transparent. For poor temporal resolution ($\Gamma = 0$), the signal is simply the weighted sum of populations $\sigma_{\alpha\alpha}$ (see Eq. (4.18)), while the perfectly time-resolved signal contains the contributions from both coherences $\sigma_{\alpha\beta}$ ($\alpha \neq \beta$) and populations $\sigma_{\alpha\alpha}$ (see Eq. (4.16)). Thus, the comparison of the signals for good and poor temporal resolution allows one to reveal the importance of coherences in the RDM.

When there is no coupling between the excited electronic states (and thus no ET), the integral signal is simply proportional to the constant (time-independent) population

of the bright state, irrespective of the time resolution [141]. The nonadiabatic coupling is therefore responsible for the time dependence of the population and the evolution of the integral optical signal. Alternatively, non-Condon effects in adiabatic systems also result in a time dependence of the integral fluorescence signal [7, 141, 142].

To learn about the interrelation between the integral signal and the population dynamics, we present below the results of explicit calculations. The system-bath interaction is described by the spectral function (4.7) with $\omega_c = \Omega$. The bath is assumed to be in equilibrium at zero temperature to emphasize quantum tunneling effects. We begin with the consideration of the effect of temporal resolution. To render the presentation more transparent, we separate the influence of the gate-pulse duration from that of the pump pulse, restricting ourselves initially to the case of impulsive excitation. In other words, the system is instantaneously excited from the ground electronic state to the donor ($|\phi_2>$) electronic state. The preparation is referred to as stationary, if there is no shift between the equilibrium configurations of the ground and excited electronic states, and as nonstationary otherwise.

4.3.2 Electronic coherence in electron transfer

We start from the consideration of an ET system in the so-called normal regime (Fig. 4.1a). The system parameters have been taken from [56]: $\Omega = 0.05\,\text{eV}$, $\Delta_1 = 3.5$, $\Delta_2 = 0$ (stationary preparation), $\varepsilon_0 = 0$ eV, $\varepsilon_1 = 1.455$ eV, $\varepsilon_2 = 1.5$ eV (the minimum of the potential surface for the donor state is higher than that for the acceptor state) and $V_{12} = \Omega$ (strong electronic coupling). The coupling to the bath is assumed to be rather weak ($\eta = 0.1$).

The donor-state population dynamics for this system is given by curve 1 in Fig. 4.2a. This particular system (stationary preparation and strong electronic coupling) is a good example for the observation of EC in the ET reaction. Since no horizontal shift is assumed between the minima of the $|g>$ and $|\phi_2>$ energy surfaces, the vibrational effects (in particular, VC) are of minor importance. The large-amplitude quantum beatings in the population dynamics reflect the presence of EC. Indeed, sufficiently large values of electronic coupling can result in coherent electronic motion ("coherent ET") between the donor and acceptor electronic states. These beatings are analogous to the well-known Rabi oscillations in optical physics.

The fast oscillations in curve 1 of Fig. 4.2a arise from the peculiarities of the initial preparation. Indeed, the WP is put at $t_0 = 0$ into the unperturbed ($V_{12} = 0$) ground vibrational state of $|\phi_2>$. However, because of the strong electronic coupling, this initial vibrational state deviates significantly from the eigenstates of the distorted adiabatic potential.

Fig. 4.2a shows the integral signals calculated for this system, assuming four different time resolutions, varying from good ($\Gamma = 2\Omega$) to poor ($\Gamma = \Omega/100$). The calculations show that for good temporal resolution (up to $\Gamma = 2\Omega$) the integral signal follows the diabatic population of the donor state. In Fig. 4.2a, the corresponding kinetics are undistinguishable from that given by curve 1: they reproduce all the features of the population dynamics, even the fast oscillations of vibrational origin. The equivalence of integral signal and population dynamics is a direct consequence of the theoretical analysis discussed above.

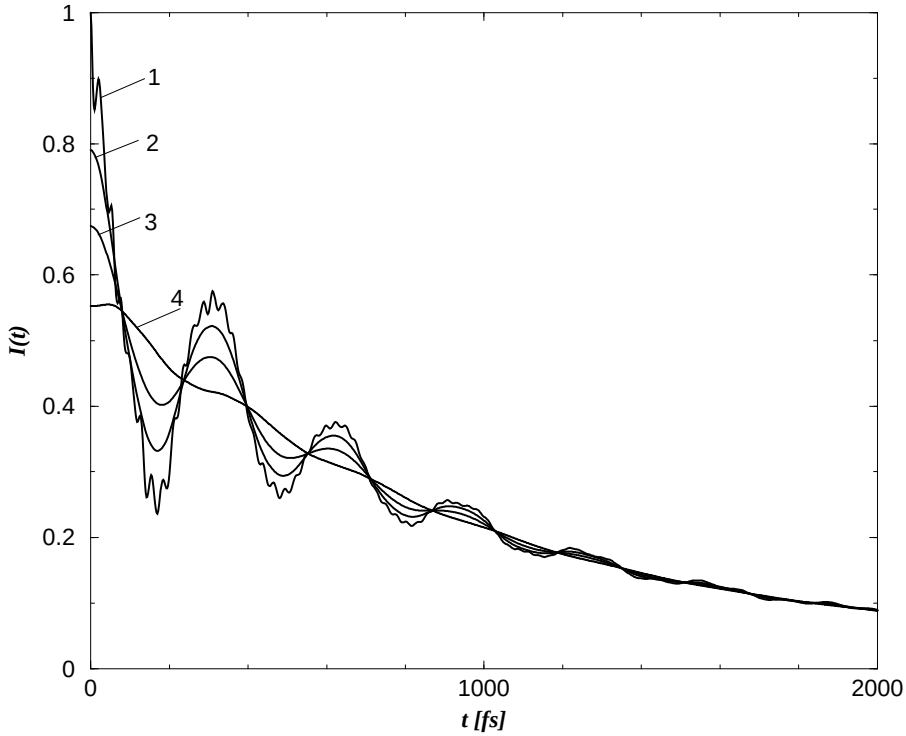

(a)

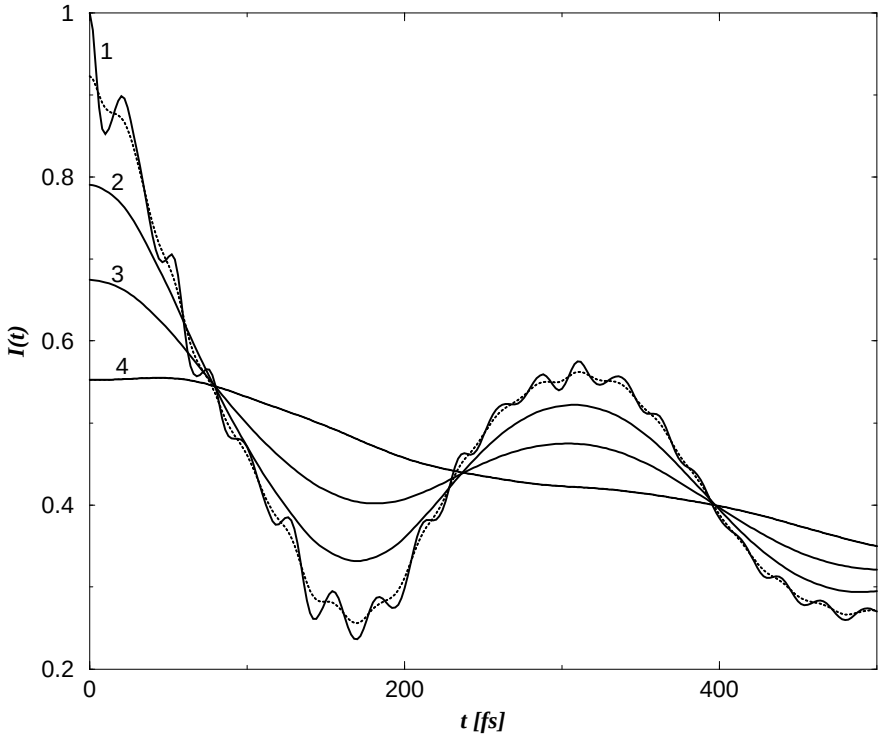

(b)

Figure 4.2: **(a)** Influence of the temporal resolution on the integral SE signal of a model ET system (normal regime, stationary preparation, strong electronic coupling) exhibiting EC: **1** : $\Gamma > 2\Omega$ (population dynamics); **2** : $\Gamma = \Omega/5$; **3** : $\Gamma = \Omega/10$; **4** : $\Gamma = \Omega/100$. **(b)** Same as in Fig. 4.2a, but for the first 500 fs. The additional dotted line corresponds to $\Gamma = \Omega$.

With decreasing Γ, the integral signal becomes smoother, but, as expected, the electronic beatings are seen in curves 2 and 3 in Fig. 4.2a ($\Gamma = \Omega/5$ and $\Gamma = \Omega/10$, respectively). Finally, when we take really poor time resolution (curve 4, $\Gamma = \Omega/100$), which corresponds to a gate pulse which is much longer than the timescale of EC, we loose the electronic beatings in the signal. For such long gate pulses, the time resolution becomes inadequate to resolve the quantum beats in the population dynamics. It is noteworthy that the smoothing of integral signal with decreasing temporal resolution looks like a time-averaging process: all the curves in Fig. 2a pass through the same intersection points. For poor resolution ($1/\Gamma$ larger than the timescale of EC) the fast system dynamics can not be resolved and one measures only the time-averaged signal, describing the rate process of the population decay from the donor to acceptor state.

Clearly, the temporal resolution $\Gamma = \Omega$ (when the gate pulse is of the order of the vibrational period) is critical for the observation of the fast-oscillating vibrational structure, originating from the peculiarities of the initial preparation. The corresponding signal is given by the dotted line in Fig. 4.2b, which shows in detail the early-time part (first 500 fs) of the the population dynamics and fluorescence signals presented in Fig. 4.2a. When $\Gamma = \Omega$, the vibrational oscillations in the integral signal disappear, but the signal still exhibits the same electronic oscillations as in the case of high temporal resolution. Although the value of the electronic coupling is equal to the vibrational frequency in this example, the period of these electronic beatings is much longer than $1/\Omega$. The explanation of this seemingly puzzling fact is simple: $V_{12} = \Omega$ does not mean that the characteristic timescale of the EC is of the order of $1/\Omega$. The frequency of the electronic quantum beats is rather determined by the electronic coupling matrix element, renormalized by the Frank-Condon overlap integral of the relevant vibrational wave functions of the diabatic potentials. One can estimate this timescale from Fig. 4.2 as $\sim$ 400 fs. Taking into account that the vibrational period corresponding to $\Omega = 0.05$ eV is $T_{vib} = 83$ fs, one can expect that electronic oscillations in the integral signal can be seen up to values $\Gamma \sim \Omega/5$. This conclusion is confirmed by the results of our calculations (see Fig. 4.2a).

This example gives a clear confirmation of our qualitative considerations on the integral signal (see discussion above). In Fig. 4.2a, the signal corresponding to good resolution (curve 1) shows contributions from both populations and coherences, while in the case of poor time resolution, the coherences are no longer present in the signal which simply reflects monotonous population decay. All curves have the same long-time decay, giving the ET rate which is independent of temporal resolution. As expected, the difference between the highly and poorly time-resolved signals is important on short timescales (when coherences are not yet destroyed). For instance, with decreasing time-resolution the absolute value of the integral signal at $t = 0$ is significantly less than 1.

The discussed model system is a good example for the observation of EC in ET. We conclude that the very existence of electronic beatings for the present ET system can be observed with gate pulses as long as $1/\Gamma = 10/\Omega \approx 830$ fs. Therefore it seems that the temporal resolution is not a critical parameter for the observation of EC; the necessary temporal resolution can be easily achieved with pulses available nowadays. Nevertheless, to the knowledge of the authors, electronic population oscillations of the type shown in Fig. 4.2a have not yet been observed in real systems. The quantum beats

observed so far in femtosecond time-resolved pump-probe and fluorescence signals for numerous ET systems appear to be of vibrational origin [6, 108]. An experiment which was especially designed to detect EC in ET has failed [106]. In real systems, extremely short (of the order of several femtoseconds) dephasing times are the most important obstacle for the observation of the EC. In the ET model system discussed here, the dephasing time was long enough to allow the observation of EC at a timescale of the order of 1 ps.

There might be another possible reason for the failure of the above-mentioned attempt to detect EC in ET. The amplitude of the EC effect is extremely sensitive to the choice of system parameters, especially the initial preparation and the electronic coupling strength. It is therefore not unlikely that for a particular molecule and for a particular configuration of experiment, EC effects are not present at all.

4.3.3 Vibrational coherence in electron transfer

Next we consider again an ET system in the normal regime (Fig. 4.1a), but two important system parameters are taken different from the previous case: $V_{12} = \Omega/5$ (weak electronic coupling) and $\Delta_1 = 5.5$, $\Delta_2 = 2$ [56]. This choice corresponds to nonstationary preparation, that is, there is a shift between the equilibrium configurations of the ground and donor electronic states. Due to the weak electronic coupling, the EC is strongly suppressed, but a new effect, VC, shows up as a consequence of the nonstationary preparation. The instantaneous excitation results in the preparation of a WP in the excited electronic state which subsequently performs coherent vibrational motion. As can be seen from Fig. 4.1a, the mean energy of the initial WP lies above the energy of the crossing point of the diabatic potentials, that is, the crossing point is accessible for the moving WP.

The population dynamics for this system calculated via Redfield theory is given by curve 1 in Fig. 4.3a. It exhibits a peculiar and easily interpretable behavior, reflecting the combined effect of vibrational WP dynamics in the donor state and ET, namely a step-like decay of donor-state diabatic population $P_2(t_0)$. Obviously, due to the presence of electronic coupling, a fraction of the WP is transferred to the acceptor state each time the moving WP hits the crossing region (at $t_0 = 2\pi n/\Omega,\ n = 1, 2, ...$). The characteristic stepwise structure thus reflects this ultrafast ET process driven by coherent WP motion, which is quenched after $\sim$ 500 fs due to vibrational damping. After the WP motion is relaxed, the donor-state population exhibits a monotonous decay, analogous to the long-time decay in the case of stationary preparation in Fig. 4.2. Similar step-like population behaviors at short times and bimodal decay curves have been obtained by several authors [100, 143–145] and also observed experimentally [7, 109]. These features appear to be generic for ultrafast ET dynamics with nonstationary preparation for systems with a single or few system vibrational modes.

Now we proceed to the discussion of the integral signals calculated for this system with different time resolutions, ranging from good ($\Gamma = 2\Omega$) to poor ($\Gamma = \Omega/50$). Fig. 4.3a shows the overall behavior, while Fig. 4.3b gives a detailed picture of the short-time dynamics. The main point is the criterion for the observation of the characteristic steps in the integral signal. Qualitatively, the influence of the time resolution is very similar to that established in the previous case (Fig. 4.2). For good temporal resolution

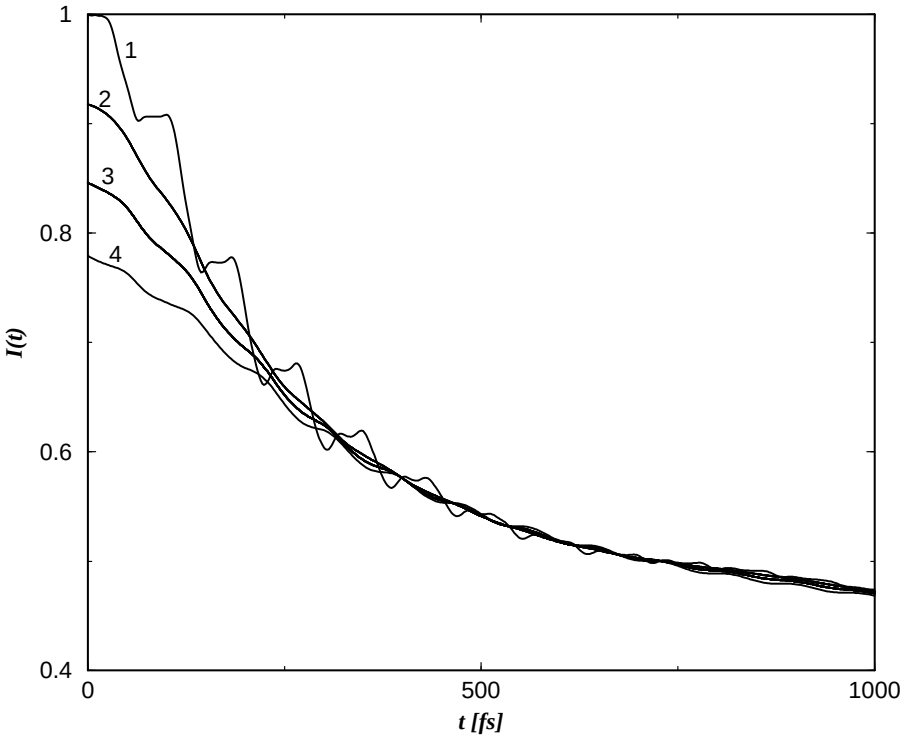

(a)

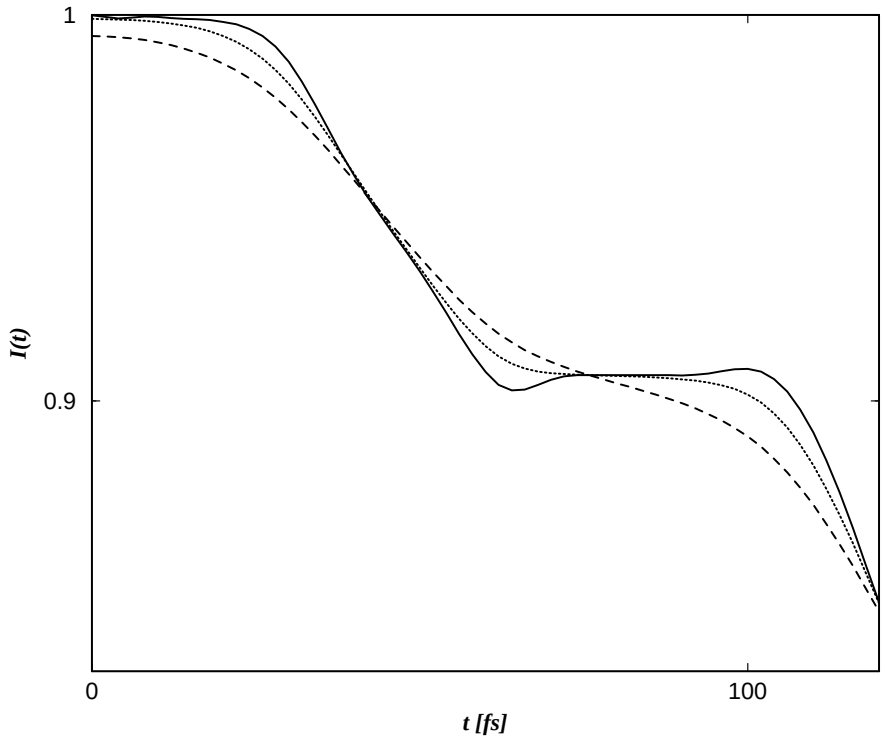

(b)

Figure 4.3: **(a)** Influence of temporal resolution on the integral SE signal of a model ET system (normal regime, nonstationary preparation, weak electronic coupling) exhibiting VC. **1** : $\Gamma > 2\Omega$ (population dynamics); **2** : $\Gamma = \Omega/10$; **3** : $\Gamma = \Omega/20$; **4** : $\Gamma = \Omega/50$. **(b)** Same as in Fig. 4.3a, but for the first 130 fs; solid line : $\Gamma > 2\Omega$; dotted line : $\Gamma = \Omega$; dashed line : $\Gamma = \Omega/2$.

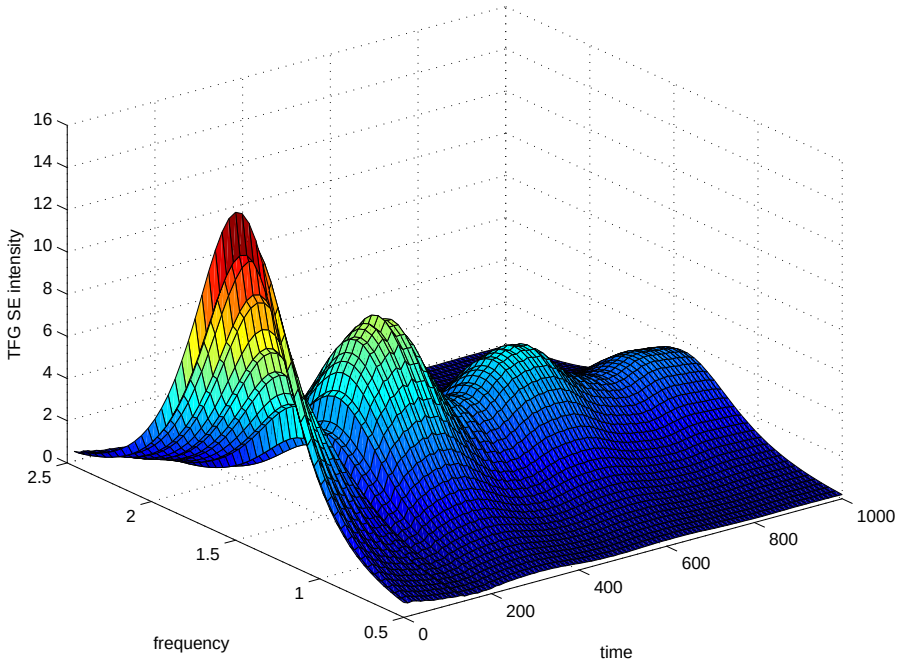

Figure 4.4: TFG SE spectrum of the ET system exhibiting EC in the case of good time and frequency resolution.

(up to $\Gamma = 2\Omega$), the integral signal coincides with the population dynamics (curve 1 in Fig. 4.3a and solid line in Fig. 4.3b); the time resolution $\Gamma = \Omega$ (dotted line in Fig. 4.3b) is at the border line for the observation of steps; for slightly worse temporal resolution (dashed line in Fig. 4.3b, corresponding to $\Gamma = \Omega/2$) the steps are washed out in the integral signal. If one further decreases the temporal resolution (curves 2-4 in Fig. 4.3a, corresponding to the temporal resolution $\Gamma = \Omega/10$, $\Gamma = \Omega/20$, and $\Gamma = \Omega/50$, respectively) the gate pulse averages out all characteristic features of the system dynamics, resulting in a smooth decay curve. The rate of the long-time exponential decay is independent of the temporal resolution. On the contrary, the short time (up to 500 fs) behavior of the signals depends significantly on the time resolution, because the coherences are not yet destroyed. In contrast to the EC, the timescale of the VC is determined by the system vibrational period, $T_{vib} = 83$ fs. Thus the timescale of the VC is much shorter than that of the EC (~ 400 fs) in our system. Therefore the characteristic features of VC disappear faster with decreasing time resolution than in the previous case. For example, a time resolution $\Gamma = \Omega/10$ is still enough to observe the EC (Fig. 4.2), while for the VC (Fig. 4.3) this is already beyond the limit of resolution.

4.3.4 Time- and frequency-gated spontaneous emission spectra

Experimentally, a TFG SE spectrum can be constructed from the data for a range of times between the excitation pulse and the gate pulse, and a range of frequency windows determined by the spectral filter. In this section we present 3D TFG spectra

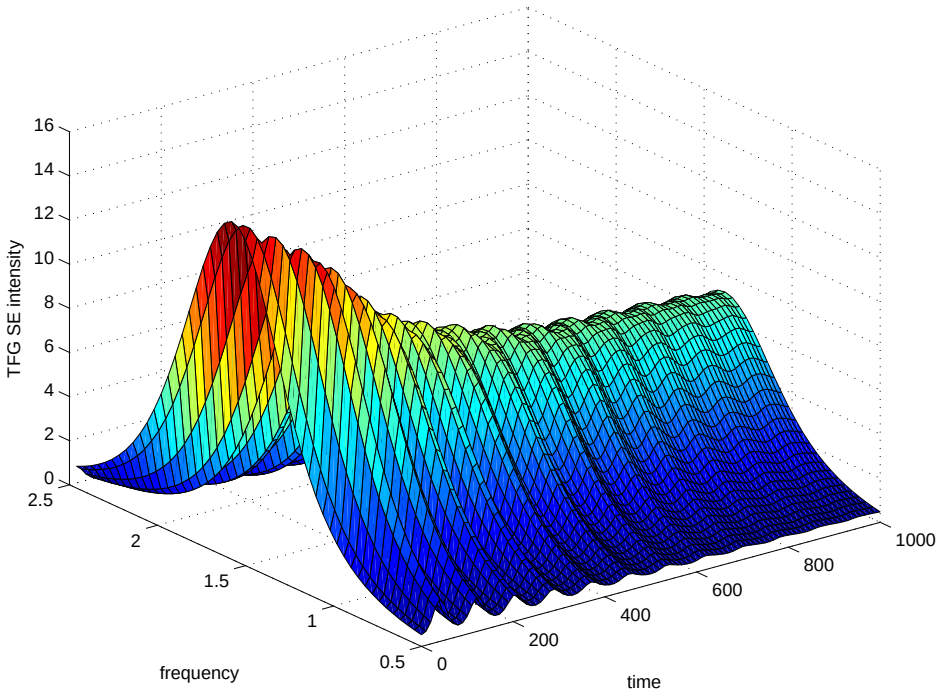

(a)

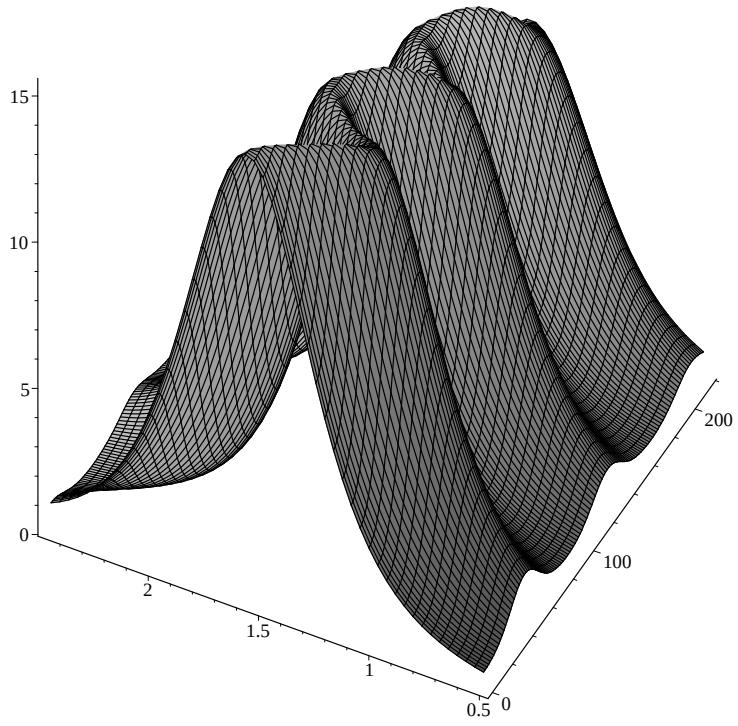

(b)

Figure 4.5: **(a)** TFG SE spectrum of the ET system exhibiting VC in the case of good time and frequency resolution. **(b)** Same as in Fig. 4.5a, but for the first two vibrational periods ($\sim$ 200 fs).

calculated using Eq. (2.57) for the systems considered in detail in a previous section. To primarily concentrate on the dynamic effects, a perfect time ($\Gamma = 10\Omega$) and frequency ($\gamma = \Omega/20$) resolution has been chosen for all calculations.

The TFG SE spectrum for the ET system with EC (system considered in Sec. 4.3.2) is presented in Fig. 4.4. The spectrum, as a function of time, qualitatively reflects the electronic population dynamics: one can clearly see the large-amplitude electronic beatings mirroring coherent ET as well as the fast oscillations due to peculiarities of the initial preparation. Cuts of the spectrum at fixed frequencies, i.e. the transients which are usually measured experimentally, in general, have very different behavior. For example, the cut at the frequency close to 0-0 transition reproduces the population dynamics almost quantitatively, while the cuts at the wings of the spectrum give a qualitatively different behavior (compare with [114, 141]). Therefore, the problem of a theoretical reproduction of experimental 3D TFG SE spectra is quite demanding, because one must achieve a coincidence for all particular frequency cuts. In turn, this imposes restrictions on the choice of system parameters. Ideally, this would help one to fit the system parameters in a unique way.

As a function of frequency, on the other hand, the TFG spectrum at $t_0 = 0$ represents the SE of the initially prepared nonequilibrium excited state. Later on, at every time moment t_0 , it represents the time evolution of the fluorescence spectrum. The area under the instantaneous spectra $S(\omega_0, t_0)$ decreases with time, reflecting the decay of the population in the donor electronic state. In the limit $t_0 \to \infty$, the TFG SE spectrum is nothing else than the relaxed fluorescence spectrum [111]. For the ET system under consideration, the donor state population tends towards zero for $t_0 \to \infty$; therefore, there is no relaxed fluorescence.

The TFG SE spectrum for the ET model with VC (system considered in Sec. 4.3.3) is depicted in Fig. 4.5a. Again, the time evolution of the signal monitors the ET dynamics: we can see the steps occurring in the donor-state population. In addition, the signal, as a function of frequency, maps directly the periodic vibrational WP motion in the excited state. To show this explicitly, the TFG SE signal is displayed in Fig. 4.5b during the first two periods. The time evolution of the spectrum within each step reminds us of that of the Brownian oscillator (see Sec. 3.3) [1, 111]. The WP exhibits quasiperiodic behavior, moving between classical turning points, where the local maxima of the peak-shift occur. If the temporal and spectral resolutions are good enough, the intensity and the shape of the spectrum do not change within each step (compare with Fig. 3.1c, where the TFG spectrum is given for a Brownian oscillator). Every time the WP comes to the crossing point of the two diabatic potentials, part of it leaks to the acceptor state, producing a step in the electronic population. Thus, the crossing point can indeed be regarded as a "sink", as it is assumed in Zusman-type models of ET [146]. This picture does not apply, on the other hand, to the description of the dynamics of the ET system with EC (Figures 4.2, 4.4), because the population dynamics in that case is not monotonous, but quasiperiodic, and cannot be described by an effective "sink".

Summarizing, both electronic and vibrational coherences contribute to the population dynamics for ultrafast ET systems. If short enough pulses are employed, both types of coherences manifest themselves in the measured TFG SE spectra. Moreover, TFG SE spectra provide us with more information on the system dynamics than

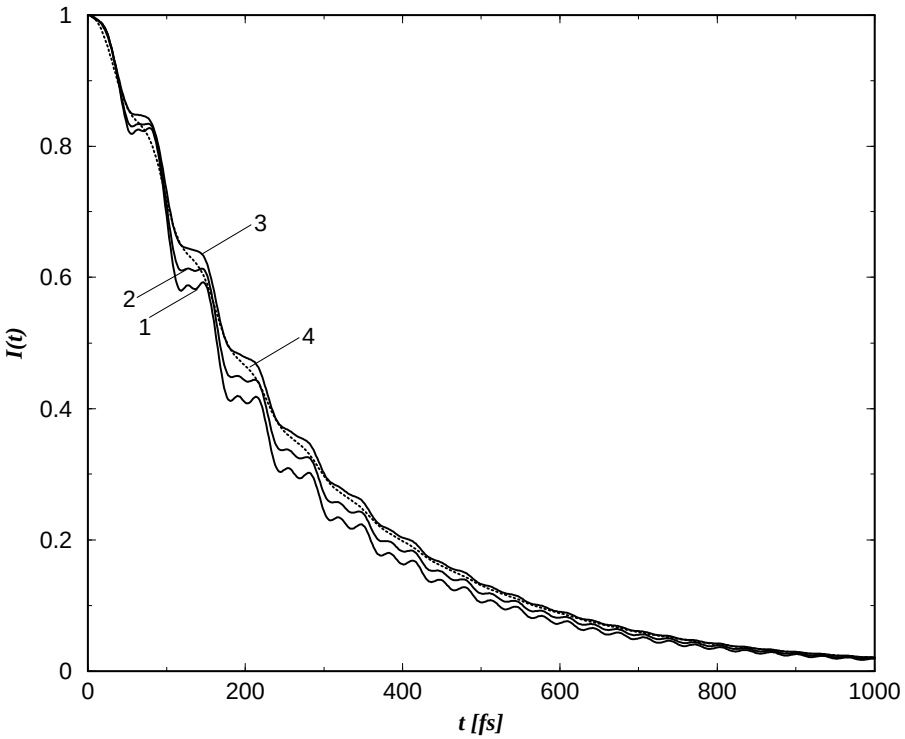

Figure 4.6: Influence of pump-pulse duration on the integral SE signal of a ET system in the inverted regime. **1** : $\Gamma_L = 10\Omega$; **2** : $\Gamma_L = 3\Omega$; **3** : $\Gamma_L = \Omega$; **4** (dotted line): $\Gamma_L = \Omega/10$.

frequency-averaged time-resolved signals or the conventional stationary fluorescence spectrum. In fact, the TFG SE signal $S(\omega_0, t_0)$ gives the actual spectral shape (e.g., Gaussian, Lorentzian, or more complicated) and shows directly the evolution of the fluorescence spectrum with time. It is thus very useful for a detailed understanding of the system dynamics.

4.3.5 Finite pump duration

Finally, we study briefly another aspect of ultrafast time-resolved spectroscopy: the effect of the system preparation by a pump pulse of finite duration. Evidently, the amount of vibrational energy and coherence initially deposited into the system is determined by the temporal and spectral properties of the excitation pulse. To separate the effect of the pump-pulse duration from that of the time-gate duration considered in Sec. 4.3.2-3, a good temporal resolution of the gate pulse ($\Gamma = 2\Omega$) is assumed in the following.

In order to analyze different scenarios of ultrafast ET within the present model, we consider a system in the so-called inverted regime. The potential-energy surfaces are given in Fig. 4.1b, and the system parameters are taken as follows [56]: $\Omega = 0.064\,eV$, $\Delta_1 = -0.8281$, $\Delta_2 = -2$, $V_{12} = 0.1\,eV$, and $\varepsilon_0 = 0$ eV, $\varepsilon_1 = 2.8741$ eV, $\varepsilon_2 = 3$ eV, $\eta = 0.4219$.

The integral signals calculated for this ET system prepared by pump pulses of different duration are plotted in Fig. 4.6. The pump pulse is described by Eq. (2.3),

so that the time-integrated intensity is kept fixed when the pulse duration is varied. The signals, on the other hand, are normalized to unity at $t_0 = 0$, i.e., $I(0) = 1$. The problem of normalization deserves further clarification. If one considers unnormalized signals calculated according to Eq. (4.13), one finds that the shorter the pump pulse, the larger is the absolute value of the signal. (This fact was well established earlier for the pump-probe spectroscopy [2].) Indeed, short pump pulses have a broad bandwidth and can excite coherently many vibrational levels, so that ET occurs from a number of initially excited levels. A long pump pulse, on the other hand, excites only a few vibrational levels, which results in a significant decrease of the absolute value of the integral signal. This must be contrasted to the time-resolution effect of the gate (Fig. 4.2). In that case, the smaller initial values of $I(t_0)$ are the result of the detection procedure: long gate pulses average over the population dynamics.

Keeping this in mind, we are in a position to analyze the dependence of the integral signal on the duration of the pump pulse (see Fig. 4.6). The effect of pump-pulse duration qualitatively looks very similar to the effect of time resolution of the gate: the step-like structure reflecting WP motion can be well detected with short pump pulses (curves 1 and 2, which correspond to $\Gamma_L = 10\Omega$, $\Gamma_L = 3\Omega$ respectively). The pump-pulse duration of the order of the vibrational period (curve 3, $\Gamma_L = \Omega$) is the critical one: the characteristic effects of coherent vibrational motion are nearly wiped out in the integral signal. For longer pump pulses (curve 4, $\Gamma_L = \Omega/10$), the system is prepared in such a way that no features of vibrational coherence can be detected, although the time resolution of the gate is sufficient to detect them.

To monitor the microscopic features of the ET dynamics in a TFG SE experiment, one must thus employ sufficiently short pump pulses to excite coherently a significant part of the vibrational levels. What is less intuitive, the structures of the integral signal are as sensitive to the pump-pulse duration as to the gate-pulse duration. To detect the mode-specific step-like structure in ultrafast spectroscopic signals of ET process, the pump-pulse duration as well as the gate-pulse duration must be shorter than the vibrational period.

4.4 Summary

We have presented the application of the theory of TFG SE signals to nontrivial examples: ultrafast ET processes. The TFG as well as frequency-integrated SE signals have been calculated for various durations of the pump and gate pulse. Our main findings can be summarized as follows.

The integral signal obtained with sufficiently short gate pulses (i.e. good temporal resolution) reflects most directly the donor-state diabatic population. If the temporal resolution decreases, system-specific features are wiped out, and the signal simply reflects monotonous decay of the population of the donor state. In the system eigenstate representation, the difference between these two limits becomes transparent. For poor time resolution, the signal is simply the weighted sum of populations $\sigma_{\alpha\alpha}$ (Eq. (4.18)), while the perfectly-resolved signal contains the contributions from both coherences $\sigma_{\alpha\beta}$ ($\alpha \neq \beta$) and populations $\sigma_{\alpha\alpha}$ (Eq. (4.16)). Thus the comparison of the signals obtained with good and poor temporal resolution allows one to estimate the importance

of coherence effects in the system dynamics. The difference between the two limits is pronounced on short timescales (when coherences are not yet destroyed). The rate of the long-time decay (ET rate) is independent of the temporal resolution.

The effect of optical preparation by pump pulses of finite duration is qualitatively similar to that of temporal resolution of the gate pulse. To monitor the mode-specific features of the ET dynamics in a TFG SE experiment, one must employ sufficiently short pump pulses to excite coherently a significant part of vibrational levels. To detect the characteristic step-like structure in ultrafast spectroscopic signals, the pump-pulse duration as well as the gate-pulse duration must be shorter than the vibrational period.

To elucidate the effect of various coherences on SE signals, we have performed simulations for ET models in which either EC or VC effects are dominant. For the observation of electronic quantum beats, the time resolution of the gate must be of the order of or shorter than the electronic beating period. Provided the time-gate duration is of the order of a vibrational period or shorter, VCs were shown to manifest themselves through the characteristic step-like structures in the electronic population. It should be noted that the prediction of such peculiar step-like structures is not limited to the case of weak system-bath coupling, which is described by Redfield theory. They manifest themselves in the population dynamics also in calculations carried out beyond this limit [145, 147, 148].

Both types of coherences can show up in measured TFG SE spectra. The TFG SE spectrum $S(\omega_0, t_0)$ as a function of time qualitatively reflects the electronic population dynamics: either electronic beatings reflecting EC or the steps occurring in the donor-state population due to VC. In addition, the frequency-dependent TFG spectrum at $t_0 = 0$ represents the SE of the initially prepared nonequilibrium excited state. Later on, at every time moment t_0 it gives the development of this fluorescence spectrum. Most importantly, the time- and frequency-resolved signal maps directly the periodic vibrational WP motion in the excited state. TFG SE spectra provide us therefore with more information on the system dynamics than frequency-averaged time-resolved signals or the conventional stationary fluorescence spectrum.

To summarize, the influence of the measuring devices (the pump pulse for preparation and the gate pulse for detection) is significant and must be accurately taken into account. The presented results illustrate the relation between the "pure" (intrinsic) dynamics of ET systems (e.g., the time-dependent electronic population dynamics) and "real" experimental observables. This aspect is new in comparison with the investigations of Jean [52]. We hope that the methods developed in this chapter may prove useful for the interpretation of TFG SE experiments on ultrafast ET systems exhibiting coherent responses.

Chapter 5

Application: time-resolved fluorescence of the TCNE-HMB complex

5.1 Introduction

There are several systems for which coherent oscillatory behavior has been observed in SE signals. These include oxazine dye molecules [30], the sodium dimer [17–20], the light-harvesting antenna of purple bacteria mutants [149], the reaction center of purple bacteria [25], and the photoactive yellow protein [28]. Here we consider vibrational coherences in a system with medium complexity: the electron donor-acceptor (EDA) complex tetracyanoethylene-hexamethylbenzene (TCNE-HMB).

This system is a member of a group of complexes, the theoretical description of which is owed to the pioneering work on ET by Mulliken and others [150]. A main feature of EDA complexes is the appearance of a new absorption band (the charge transfer (CT) band) when two molecules form a complex; the optical transition to this band causes a charge separation. It is well established that the ground state of such a complex is weakly bound and only slightly polar, whereas the electronically excited state that absorbs in the visible region involves the transfer of an electron from the donor to the acceptor. Upon photoexcitation to the CT band of a "weak" EDA complex, an electron is transferred from the HOMO orbital located mainly on the donor to the LUMO orbital located mainly on the acceptor molecule [150, 151]. So the absorption of a photon is accompanied by the electron transfer from a donor to an acceptor.

TCNE-HMB system is well suited for a theoretical analysis of the CT process: on the one hand, it exhibits coherent responses in ultrafast time-resolved fluorescence signals [7, 21, 110]; on the other hand, this ET system is one of the most intensively theoretically studied EDA complexes [71, 150–154].

5.1.1 Experiments

Early studies of resonance Raman profiles and the near-infrared fluorescence spectrum [155,156] of TCNE-HMB have identified spectroscopically active vibrational modes and

have provided their initial assignment [152, 153].

Recently, the dynamics of ultrafast ET in this EDA complex has been studied by different time-resolved methods [7, 21, 110, 157, 158]. Although TCNE-HMB is formed by relatively large organic molecules with many inter- and intramolecular vibrational modes, a VC in a single vibrational mode manifests itself in this complex: underdamped oscillatory responses with only one dominant frequency have been clearly observed at an ultrafast time scale via pump-probe and time-resolved fluorescence spectroscopy. In the transient absorption experiment by Hochstrasser's group [157, 158] an oscillation with the frequency of 162 cm^{-1} excited by impulsive stimulated Raman scattering was observed in a bleach recovery signal; the oscillation was assigned to a vibration in the ground state. The time-resolved spectra measured by Rubtsov and Yoshihara [7,21,110] showed quantum beats of 159 cm^{-1} with an ultrafast decay component. As spontaneous fluorescence reflects only the excited-state properties, the oscillation in this case results from a coherent vibration in the excited electronic state of the complex.

Oscillatory signals with very similar oscillation frequencies have been observed in three types of experiments (resonance Raman, transient absorption, and time-resolved fluorescence) and for complexes with different donors and a common acceptor [21]. This has lead to the conclusion that an intramolecular acceptor mode is responsible for the observed oscillations. In particular, it has been assigned to the out-of-plane bending mode of acceptor [21].

5.1.2 Previous simulations and theoretical interpretations

There have been several theoretical efforts to understand and explain the origin of the observed oscillations [152,153,155,157]. Despite of a certain progress, there still remain some discrepancies in previous studies regarding the spectral modeling and dynamics of this complex:

- different groups (Myers and co-workers [155,156], and Hochstrasser's group [157, 158]) reported back electron-transfer rates which differ by a factor of 3-8.
- Myers' group [155, 156] derived a solvent reorganization energy which is about 2 orders of magnitude larger than that predicted by classical continuum theory.
- Hochstrasser and collaborators [157, 158] had to assume a large displacement for the electronically excited potential surface along the coordinate of the 165 cm^{-1} mode (increasing the displacements of Myers' by 23%) and had to change the 0-0 energy gap from 11 600 cm^{-1}, which was obtained by Myers' group as 13 860 cm^{-1}, in order to fit the observed absorption spectrum.

To resolve these discrepancies, Hayashi and Lin investigated this complex theoretically [71, 154]. First, they performed ab initio molecular orbital (MO) calculations and identified all vibrational modes of the electronic ground state [154]. Based on the results of MO calculations, they have proposed a new theoretical model consisting of the ground state and two excited CT states (CT1 and CT2) having a small energy gap. Absorption occurs from the ground state to both CT states. CT2 non-radiatively relaxes to CT1 which undergoes a transition to the ground state via both back electron

transfer and emission of fluorescence light. Using this model and the results of previous experiments, they have been able to reproduce the experimental stationary absorption and fluorescence spectra of the TCNE-HMB complex in CCl_4 [154].

In subsequent work, these authors tried to simulate the time-resolved experiments, in particular, to describe both spectral features and ultrafast dynamics of the TCNE-HMB complex [71]. For this purpose, they have adopted a simple model consisting of the three above mentioned electronic states and a single vibrational mode (which is equivalent to our ET model system in the normal regime, Fig. 4.1a). The pump pulse excites the system into CT state. The ultrafast dynamics takes place between CT1 and CT2 manifolds. For the system dynamics calculation they used the RDM formalism including explicitly vibrational relaxation and dephasing of optical coherences. They analyzed the femtosecond time-resolved pump-probe and fluorescence signals on the basis of this single-mode model. They roughly estimated the vibrational relaxation and dephasing rate constant for the CT1 and CT2 states. But there are still several problems which deserve further investigation:

- the quality of their fits is only "semi-qualitative" [71].
- they did not take into account the finite duration of the gate pulse, i.e. there is no analog of the window function in their formalism.
- they have considered only one time-dependent transient from several available experimental ones; they did not discuss the integrated signal and the TFG signal.
- There are some inconsistencies in their theory and interpretation of the experiment. They identify two processes: (i) fast exponential decay due to vibrational relaxation (if photon has an excess energy, that is its frequency is larger than 0-0 energy, then the fast relaxation starts) and (ii) oscillations due to the following two mechanisms: modulation of transition frequency or modulation of transition dipole moment (non-Condon effect). This is a very important point: the nature of ultrafast initial dynamics is attributed to vibrational relaxation, but not to nonadiabatic electronic coupling. We propose a "more economic" model which does not require some of these additional assumptions.

5.1.3 Our goals

With the theory developed in this thesis, we are in the position to develop an improved analysis of the experimental time-resolved fluorescence signals measured in [7, 21, 110]. Our particular goals are:

- to calculate (i) the time- and frequency-resolved (3D) fluorescence signal; (ii) the cuts (or slices) of the general TFG SE spectrum at different wavelengths presented in experimental papers [7, 21, 110]; (iii) the frequency-integrated fluorescence signal.
- to give a consistent interpretation of the experiments in the framework of a model involving one relevant system mode. Nonadiabatic coupling (without non-Condon effects) is sufficient to reproduce (at least qualitatively) all the observed features.

- to consider explicitly the effect of the time resolution (gate pulse duration) introducing the window function into theory.

- to systematically study the effect of different system parameters (in particular, the role of nonadiabatic coupling) on the signal.

5.2 Computational details

The plan outlined in Sec. 2.5 is realized here to describe the above mentioned experiments. We have developed a model involving three (ground and two nonadiabatically coupled excited) electronic states and a single reaction mode (see Fig. 4.1a). As the starting point, we take the results of ab initio MO calculations [154] (for the system parameters) and the data from [21,110] (for the experimental parameters). The model parameters producing the best fit are obtained from the simulation. We have studied the effect of the following parameters on the signal:

1) System parameters
Part of the system parameters, namely, the oscillator frequency Ω, the vertical energy shifts (ε_1, ε_2), and the horizontal displacements (Δ_1, Δ_2) have been kept fixed since these are the results of ab initio calculations. We have checked, furthermore, that small changes of these parameters had a little effect on the signals. This allowed us to reduce the number of variable parameters.

Hayashi and Lin [71,154] give the value of 1/3 for the ratio of electronic dipole moments of the CT1 and CT2 states from the fit of absorption spectrum. We have shown that the introduction of the second partially bright state ($\mu_{10} = \mu_{20}/3$) into the doorway and window functions only slightly changes the signal. The point is that a horizontal shift of CT1 is smaller, than that of CT2, the corresponding Franck-Condon factors are also smaller, and they are additionally divided by 3. So further we assume that the CT1 state is dark. In that case, moreover, the integral signal is directly related to the diabatic population (if the second state is partially bright, it is not so).

The remaining system parameter, the nonadiabatic electronic coupling V_{12}, is shown to influence drastically the signal behavior. In our theory, it is the most important parameter which is responsible for the ultrafast dynamics.

2) Relaxation parameters
We have introduced dissipation effects within the Redfield formalism (see Section 4.2.2) and studied the influence of the system-bath coupling on the signals.

In order to achieve an agreement between the experimental transients and calculated signals, we have introduced an additional optical dephasing Γ_{deph} into the doorway and window functions (Eqs. (2.46), (2.47)). That parameter controls the "lifetime" of the optical coherence. In the window function this results in a redefined frequency filter (Eq. (2.4)) with $\widetilde{\gamma} = \gamma + \Gamma_{deph}$. In general, the introduction of optical dephasing leads to the qualitatively expected effect: when increasing Γ_{deph} , the amplitude of oscillations becomes smaller; more precisely, the oscillations minima shift up and maxima remain in their positions.

3) Experimental parameters
We have found very little effect of the time resolution (Γ) on the signals: our model represents a single vibrational mode with a period which is well resolved with the pulses used in the experiments. Indeed, $40 \div 55$ fs corresponds to $\Gamma = 4 \div 5\,\Omega$. This is within the good resolution limit, as has already been discussed in detail in Chapter 4. So the experimental TFG spectrum is close to an ideal (snapshot) one.

The temperature effect is also not big but observable when changing from finite (fixed to 300 K in the experiments) to zero temperature. For higher temperatures, more vibrational states are populated which results in more smoothed signals.

Best-fit parameters of the model
We obtained the best fit of the experimental results with the following set of parameters:

- oscillator frequency $\Omega = 160$ cm^{-1}, vertical excitation energies $\varepsilon_1 = 13910$ cm^{-1}, $\varepsilon_2 = 14310$ cm^{-1}, horizontal displacements $\Delta_1 = -1.28$, $\Delta_2 = 1.57$,
- nonadiabatic coupling $V_{12} = 49$ cm^{-1} $= 0.3\Omega$,
- electronic transition dipole moment of CT1 state $\mu_{10} = 0$,
- temperature $T = 300$ K,
- pump pulse central frequency $\omega_L = 15748$ cm^{-1}, pulse durations: $\Gamma_L = 5\Omega$ for the pump and $\Gamma = 5\Omega$ for the gate pulse,
- cutoff frequency $\omega_c = \Omega$, system-bath coupling strength $\eta = 0.45$,
- optical dephasing rate $\Gamma_{deph} = \Omega$.

5.3 Results and interpretations

The time-resolved fluorescence signals are calculated for the model developed above. To perform the explicit comparison with the experimental signals, we start with a detailed analysis of particular cuts.

5.3.1 Cut at $\lambda = 774$ nm

Figure 5.1 demonstrates the calculated time-resolved signal at $\lambda = 774$ nm (which corresponds to $\omega_0 = 13405$ cm^{-1}), as well as the experimental signal reported by Rubtsov and Yoshihara [21]. It is seen that we can qualitatively reproduce the main effects contained in the experimental signal (and semiquantitatively the signal itself): the oscillatory behavior and the overall decay. Moreover, since the experimental time resolution is quite good (pulses are short), we can achieve rather good agreement even at short times (overlapping-pulse effects are not contained in the calculations). The theoretical and experimental cuts differ in the vicinity of $t_0 = 200$ fs where the calculated signal exaggerates oscillatory features. A more detailed discussion of this discrepancy is given below. Here we just note that, according to our assumptions, some

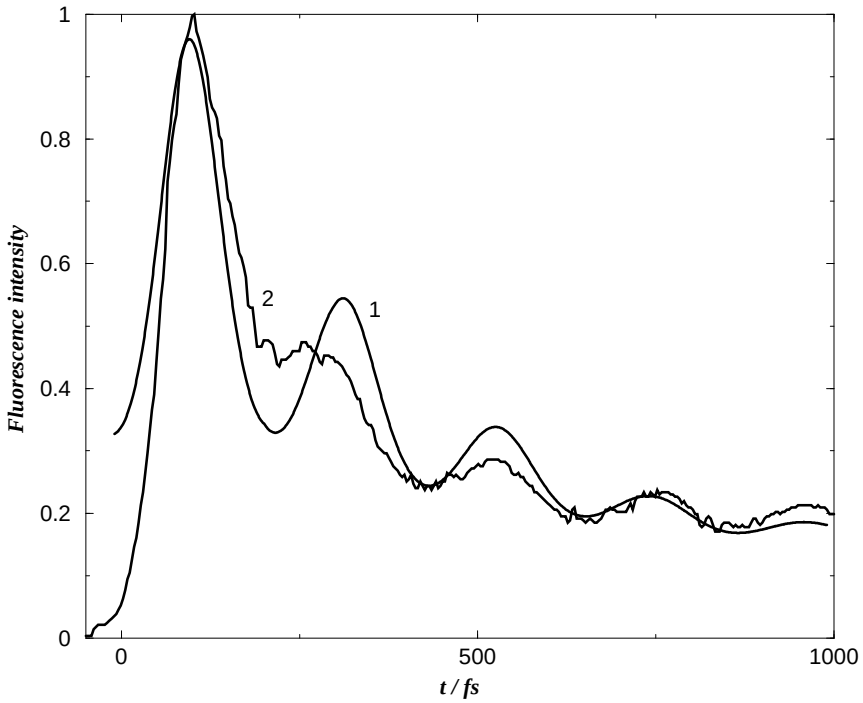

Figure 5.1: Cut at $\lambda = 774$ nm. **1** - calculated, **2** - experimental (taken from [21]).

dephasing effects, which are the consequence of the multimode nature of the system under study, are not taken into account in the present model. To arrive at a more quantitative agreement, one may add to the single optically active mode (which is treated within the Redfield formalism) one (or several) other system modes.

The system under study provides us with a typical example of an electron-transfer system with vibrational coherence. The model parameters determined above [moderate nonadiabatic electronic coupling, a significant shift between the minima of the ground and excited electronic states, and an excess energy of $\sim 9\Omega$ provided by the short pump pulse] allow the creation of a vibrational wave packet in the excited state. The oscillations in the signal (Fig. 5.1) cannot be interpreted as a signature of EC: these oscillations appear in the time cut at a fixed frequency, but not in the integral signal. As will be shown below, the integral signal has a characteristic step-like behavior, reflecting a WP motion in the excited electronic state. The oscillations in the cut (Fig. 5.1) reflect the same effect but in a different way: the maxima correspond to the steps in the integral signal. Obviously, due to the presence of an electronic coupling, a fraction of the WP is transferred to the acceptor state each time the moving WP hits the crossing region (at $t_0 = 2\pi n/\Omega$, $n = 1, 2, ...$), i.e., when the system tunnels to a (dark) acceptor state, producing an abrupt loss of the amplitude in the cut at a given frequency.

5.3.2 Peak-shift

As another check of our simulations, we have calculated the peak shift of the fluorescence signal. The time-behavior of the peak position of the SE spectrum $\nu_{max}(t)$ is shown in Fig. 5.2b (to highlight the shift, the y-axis origin is chosen as $\nu_{max}(0)$).

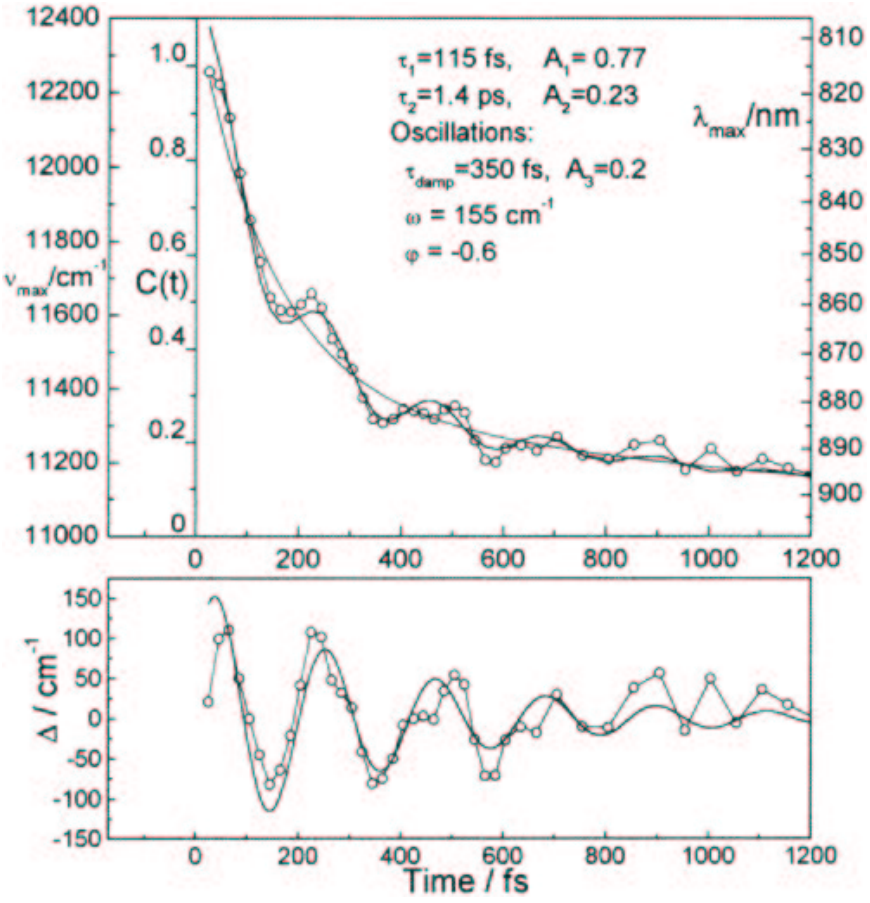

(a)

Maximum of fluorescence spectrum $\nu(t)$ time behavior. The normalized spectral shift correlation function $C(t) = [\nu(t) - \nu(\infty)]/[\nu(0) - \nu(\infty)]$ is shown as additional Y axis. The oscillating component determined as a difference between experimental data and fit with eq 1 where the oscillating component was set to zero is shown at the bottom.

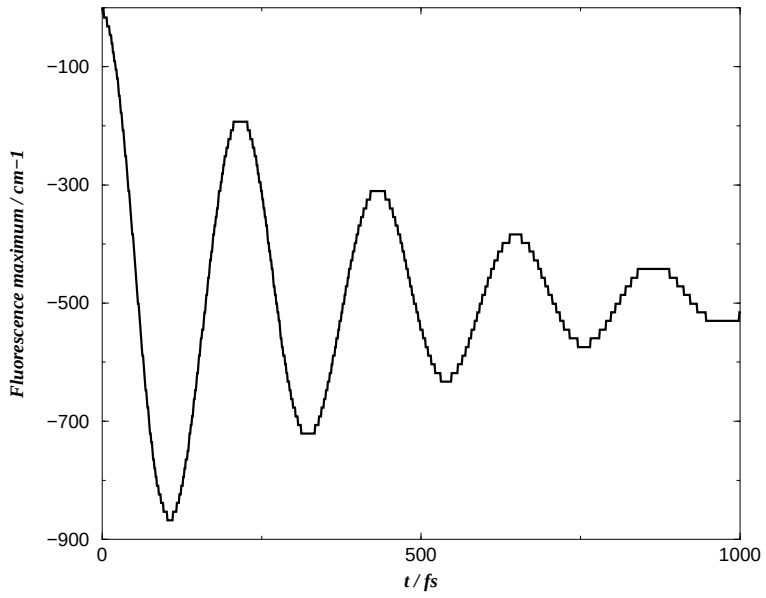

(b)

Figure 5.2: Peak shift. **(a)** - experimental (taken from [21]), **(b)** - calculated.

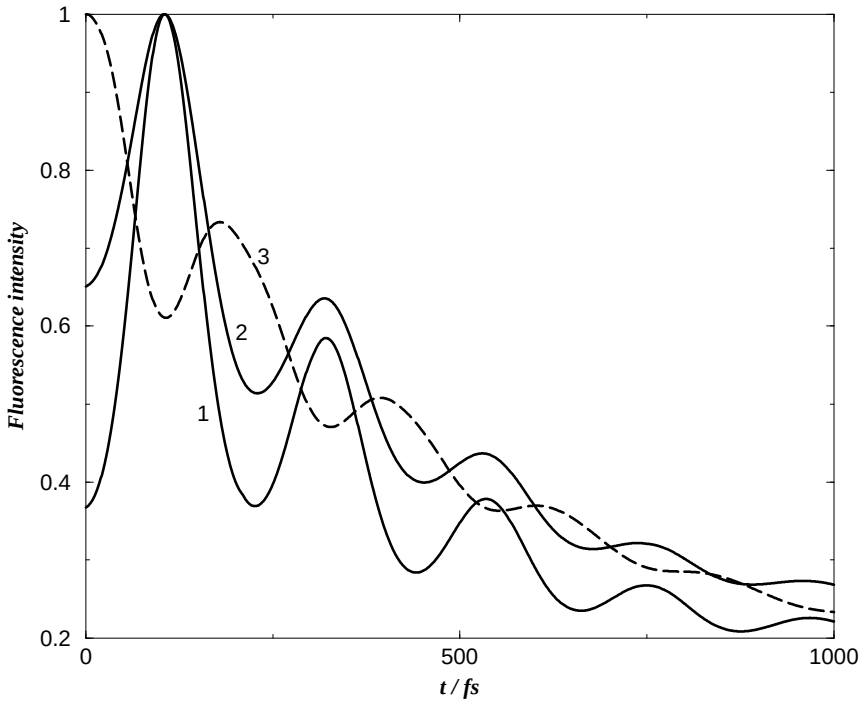

Figure 5.3: Comparison of several cuts (normalized). **1** - cut at 774 nm, **2** - cut at 907 nm, **3** (dashed line) - cut at 660 nm. All the curves are normalized to their maxima.

For comparison, the experimental results (figure 2 from [21]) are given in Fig. 5.2a. The experimental peak-shift consists of an oscillatory (which is given separately in the lower panel of Fig. 5.2a) and an exponential part. The model reproduces very well the weakly damped oscillatory part of the peak shift: the spectral position of the fluorescence is oscillating due to WP motion in the excited state of the complex. But the model does not describe the large Stokes shift of 1400 cm^{-1}. This reflects the fact that our single-mode model does not take into account other system modes and, what is more important, solvent modes, which contribute to the overall shift of the SE spectrum. The model may be improved by including an additional overdamped or solvation coordinate.

5.3.3 Comparison of several cuts

With the present model, we can predict cuts of the fluorescence signal at any detection frequency. The phase of the oscillations is better observed when all the cuts are normalized to their maxima, see Fig. 5.3 , showing cuts at 774, 907 and 660 nm. Unfortunately, all experimental cuts have been measured to the red side from the vertical transition. In this case, the different transients show no observable phase shift. To demonstrate the existence of this effect, an additional time-transient for the detection wavelength 660 nm, which is to the blue side from the vertical transition, is shown in Fig. 5.3 (dashed line). The transients taken at different sides of the vertical excitation energy clearly show a phase shift of π which can be understood from WP motion: these cuts have their maxima when the WP reaches the corresponding turning points.

When the cuts are not normalized to their maximum values, other effects can be

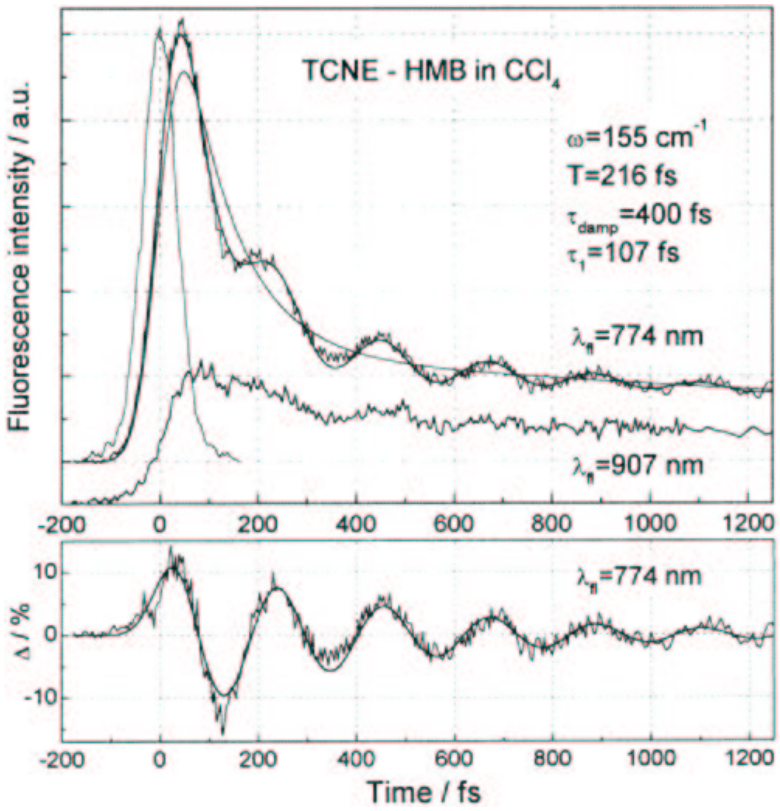

(a)

Fluorescence decays of the TCNE-HMB complex in CCl_4 at 774 and 907 nm. The best fit of convolution of f(t) function with instrument response function is shown. Instrument response function of 85 fs (fwhm) used for the convolution is also shown. The oscillatory component for the signal at 774 nm is emphasized separately at the bottom.

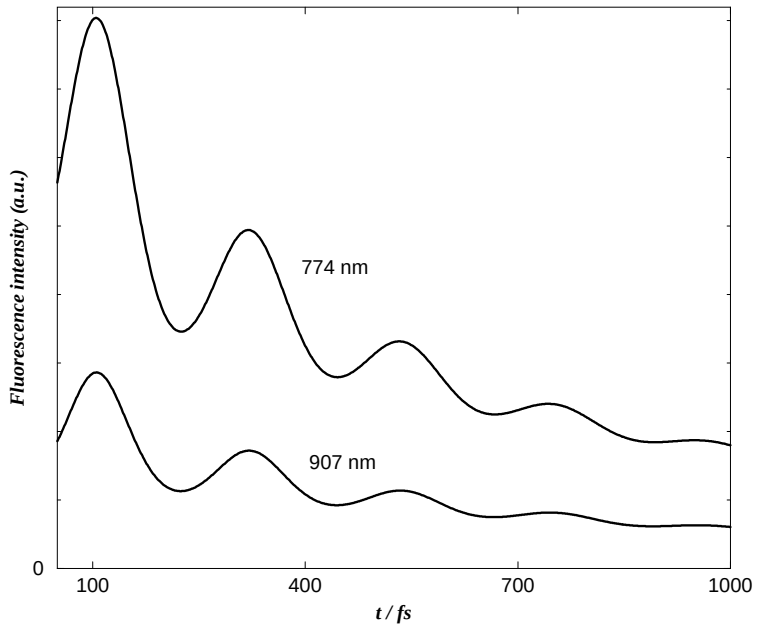

(b)

Figure 5.4: Comparison of several cuts (unnormalized). **(a)** - experimental (taken from [21]); **(b)** - calculated.

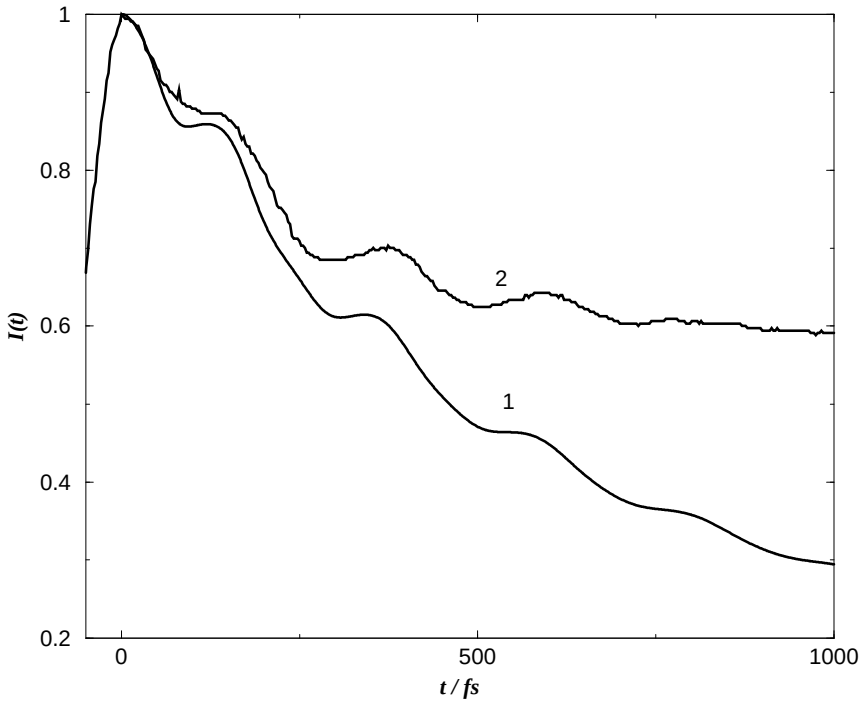

Figure 5.5: Frequency-integrated fluorescence signal. **1** - calculated, **2** - experimental (taken from [21]).

extracted. In Fig. 5.4b two different cuts are shown: at 774 nm (which we have fitted above) and at 907 nm (which is near the red tail of the spectrum); the corresponding experimental signals (figure 3 from [21]) are given in Fig. 5.4a. It is seen that for detection wavelengths which are closer to the vertical transition the signal amplitude is larger. Our simulation nearly reproduces the ratio of the amplitudes of these two experimental cuts (e.g., 1/3 for the ratio of the first maxima). On the other hand, our model does not reproduce another effect observable in the experimental transients: at the red tail of the spectrum, the long-time limit of the experimental signal is higher, which indicates that the overall decay is very slow. In our model the decay is approximately the same for all frequencies (compare the normalized cuts 1 and 2 in Fig. 5.3).

5.3.4 Integral signal

The developed model correctly reproduces general behaviors and trends in the experimental cuts measured at different detection wavelengths. We proceed next to the discussion of the frequency-integrated fluorescence signal. The signal, calculated with the set of model parameters determined above, is given in Fig. 5.5, along with the experimental one. Both of them show the characteristic step-like behavior which is typical for ET systems with VC (compare, e.g., with Fig. 4.3). There are several factors which determine the dynamics of the ET process, among which the most important are the nonadiabatic electronic coupling and the dissipation strength. Our explanation and those of others [21, 154] agree in that the steps (oscillations) in the signal are due to WP motion and that their period is determined by the oscillator frequency Ω. How-

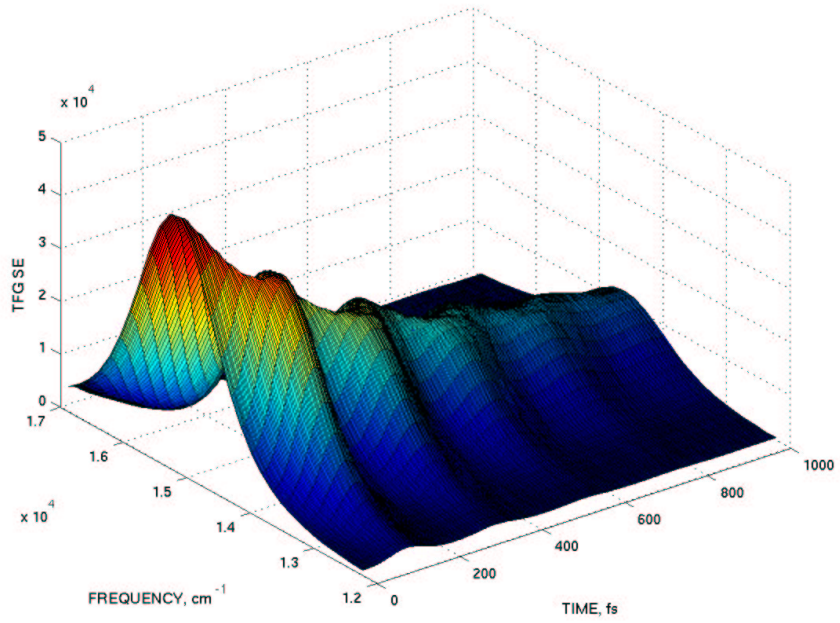

Figure 5.6: TFG SE spectrum of the TCNE-HMB complex.

ever, the explanations differ in an important point: the nature of the ultrafast initial dynamics. Rubtsov and Yoshihara [7, 21, 110] give an explanation in terms of vibrational relaxation, while in our model the short-time dynamics is mostly determined by the nonadiabatic electronic coupling. Moreover, we do not need to invoke non-Condon effects (as Rubtsov and Yoshihara did) to explain the coherent oscillations. (Actually, a WP moving between the dark and bright states is, in a sense, a non-Condon effect.)

Fig. 5.5 shows significant deviations of the calculated integral signal (curve 1) from the experimental one (curve 2). Two sets of the experimental data, i.e. the cuts and the frequency-integrated signal, can not simultaneously be fitted (even semi-qualitatively) within our model. Roughly speaking, the experimental cuts decay to 0.2 in 1000 fs and $I(t)$ decays to 0.6 during the same time. In contrast, the two types of signals calculated within our model exhibit nearly the same long-time decay: when making a reasonable fit of the cuts (see above), the integral signal also decays to 0.2 in 1000 fs, which is much below the corresponding experimental signal. Different decay rates for the integral signal and cuts could be, in principle, due to the effect of nonadiabatic coupling or due to brightness of the second state. For example, for the limiting situations $V_{12} = 0$ or $\mu_{10} = \mu_{20}$, one gets $I(t) \equiv 1$, irrespective of the system-bath coupling. But a variation of V_{12} and μ_{10} (within the limits which give a reasonable fit of the cuts) is shown to result in no substantial improvements of the quality of the fit of the integral signal. This may indicate that our model need be extended (see several suggestions in the next section). However, we must mention another possible reason for the different decay rates for the cuts and $I(t)$. The experimental frequency-integrated signal is not very reliable, since it has been constructed on the basis of only 5-6 points in the spectrum, while the cuts at fixed wavelengths are very accurate [159]. Therefore in the

experimental determination of the integral signal, part of the spectrum may have been missed. This could lead to an underestimated decay rate of the experimental $I(t)$.

5.3.5 Time-resolved fluorescence spectrum

The TFG SE spectrum as a function of both detection frequency and delay time, calculated for the TCNE-HMB complex, is shown in Fig. 5.6. We see that it is very similar to Fig. 4.5 (system with VC) and, therefore, its interpretation is pretty much the same. The time evolution of the signal monitors the ET dynamics: qualitatively it reflects the combined effect of ET and damped vibrational WP dynamics in the donor state, which give rise to a characteristic step structure. Due to the presence of electronic coupling, a fraction of the WP is transferred to the (dark) acceptor state each time the moving WP hits the crossing region, producing a sudden loss (jump) of the amplitude in the cut at a given frequency. In addition, the signal maps directly the periodic coherent WP motion in the excited state between classical turning points, where the local maxima of the peak-shift occur (see Chapter 4 for details). As we have already emphasized, it is far more demanding to construct experimentally the time- and frequency-gated spectrum since this requires measurements for detection frequencies over the whole fluorescence spectrum.

5.3.6 Comparison with the single-excited-state model

One may ask whether the oscillatory cuts and the overall behavior of the TFG SE spectra reflecting WP motion may be reproduced by a harmonic oscillator model involving a single excited-state surface. So one may try to model ET system by a single excited (damped harmonic oscillator) state superimposed with an additional phenomenological population decay e^{-t/T_1}, where T_1 is the excited-state lifetime. Here we would like to demonstrate that the more sophisticated model developed in the present thesis has a considerable advantage over phenomenological harmonic oscillator models in describing the time-resolved signals. The comparison can be performed on the basis of Fig. 5.7 where we present the best fit of the cut at 774 nm (curve 1 from Fig. 4) calculated within our model and the corresponding results for a single excited-state model ($V_{12} = 0$). Curve 3 has been obtained for the same set of parameters as curve 2, except $V_{12} = 0$. The signal has an asymptotic value (which corresponds to a relaxed fluorescence spectrum) of ~ 0.6 and cannot be made lower by varying damping η and dephasing time Γ_{deph}. These two parameters will only change the manner of approaching this asymptotic value. We can change the asymptotic value by varying *significantly* some system parameters. For example, curve 4 has been obtained by changing the horizontal shift between the ground and excited state along the system mode from 1.57 to 2.57. The new asymptotic value is indeed lower (~ 0.4), but the behavior is still very different from the results of calculations involving two electronically coupled excited states and/or the experimental signal: there is a very strong first recurrence and the oscillatory behavior is exaggerated. This has a clear explanation: in a single-excited-state model there is no loss of the amplitude via decay to the dark state. This can be achieved only by introducing the above mentioned phenomenological decay e^{-t/T_1}. So, in fact, a single cut probably can be fitted even within this simple model, but only for

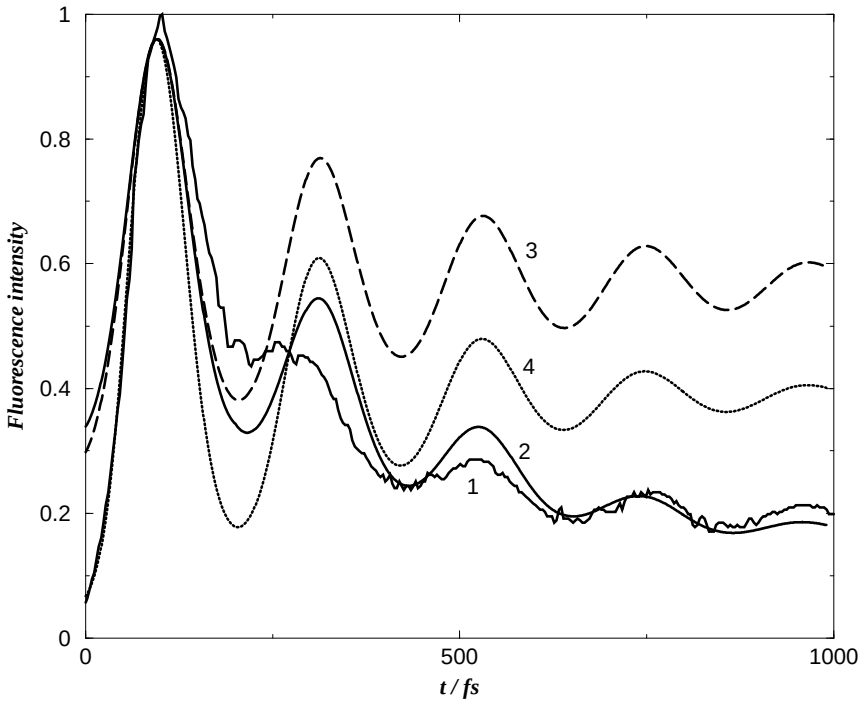

Figure 5.7: Present model vs. single-excited-state model. Cut at 774 nm: **1** - experimental (taken from [21]), and calculated within the: **2** - present model, **3** - single-excited-state model ($V_{12} = 0$), other parameters are the same, **4** - single-excited-state model ($V_{12} = 0$), $d_2 = 2.57$, other parameters are the same.

a single cut, not for the integral signal. In the single-excited-state model, $I(t) = e^{-t/T_1}$, i.e., this model predicts structureless, simple exponential decay and cannot reproduce the step-like structures in the integral signal.

5.4 Possible improvements of the model

As it is evident from the above results, our single-mode model appears to be too simple to describe quantitatively all features in the experimental signals. There are several possible improvements which should be considered in the future.

1) Overlapping pulses
Our theory does not yet describe overlapping excitation and gate pulses. It is rather difficult to describe overlapping-pulse effects within the perturbative treatment. At the moment we are working on the nonperturbative approach (see Appendix B) in which this problem can be straightforwardly solved.

2) Dissipation mechanism
The dissipation mechanism used in the present model (one relevant mode coupled to a bath consisting of other system modes and environment) is probably too simple to describe the actual situation of a complex formed by large molecules in solution.

The Redfield formalism creates an additional limitation on the system-bath coupling strength.

As discussed above, the present model cannot account for the large Stokes shift of the fluorescence. This problem can be solved by including an additional effective overdamped (or solvation) coordinate.

The assumption that the system is dissipation-free during the interaction with the external fields may also be called in question. The corresponding generalization of the theory requires the numerical evaluation of the doorway and window functions with account of dissipation, which will be computationally expensive.

3) Multimode effects

The issue of multimode effects is closely related to the problem of dissipation. The idea to use a single 160 cm^{-1} mode for the description of the experiments [71] is not entirely consistent: although a number of intramolecular vibrational modes is observed in the resonance Raman spectra, it has been assumed [71, 154] that only the 137 cm^{-1} mode (which is actually an effective mode resulting from the averaging of 14 TCNE and/or HMB modes ranging from 80 to 210 cm^{-1}) is associated with the 160 cm^{-1} mode reported in [21, 110, 155–158], and plays a dominant role in time-resolved experimental signals. In a more comprehensive model, more intramolecular vibrational modes should explicitly be taken into account.

5.5 Summary

The developed theory for the description of time- and frequency-gated spontaneous emission spectra has been applied to the interpretation of recent time-resolved fluorescence experiments of Yoshihara and coworkers on the ultrafast electron transfer reaction in the donor-acceptor complex TCNE-HMB. A theoretical model has been constructed which describes the ground state and two nonadiabatically coupled excited electronic states which are strongly coupled to a single reaction mode. The system parameters have been obtained from ab initio calculations [154] and by a fitting of the experimental signals. It is demonstrated that the developed model correctly reproduces general trends in various experimentally measured responses, which include cuts of time- and frequency-gated spectra at particular frequencies, oscillatory peak-shifts of the fluorescence spectra, and frequency-integrated signals. Moreover, the relative shapes and intensities of the spectral cuts at different frequencies are correctly reproduced. A clear distinction between the predictions of a single-surface harmonic oscillator model and the nonadiabatic model of electron transfer is established. It has been shown that the essential features of the signal can be rationalized in a nonadiabatic ET model without introducing non-Condon effects.

Chapter 6

Phenomenological relaxation model

6.1 Introduction

The aim of the present chapter is to develop a simple reference model which allows the explicit calculation of RFs for electronically nonadiabatic systems coupled to a heat bath. The model is based on a phenomenological dissipation ansatz which describes the major bath-induced relaxation processes: excited-state population decay, optical dephasing, and vibrational relaxation. The model is constructed in such a way that it allows us to express the nonlinear RFs of a dissipative material system through those of the corresponding bath-free system.

The idea to express the RFs of a dissipative system through the corresponding bath-free ones is not new, of course. For instance, the strong collision model (which is similar in spirit to the present model) allows one to express various translational and rotational CFs through their bath-free counterparts [160]. The phenomenological dissipation model certainly oversimplifies the relaxation processes. It therefore cannot be invoked for gaining detailed, state-selected information. It is hoped, however, that the model still captures the essential features of the relaxation process, so that its use for the calculation of averaged quantities, like the RFs, is justified. The main impetus for developing the model is to supply a simple tool which can be useful for the interpretation of ultrafast spectroscopic measurements.

6.2 The model

Adopting the electronic two-level system Hamiltonian (2.29) introduced in Section 2.3, we postulate the following kinetic equation for the DM:

$$\rho(t) \equiv \begin{pmatrix} \rho_g(t) & \rho_{ge}(t) \\ \rho_{eg}(t) & \rho_e(t) \end{pmatrix}, \tag{6.1}$$

$$\partial_t \rho(t) = -\frac{i}{\hbar}[H, \rho(t)] - (\Gamma_{el} + \Gamma_{vib})\rho(t). \tag{6.2}$$

The first term in Eq. (6.2) just describes the DM evolution under dissipation-free conditions. The damping operators are defined as follows:

$$\Gamma_{el}\rho(t) = \xi_e|e><\rho_e(t)<e| + (\xi_{eg}|e><\rho_{eg}(t)<g| + H.c.), \tag{6.3}$$

$$\Gamma_{vib}\rho(t) = \sum_{a=e,g} \nu_a(1-\rho_a^B Tr)\,|a><\rho_a(t)<a|. \tag{6.4}$$

Here a bra-ket notation for the electronic states is used, Tr means the trace over vibrational (not electronic) coordinates,

$$\rho^B \equiv \begin{pmatrix} \rho_g^B & 0 \\ 0 & \rho_e^B \end{pmatrix},\ \rho_a^B \equiv Z_a^{-1} e^{-H_a/kT} \tag{6.5}$$

is the equilibrium Boltzmann vibrational distribution, and Z_a are the corresponding partition functions.

The proposed damping operator consists of the two contributions, Γ_{el} and Γ_{vib}, which are responsible for the electronic and vibrational relaxation, respectively. The first term in the operator (6.3) reflects the excited-state population decay, so that $T_1 \equiv 1/\xi_e$ is simply the excited state lifetime. The second term in (6.3) is responsible for the relaxation of coherences, and $T_2 \equiv 1/\xi_{eg}$ is the corresponding optical dephasing time. Explicitly, $1/T_2 \equiv 1/(2T_1) + 1/\overline{T}$, where $\overline{T}$ is the pure dephasing time. Γ_{vib} has been introduced to ensure vibrational relaxation of the DM in each electronic state to its equilibrium form, so that $\tau_a \equiv 1/\nu_a$ can be regarded as vibrational relaxation times ($a = e,\, g$). The damping term Γ_{el} corresponds to the the optical dephasing model proposed by Domcke and Stock [2, 122, 126]. In these papers, one can also find an explanation and justification for the proposed form of the electronic damping operator. Γ_{vib} describes (in a simple phenomenological way) vibrational relaxation in the ground and excited electronic states. In the literature, the ansatz of the kind (6.4) is referred to as a "relaxation time approximation" [161], or a "strong collision model" [160, 162], or the "Bhatnagar-Gross-Krook (BGK)" model [163]. It is frequently used for the treatment of translational [161, 163], rotational [160], and vibrational [162] relaxation.

The solution of Eq. (6.2) with an arbitrary initial condition $\rho(t) = \rho(0)$ reads

$$\rho_a(t) = \exp\{-\xi_a t\}\left[\rho_a(t)^{fr}\exp\{-\nu_a t\} + \rho_a^B\,(1-\exp\{-\nu_a t\})\right] \tag{6.6}$$

($a = e, g$; naturally, $\xi_g = 0$),

$$\rho_{eg}(t) \equiv \rho_{ge}^*(t) = \rho_{eg}(t)^{fr}\exp\{-\xi_{eg}t\}\,. \tag{6.7}$$

Hereafter, the label "fr" ("free") designates the object, evaluated according to Eq. (6.2) with the dissipation term omitted, i.e.

$$\rho_a(t)^{fr} = \exp\left\{-\frac{i}{\hbar}H_a t\right\}\rho_a(0)\exp\left\{\frac{i}{\hbar}H_a t\right\}, \tag{6.8}$$

$$\rho_{eg}(t)^{fr} = \exp\left\{-\frac{i}{\hbar}H_e t\right\}\rho_{eg}(0)\exp\left\{\frac{i}{\hbar}H_g t\right\}. \tag{6.9}$$

Eqs. (6.6), (6.7) clarify the meaning of the model. One sees that the time evolution of coherences (6.7) is governed by a simple exponential decay, while the populations (6.6) undergoes relaxation from an arbitrary initial distribution to equilibrium. The timescale for this relaxation is determined by the parameter τ_a. The damping ansatz

(6.3), (6.4) thus ensures that any DM relaxes to its equilibrium Boltzmann form (6.5). If one takes into account the phenomenological excited state decay time $T_1 \equiv 1/\xi_e$, the long-time asymptote for the DM is

$$\rho(\infty) \equiv \begin{pmatrix} \rho_g^B & 0 \\ 0 & 0 \end{pmatrix}. \tag{6.10}$$

As is seen from Eqs. (6.4)-(6.7), the DM populations $\rho_e(t)$ and $\rho_g(t)$ experience vibrational relaxation, but no vibrational relaxation occurs for coherences $\rho_{eg}(t)$ and $\rho_{ge}(t)$. This evident limitation of the present model can be justified by the following observations. First, if the coherence dephasing time T_2 is shorter than a characteristic vibrational relaxation time, one does not need to take into account vibrational relaxation during this time interval. Second, the present theory is intended for the description of ultrafast spectroscopies in terms of RFs. While calculating such spectroscopic signals, the contributions of the electronic coherences to the RFs are limited by the corresponding pulse durations. Therefore, if the pulses are short enough, one can neglect relaxation of vibrational coherences.

To better understand the physical content of the damping ansatz (6.3), (6.4), it is insightful to introduce the complete set of the eigenfunctions and eigenvalues for the ground and excited state Hamiltonians:

$$H_g|n>=E_n|n>,\ H_e|\alpha>=E_\alpha|\alpha>, \tag{6.11}$$

$$\rho_g^B(n) = Z_g^{-1}\exp\left\{-E_n/kT\right\},\ \rho_e^B(\alpha) = Z_e^{-1}\exp\left\{-E_\alpha/kT\right\}. \tag{6.12}$$

Expanding Eq. (6.6) over the complete set of the eigenfunctions for, e.g., the excited state, one arrives at the result

$$\rho_e^{\alpha\beta}(t) = \exp\left\{-(i\omega_{\alpha\beta}+\nu_e)t\right\}\rho_e^{\alpha\beta}(0) + \rho_e^B(\alpha)\delta_{\alpha\beta}\left(1-\exp\left\{-\nu_e t\right\}\right) \tag{6.13}$$

(here $\delta_{\alpha\beta}$ is the Kronecker symbol and we put $\xi_e = 0$). Eq. (6.13) helps one to visualize how vibrational relaxation proceeds according to our model within a particular vibrational manifold. Both the populations and coherences decay with the same relaxation time $\tau_e \equiv 1/\nu_e$: $\rho_e^{\alpha\beta}(t) \sim \exp\{-t/\tau_e\}$ (note, that we speak here of vibrational, not electronic, coherences). This behavior should be contrasted to that for the Redfield equation for a damped harmonic oscillator. Let us denote by ρ_{ij} the DM elements in the harmonic oscillator basis. Then, after a certain transient time of the order of a vibrational period, one also obtains a quasi-exponential state-independent population decay $\rho_{ii}(t) \sim \exp\{-t/\tau(t)\}$. The coherence damping is, however, state-dependent: $\rho_{ij}(t) \sim \exp\{-|i-j|t/(2\tau(t))\}$, $(i \neq j)$ [164]. The quantity $1/\tau(t)$, after the averaging over a vibrational period, gives just the constant friction in the Redfield equation. It is surprising that the two drastically distinct models give rise, roughly, to the same law of the population decay and differ only in the coherence decay. One hardly may expect the damping ansatz (6.3), (6.4) to accurately describe the state-dependent vibrational relaxation rates. Of course, it is not very realistic to assume a constant, level-independent decay rate for all the populations and coherences of a vibrational manifold. We stress, however, that our model is certainly correct in the two limiting cases: $t = 0$ (no relaxation has occurred yet) and $t \to \infty$ (the system has already

relaxed to its equilibrium distribution). The ansatz (6.4), in fact, interpolates linearly between the two extremes via a single parameter, which is the vibrational relaxation time τ_a. It is hoped that, although our model is unable to describe state-dependent rates for particular vibrational levels, it still gives a reasonably good description for various averaged quantities, like the total (diabatic or adiabatic) populations and RFs.

It is of importance that Eq. (6.2) with the damping operator (6.3), (6.4) is of Lindblad form [165], so that the positiveness of the DM is guaranteed for an arbitrary time interval and for any values of the parameters of the model. Therefore, our approach is not limited to the case of weak system-bath coupling. In addition, the vibrational relaxation operator (6.4) is formulated in a representation-free form. This ensures relaxation to an "actual" equilibrium excited-state distribution (6.5) determined by a (nonadiabatic) Hamiltonian H_e. So, in the present formulations one avoids the problems inherent, e.g., in the diabatic damping approximation in the Redfield theory [2].

To summarize, the damping ansatz (6.3), (6.4) is uniquely determined by four parameters. These are the population decay rate ξ_e , the optical dephasing rate ξ_{eg}, and the two vibrational damping rates ν_e and ν_g .

6.3 Analytic expressions for nonlinear response functions

So far, we have discussed the kinetic equation (6.2) without explicit consideration of the time-dependent field-system interactions. To apply the model for the calculation of nonlinear RFs, one has to start from the total system+field Hamiltonian in the dipole approximation,

$$H(t) = H + H_{SF}(t),\ H_{SF}(t) = -E(t) \begin{pmatrix} 0 & V_{ge} \\ V_{eg} & 0 \end{pmatrix}. \tag{6.14}$$

Here $E(t)$ is the electric field and V_{eg} is the transition dipole moment, which is still an operator in the nuclear space. Substituting H for $H(t)$ in Eq. (6.2), and solving the resulting equation perturbatively with respect to $H_{SF}(t)$, one can analytically express the third-order nonlinear RFs of the dissipative system in terms of those of the corresponding dissipation-free system. The result reads:

$$R_1(t_3,t_2,t_1) = \exp\{-\xi_{eg}(t_1+t_3) - \xi_e t_2\} \times \tag{6.15}$$

$$\left[R_1(t_3,t_2,t_1)^{fr} \exp\{-\nu_e t_2\} + J_g(t_1)J_e(t_3)\left(1-\exp\{-\nu_e t_2\}\right)\right];$$

$$R_2(t_3,t_2,t_1) = \exp\{-\xi_{eg}(t_1+t_3) - \xi_e t_2\} \times \tag{6.16}$$

$$\left[R_2(t_3,t_2,t_1)^{fr} \exp\{-\nu_e t_2\} + J_g^*(t_1)J_e(t_3)\left(1-\exp\{-\nu_e t_2\}\right)\right];$$

$$R_3(t_3,t_2,t_1) = \exp\{-\xi_{eg}(t_1+t_3)\} \times \tag{6.17}$$

$$\left[R_3(t_3,t_2,t_1)^{fr}\exp\{-\nu_g t_2\} + J_g^*(t_1)J_g(t_3)\left(1-\exp\{-\nu_g t_2\}\right)\right];$$

$$R_4(t_3,t_2,t_1) = \exp\{-\xi_{eg}(t_1+t_3)\}\times \tag{6.18}$$

$$\left[R_4(t_3,t_2,t_1)^{fr}\exp\{-\nu_g t_2\} + J_g(t_1)J_g(t_3)\left(1-\exp\{-\nu_g t_2\}\right)\right].$$

Here the standard bath-free third-order nonlinear RFs are given by the Eqs. (2.30)-(2.33). The quantities

$$J_g(t) = Tr\left[\exp\left\{\frac{i}{\hbar}H_g t\right\}V_{ge}\exp\left\{\frac{-i}{\hbar}H_e t\right\}V_{eg}\rho_g^B\right], \tag{6.19}$$

$$J_e(t) = Tr\left[\exp\left\{\frac{i}{\hbar}H_e t\right\}V_{eg}\exp\left\{\frac{-i}{\hbar}H_g t\right\}V_{ge}\rho_e^B\right] \tag{6.20}$$

are the first order RFs, whose Fourier-spectra represent the absorption (6.19) and relaxed fluorescence (6.20) [1]. The set of equations (6.15)-(6.18) embodies the major result of this section. To put it in a different way, the proposed approach supplies us with a kind of regression theorem, which allows us to calculate various RFs for a dissipative system from those for the corresponding non-dissipative system. Having reduced the problem of the evaluation of dissipative RFs to that for bath-free RFs, one can apply various approximate approaches available for bath-free RFs (see, e.g., [49,166]) to calculate and analyze the corresponding dissipative RFs.

If a direct diagonalisation of the excited and ground state Hamiltonians is feasible, evaluation of the nonlinear RFs (6.15)-(6.18) presents no difficulties (see below). It is a frequently occurring situation, however, that the eigenfunctions (6.11) are available analytically for the ground state Hamiltonian only. This may be the case for many nontrivial problems if, e.g., H_g is represented through a collection of harmonic and/or one-dimensional rotational (isomerization) modes [2,61] or, for instance, Morse oscillators [42,60,66]. We may thus adopt the eigenvalue representation for the ground state, while the treatment of the excited-state dynamics will be representation free. This is precisely the strategy pursued in [2,122,126]. In doing so, one is able to express all the nonlinear RFs in terms of matrix elements of the excited-state propagator

$$\Phi_{nm}(t) = < n|V_{ge}\exp\{\frac{-i}{\hbar}H_e t\}V_{eg}|m> . \tag{6.21}$$

Indeed,

$$R_1(t_3,t_2,t_1)^{fr} = \sum_{n,m}\rho_g^B(n)\exp\left\{\frac{i}{\hbar}(E_n^g t_1 + E_m^g t_3)\right\}\Phi_{nm}^*(t_2)\Phi_{mn}(t_1+t_2+t_3), \tag{6.22}$$

$$R_2(t_3,t_2,t_1)^{fr} = \sum_{n,m}\rho_g^B(n)\exp\left\{\frac{-i}{\hbar}(E_n^g t_1 - E_m^g t_3)\right\}\Phi_{nm}^*(t_1+t_2)\Phi_{mn}(t_2+t_3), \tag{6.23}$$

$$R_3(t_3,t_2,t_1)^{fr} = \sum_{n,m} \rho_g^B(n) \exp\left\{\frac{-i}{\hbar}\left[E_n^g(t_1+t_2) - E_m^g(t_2+t_3)\right]\right\} \Phi_{mn}^*(t_1)\Phi_{nm}(t_3), \tag{6.24}$$

$$R_4(t_3,t_2,t_1)^{fr} = \sum_{n,m} \rho_g^B(n) \exp\left\{\frac{i}{\hbar}\left[E_n^g(t_1+t_2+t_3) - E_m^g t_2\right]\right\} \Phi_{mn}(t_3)\Phi_{nm}(t_1); \tag{6.25}$$

$$J_g(t) = \sum_n \rho_g^B(n) \exp\left\{\frac{i}{\hbar} E_n^g t\right\} \Phi_{nn}(t), \tag{6.26}$$

$$J_e(t) = Z_e^{-1} \sum_n \exp\left\{\frac{i}{\hbar} E_n^g t\right\} \Phi_{nn}(-t - \frac{i\hbar}{kT}). \tag{6.27}$$

When one considers the zero temperature case, $\rho_g^B(n) \to \delta_{n0}$, summation over n in Eqs. (6.22)-(6.26) disappears and one arrives at much simpler expressions, since everything is expressed through the zero-temperature propagator $\Phi_{0m}(t)$. Of course, in the case of no vibrational relaxation ($\nu_a = 0$), one then recovers the results of Domcke and Stock [2, 122, 126]. Provided a direct diagonalisation of the excited state Hamiltonian is also feasible, one gets

$$\Phi_{nm}(t) = \sum_\alpha V_{n\alpha} \exp\{\frac{-i}{\hbar} E_\alpha t\} V_{\alpha m}, \;\; V_{\alpha n} \equiv < \alpha | V_{eg} | n > . \tag{6.28}$$

After the insertion of this expression into Eqs. (6.22)-(6.25) one recovers the standard eigenvalue representation for the bath-free nonlinear RFs [1] and further, through Eqs. (6.15)-(6.18), (6.26), (6.27), one obtains the corresponding expressions for the nonlinear RFs of the dissipative system.

6.4 Time- and frequency-gated spontaneous emission in the framework of the phenomenological relaxation model

To illustrate the application of the expressions of the preceding section, we apply the present theory for the calculation of TFG SE spectra. *All other spectroscopic signals can be expressed through the nonlinear RFs in much the same manner* (see as an example the explicit expression for the pump-probe signal in Appendix C). The formalism developed in this chapter allows one to calculate the TFG SE signals for overlapping pump and gate pulses, because these are straightforwardly determined by the nonlinear RFs [1, 85, 111]. The main intention of this section is, however, to demonstrate the computational aspects of our method. Therefore, we restrict ourselves to the case when the pulses are well temporally separated. This allows us to adopt the DW representation for the signal (see Chapter 2) and, subsequently, to demonstrate several simplifying features. In this section we emphasize how the DW representation is specified in the framework of the present model.

The TFG SE spectrum is expressed through the nonlinear RFs according to Eq. (2.36). If one additionally neglects the transient effects occurring on the time scale of the order of duration of the pump and gate pulses, one may further invoke the DW representation. For the present dissipative model, the desirable DW representation can immediately be retrieved from the corresponding bath-free formulas (see Chapter 2) [1, 111]. Indeed, each of the third-order nonlinear RFs (6.15)-(6.18) consists of two contributions which can loosely be labeled as "free" and "relaxed" one. The DW formulas also split into the corresponding parts:

$$S_{st}(t_0,\omega_0) \sim Tr[W^{fr}(\omega_0)G^{fr}(t_0)D^{fr}(\omega_L)] + W^{rel}(\omega_0)G^{rel}(t_0)D^{rel}(\omega_L). \tag{6.29}$$

Here the D and W operators are determined via the expressions

$$D^j(\omega_L) = \int_{-\infty}^{\infty} dt' \int_0^{\infty} dt_1\, E_L(t')E_L(t'-t_1)e^{(i\omega_L-\xi_{eg})t_1}\, D^j(t',t_1) + H.c.\,, \tag{6.30}$$

$$W^j(\omega_0) = \int_{-\infty}^{\infty} dt \int_0^{\infty} dt_3\, E_t(t+t_3)E_t(t)e^{(i\omega_0-\gamma-\xi_{eg})t_3}\, W^j(t,t_3) + H.c. \tag{6.31}$$

in which

$$D^{fr}(t',t_1) = e^{iH_e t'}\, e^{-iH_e t_1}\, V_{eg}\rho_g^{eq}\, e^{iH_g t_1}\, V_{ge}\, e^{-iH_e t'}, \tag{6.32}$$

$$W^{fr}(t,t_3) = e^{iH_e t}\, V_{eg}\, e^{iH_g t_3}\, V_{ge}\, e^{-iH_e t_3} e^{-iH_e t}; \tag{6.33}$$

$$D^{rel}(t',t_1) = J_g(t_1),\ W^{rel}(t,t_3) = J_e(t_3). \tag{6.34}$$

The excited state propagators are determined as follows:

$$G^{fr}(t_0)X = e^{-iH_e t_0} X e^{iH_e t_0}\, e^{-(\nu_e+\xi_e)t_0} \quad \forall X, \tag{6.35}$$

$$G^{rel}(t_0)X = e^{-\xi_e t_0}(1-e^{-\nu_e t_0})X \quad \forall X. \tag{6.36}$$

In the derivation of Eqs. (6.34) we have assumed again that the pump and gate pulses are short enough, so that no bath-induced excited-state population relaxation occurs during the pump and probe processes. The introduced DW-representation for the TFG SE makes the contributions of various relaxation processes to the signal transparent. Since the "free" term is basically determined by the standard bath-free formulas, we shall not consider it here in detail, because a very similar analysis has been given elsewhere [2, 122, 126]. By adopting the eigenvalue representation for the ground state, one may express the "free" contribution to the TFG SE signal (6.29) through the excited state propagator (6.21). As to the "relaxed" contribution, one can further simplify the problem by assuming that the time-gate functions and the excitation pulses are exponential (2.3). Using these formulas, one can analytically perform one of the time integrations in Eqs. (6.30) and (6.31) for the "relaxed" terms (6.34):

$$D^{rel}(\omega_L) = \int_0^{\infty} dt\, (t+\Gamma_L^{-1})\, e^{-(\overline{\Gamma}_L - i\omega_L)t}\, J_g(t) + c.c., \tag{6.37}$$

$$W^{rel}(\omega_0) = \int_0^\infty dt\,(t+\Gamma^{-1})\,e^{-(\overline{\Gamma}-i\omega_0)t}\,J_e(t) + c.c., \tag{6.38}$$

$$\overline{\Gamma}_L \equiv \Gamma_L + \xi_{eg},\ \overline{\Gamma} \equiv \Gamma + \gamma + \xi_{eg}. \tag{6.39}$$

If, additionally, the problem can be handled in the eigenvalue representation for the excited state Hamiltonian (for electronically nonadiabatic systems, this strategy is feasible for Hamiltonians containing several vibrational modes [2, 55–57]) one arrives, in fact, at analytical formulas:

$$S_{st}(t_0,\omega_0) \sim \sum_{\alpha,\beta}\left\{W^{fr}_{\alpha\beta}(\omega_0)e^{-(i\omega_{\alpha\beta}+\nu_e+\xi_e)t_0}D^{fr}_{\beta\alpha}(\omega_L)\right\} \tag{6.40}$$

$$+(1-e^{-\nu_e t_0})W^{rel}(\omega_0)e^{-\xi_e t_0}D^{rel}(\omega_L).$$

Explicitly

$$D^{fr}_{\alpha\beta}(\omega_L) = \sum_n V_{\alpha n}V_{n\beta}\rho^B_g(n)\left\{\frac{1}{\overline{\Gamma}_L - i\omega^L_{\alpha n}}\frac{1}{\overline{\Gamma}_L - i\omega^L_{\beta n}}\right. \tag{6.41}$$

$$\left.+\frac{1}{2\Gamma_L - i\omega_{\alpha\beta}}\frac{1}{\overline{\Gamma}_L - i\omega^L_{\beta n}} + \frac{1}{2\Gamma_L + i\omega_{\alpha\beta}}\frac{1}{\overline{\Gamma}_L - i\omega^L_{\alpha n}}\right\} + c.c.,$$

$$W^{fr}_{\alpha\beta}(\omega_0) = \sum_n V_{\alpha n}V_{n\beta}\left\{\frac{1}{\overline{\Gamma} - i\omega^0_{\alpha n}}\frac{1}{\overline{\Gamma} - i\omega^0_{\beta n}}\right. \tag{6.42}$$

$$\left.+\frac{1}{2\Gamma - i\omega_{\alpha\beta}}\frac{1}{\overline{\Gamma} - i\omega^0_{\beta n}} + \frac{1}{2\Gamma + i\omega_{\alpha\beta}}\frac{1}{\overline{\Gamma} - i\omega^0_{\alpha n}}\right\} + c.c.,$$

$$D^{rel}(\omega_L) = \sum_{n,\alpha}\frac{V^2_{\alpha n}\rho^B_g(n)}{\overline{\Gamma}_L - i\omega^L_{\alpha n}}\left\{\frac{1}{\overline{\Gamma}_L - i\omega^L_{\alpha n}} + \frac{1}{\Gamma_L}\right\} + c.c., \tag{6.43}$$

$$W^{rel}(\omega_0) = \sum_{n,\alpha}\frac{V^2_{\alpha n}\rho^B_e(\alpha)}{\overline{\Gamma} - i\omega^0_{\alpha n}}\left\{\frac{1}{\overline{\Gamma} - i\omega^0_{\alpha n}} + \frac{1}{\Gamma}\right\} + c.c. \tag{6.44}$$

Here

$$\omega^L_{\alpha n} \equiv \omega_L - \omega_{\alpha n},\ \omega^0_{\alpha n} \equiv \omega_0 - \omega_{\alpha n}. \tag{6.45}$$

Eqs. (6.40)-(6.44) provide an explicit recipe for the calculation of the TFG SE signal for any material system, which can be handled in terms of the eigenvalues and eigenfunctions. The equations also generalize the treatments of Kowalczyk et al. [79] and Santoro et al. [78] to dissipative systems.

6.5 Applications of the model

We are now in a position to compare the results of the present alternative model with those obtained by various more accurate methods.

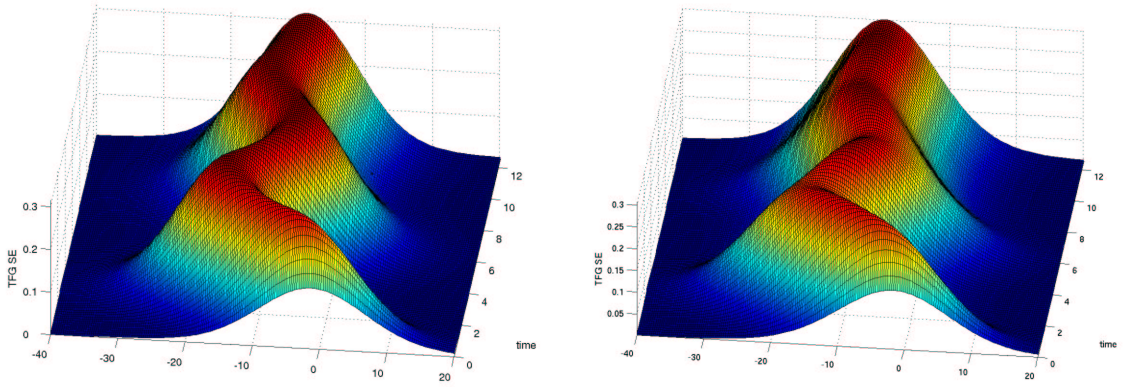

(a) (b)

Figure 6.1: Time evolution of the TFG SE spectrum in the case of satisfactory time and frequency resolution ($\gamma = 0.3$; $\Gamma = 1$) for an underdamped displaced ($\lambda = 5$) classical ($\epsilon = 0.1$) harmonic oscillator. **(a)** $\Lambda = 0.3$ (standard model); **(b)** $\nu_e = 0.3$ (present model). The TFG SE intensity is given in arbitrary units. All the parameters are dimensionless, the inverse of the free oscillator frequency Ω is taken as the time unit. The frequency origin is chosen as ω_{eg} .

6.5.1 Comparison with a Brownian oscillator model

We start with the Brownian oscillator model considered in Section 3.2. For the Brownian oscillator model the nonlinear RFs are determined by a line shape function $g(t)$ (3.14). On the other hand, within the present model, the nonlinear RFs are expressed through the pertinent bath-free ($\Lambda = 0$) function $g_{fr}(t)$. That allows us to compare the results of the approaches with each other. To make this comparison more transparent, here we also restrict ourselves to the case of impulsive excitation which gives an explicit expression for the TFG SE spectrum (see Eq. (3.6)). For our purposes, however, we rewrite that equation as

$$S_{st}(t_0, \omega_0) \sim Re \int_0^\infty dt \int_0^\infty dt_3 \, E_t(t - t_0) E_t(t - t_3 - t_0) e^{[-\gamma + i(\omega_0 - \omega_{eg})]t_3} \Psi(t, t_3). \quad (6.46)$$

In Eq. (6.46), the standard damped harmonic oscillator model corresponds to

$$\Psi(t, t_3) = e^{-g^*(t_3) - 2i[g''(t) - g''(t - t_3)]}, \quad (6.47)$$

while the phenomenological dissipation model results in the expression

$$\Psi(t, t_3) = e^{-g^*_{fr}(t_3)} \left\{ e^{-2i[g''_{fr}(t) - g''_{fr}(t - t_3)]} e^{-\nu_e(t - t_3)} + e^{-2i\lambda(t - t_3)} (1 - e^{-\nu_e(t - t_3)}) \right\}. \quad (6.48)$$

We have put $\xi_{eg} = \xi_e = 0$, since these parameters are irrelevant for the present comparison.

The formulas (6.46)-(6.48) allow us to calculate the TFG SE spectra within both approaches for different values of the dynamic parameters and for various qualities

of the time and frequency filters. Since we are primarily interested in how the phenomenological approach describes the material system dynamics, we shall not study the influence of the quality of temporal and spectral filtering on the TFG SE signals. Instead, we have chosen a representative time and frequency resolution and have calculated the TFG SE spectra within the standard damped harmonic oscillator model (Fig. 6.1a) and the present approach (Fig. 6.1b) for weak dissipation. Both approaches are seen to give rise to qualitatively similar results, since the ansatz (6.3), (6.4) does describe vibrational relaxation in the excited state and, therefore, the TFG SE spectrum evolves into the relaxed fluorescence spectrum, which experiences the Stokes shift of 2λ. Without the "relaxed" contribution to the nonlinear RFs, one simply gets the free oscillator TFG SE spectrum (with no Stokes shift) multiplied by an exponential decay factor, which just decreases the SE intensity.

Evidently, the two approaches coincide in the case of bath-free oscillators ($\nu_e = \Lambda = 0$), and also in the case of very rapid vibrational relaxation in the excited state (ν_e, $\Lambda \to \infty$). However, the parameters ν_e and Λ, which govern the dissipation strength, need not have the same physical origin. Thus, the models do not necessarily coincide for intermediate values of these parameters. It comes as a surprise that the TFG SE spectra in Figs. 6.1a and 6.1b coincide semiquantitatively for $\nu_e = \Lambda$. This provides additional support for our model description. In general, the calculations have revealed that our approach reproduces the TFG SE spectra for a damped harmonic oscillator rather well in the entire domain of the parameters of the model and for an arbitrary dissipation strength.

6.5.2 Comparison with Redfield theory for electron transfer model systems

Now we proceed to a more crucial test and consider the TFG SE for ultrafast ET system presented in Chapter 4. As in the previous consideration of damped harmonic oscillators, we restrict ourselves to the case of impulsive excitation. Therefore, the initial ground-state vibrational distribution is instantaneously transferred to the origin of the vibrational coordinate of the donor potential well. To provide a comparison of our theory with more elaborate approaches, the subsequent evolution of the WP in the electronically excited state is treated within the Redfield formalism, as has been described in detail in Chapter 4:

$$S_{st}(t_0, \omega_0) \sim Tr[W^{fr}(\omega_0) G^R(t_0) D^{fr}(\omega_L)]. \tag{6.49}$$

Here $G^R(t_0)$ is the excited-state propagator of the Redfield theory, and the D and W functions are given by Eqs. (6.41) and (6.42), respectively. For the further analysis it is important to realize that the Redfield propagator $G^R(t_0)$ is uniquely determined by the system Hamiltonian parameters (4.3), (4.7) and by the bath spectral function $J(\omega)$ which is taken in the Ohmic form with exponential cutoff (4.7).

The TFG SE spectra within the present approach were computed according to Eqs. (6.40)-(6.45). Roughly speaking, η determines the strength of the bath-induced relaxation in the Redfield theory and ν_e does in our approach, but, of course, there is no one-to-one correspondence between the two parameters.

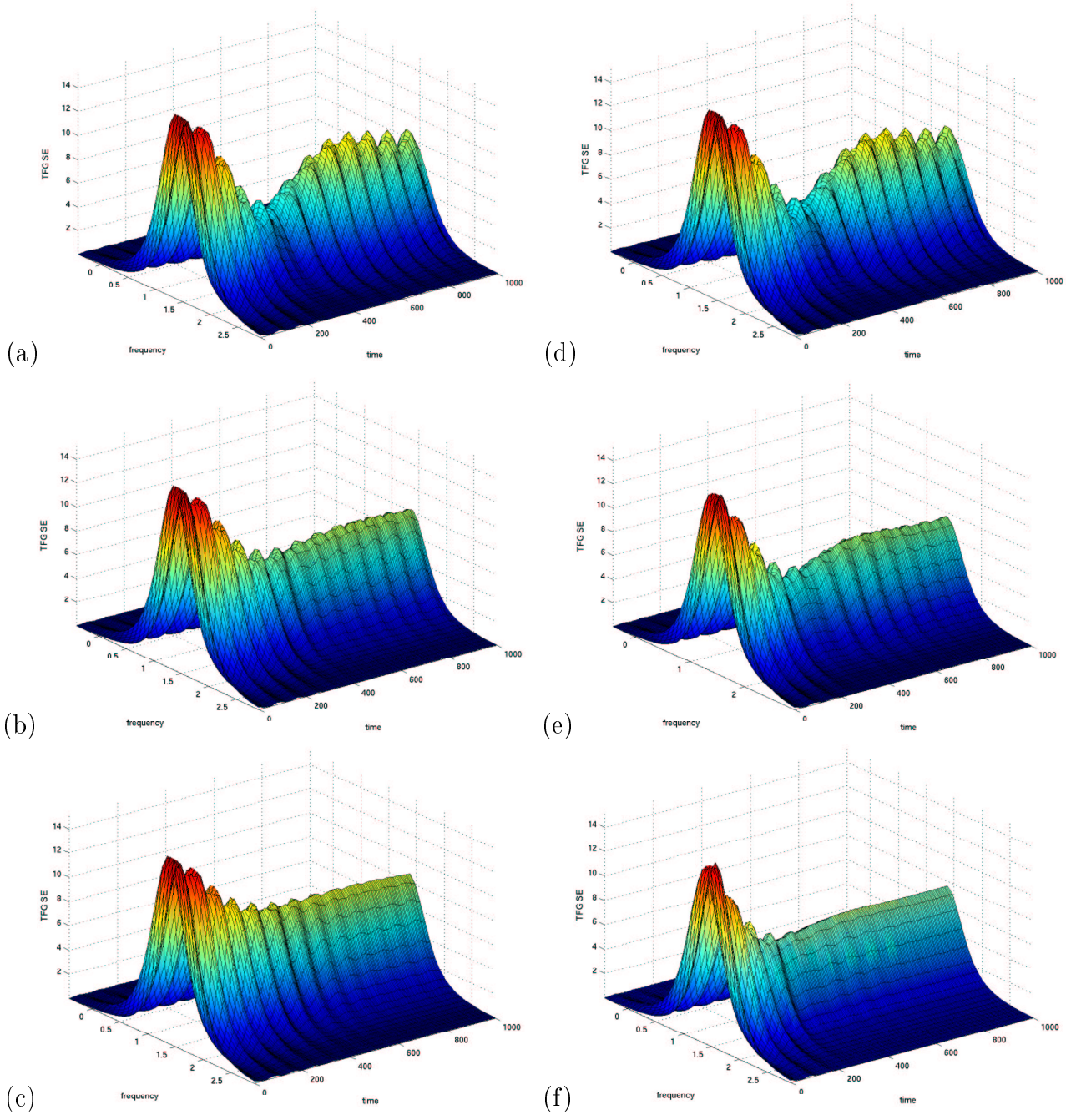

Figure 6.2: Time-evolution of the TFG SE spectrum towards the relaxed fluorescence spectrum for a model ET system in the symmetric regime. DW-Redfield theory: **(a)** $\eta = 0.005$ (weak damping), **(b)** $\eta = 0.05$ (intermediate damping), **(c)** $\eta = 0.1$ (stronger damping). Present model: **(d)** $\nu_e = 0.004\Omega$ (weak damping), **(e)** $\nu_e = 0.03\Omega$ (intermediate damping), **(f)** $\nu_e = 0.06\Omega$ (stronger damping). The TFG SE intensity is given in arbitrary units, time is measured in fs and frequency in eV.

To primarily concentrate on the dynamic effects, a perfect time ($\Gamma = 10\Omega$) and frequency ($\gamma = \Omega/20$) resolution has been chosen for all calculations.

We start from the consideration of the TFG SE spectra for ET in the symmetric case, when the minima of the potential surfaces for both donor and acceptor states are at the same level [Fig. 4.1a with $\varepsilon_2 = \varepsilon_1$]. The system parameters have been taken as those from Ref. [56]: $\hbar\Omega = 0.05\,\mathrm{eV}$, $\Delta_1 = 5.5$, $\Delta_2 = 2$, and $V_{12} = 0.2\Omega$ (relatively weak electronic coupling). We have chosen the symmetric system, since it, even in the case of zero temperature, possesses high equilibrium diabatic state population ($P_1 = P_2 = 0.5$), which is responsible for the relaxed fluorescence. To illustrate the development of the TFG SE spectra with increasing strength of the system-bath coupling, we have calculated them via DW-Redfield theory for $\eta = 0.005$ (weak damping, Fig. 6.2a), $\eta = 0.05$ (intermediate damping, Fig. 6.2b), and $\eta = 0.1$ (stronger damping, Fig. 6.2c). The TFG SE spectra computed within the present model are presented in Fig. 6.2d for $\nu_e = 0.004\Omega$ (weak damping), in Fig. 6.2e for $\nu_e = 0.03\Omega$ (intermediate damping), and in Fig. 6.2f for $\nu_e = 0.06\Omega$ (stronger damping). In general, both approaches give rise to similar scenarios of the TFG SE behavior. Namely, the short time portion of the spectrum reflects the vibrational WP dynamics in the donor state. At $t = 2\pi n/\Omega, n = 1, 2, \ldots$, the WP leaks rapidly to the dark acceptor state due to the presence of electronic coupling. This ultrafast process manifests itself through the characteristic stepwise structure of the TFG SE spectrum (compare with [56]). These periodic excursions of the WP to the acceptor state are superimposed on vibrational relaxation, and the TFG SE spectrum gradually transforms into the relaxed fluorescence spectrum with increasing delay time. The latter just coincides with the "relaxed" window function $W^{rel}(\omega_0)$.

As expected, both approaches predict very similar TFG SE spectra for weak system-bath couplings (Figs. 6.2a and 6.2d). The spectra reflect, obviously, underdamped WP dynamics in the donor state. The dip at $t = 300$ fs and the second hump at 600 fs are the spectral manifestations of the electronic beatings in the system. When the system-bath coupling further increases, these bath-free features gradually disappear, resulting in a more monotonous dependence of the spectra on the pulse delay time. Although Figs. 6.2b and 6.2e look very similar, a closer inspection reveals that the present approach exaggerates slightly the contributions due to free motion of the WP: the aforementioned dip and hump are more pronounced in Fig. 6.2e than in Fig. 6.2b. Fig. 6.2c corresponds to quite a substantial bath-induced damping, in the sense that the TFG SE spectrum exhibits a monotonous dependence on the delay time and exhibits little similarity with the corresponding bath-free spectrum. As is shown elsewhere [148], the Redfield theory is still correct for such values of the system-bath coupling. If one further increases the dissipation strength in the Redfield approach (its validity may become questionable for higher dampings), the relaxation rate of the TFG SE spectra decreases, and they tend very slowly to the relaxed fluorescence spectrum. The present model, on the contrary, predicts more rapid vibrational relaxation if ν_e increases, and the TFG SE spectra evolve to the relaxed fluorescence spectrum on the time scale of τ_e (Fig. 6.2f), in a manner which is similar to the evolution of the TFG SE spectrum for the overdamped harmonic oscillator [111]. Therefore, the slow relaxation regime predicted by the Redfield approach at relatively high dampings can not be reproduced within this model. As has been explained earlier, the case of

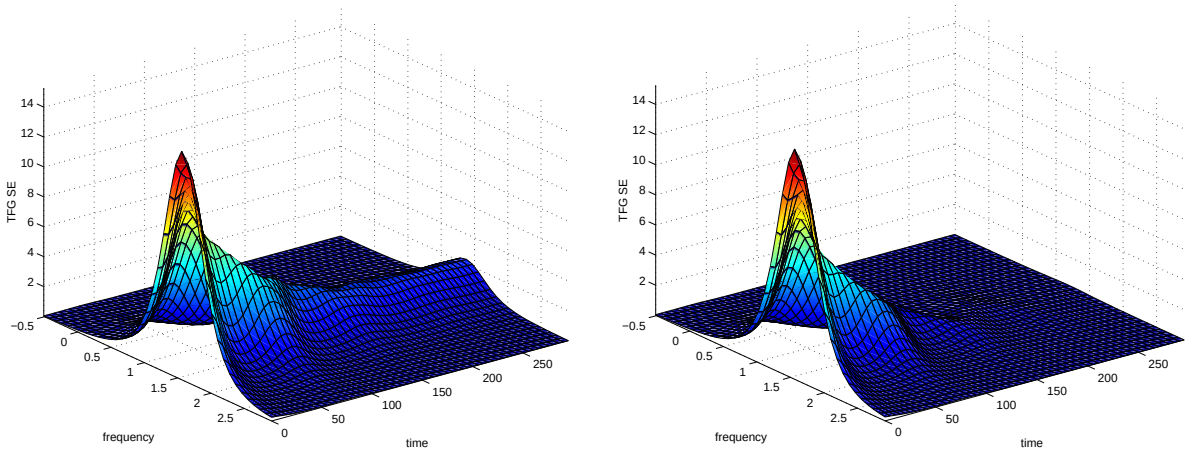

(a) (b)

Figure 6.3: TFG SE spectrum for a model ET system in the normal regime calculated within the present theory ($\nu_e = 0.2\Omega$) at **(a)** low ($T = 0$ K) and **(b)** room ($T = 300$ K) temperature. The TFG SE intensity is given in arbitrary units, time is measured in fs and frequency in eV.

intermediate dissipation strengths is the most unfavorable for testing the validity of our model: it is certainly valid for small and high dampings, while for intermediate system-bath couplings it can be only qualitatively correct. On the other hand, one cannot reproduce a rapid (overdamped) vibrational relaxation by merely increasing friction in the Redfield theory, even in the simplest case of one-dimensional harmonic oscillator [167]. Within the present approach, however, this regime is readily amenable to the description (see below).

Let us next study the ET in the normal regime [Fig. 4.1a]. The system parameters are chosen exactly as those for the previous symmetric case, but the donor state is now vertically displaced relative to the acceptor state: $\varepsilon_2 - \varepsilon_1 - \hbar\Omega(\Delta_1^2 - \Delta_2^2)/2 = 0.045\, eV$. From the point of view of the present consideration, this configuration is peculiar in the sense that the equilibrium diabatic state population is considerable ($P_2 = 0.17$) at room temperature ($T = 300$ K), while it goes to zero with decreasing temperature. The TFG SE spectra calculated within the present approach for a rather large value of the vibrational relaxation rate ($\nu_e = 0.2\Omega$) are shown in Fig. 6.3a ($T = 300$ K) and in Fig. 6.3b ($T = 0$). The figures illustrate the applicability of the phenomenological dissipation model for the description of rapid vibrational relaxation (note the shorter time scale for these figures), when the nuclear mode under study can be regarded overdamped. The initial "hot" fluorescence spectrum is seen to rapidly transform to its relaxed counterpart (Fig. 6.3a) while at $T = 0$ the signal merely vanishes at the same time scale (Fig. 6.3b). This regime of fast vibrational relaxation cannot be described via Redfield theory, because the latter is applicable only in the case of weak system-bath coupling.

As a final example we consider ET in the inverted regime [Fig. 4.1b]. The system

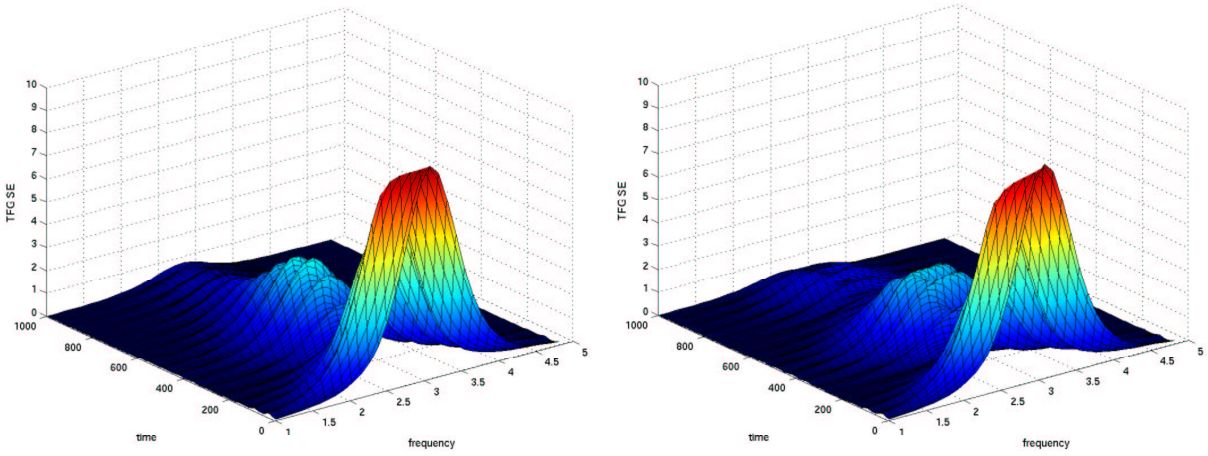

(a) (b)

Figure 6.4: TFG SE spectrum for a model ET system in the inverted regime at room ($T = 300$) temperature. **(a)** DW-Redfield theory, $\eta = 0.1$; **(b)** present model, $\nu_e = 0.03\Omega$. The TFG SE intensity is given in arbitrary units, time is measured in fs and frequency in eV.

parameters are taken as follows [56]: $\hbar\Omega = 0.064\,eV$, $\Delta_1 = -0.8281$, $\Delta_2 = -2$, $V_{12} = 0.1\,eV$, and $\varepsilon_2 - \varepsilon_1 - \hbar\Omega(\Delta_1^2 - \Delta_2^2)/2 = 0.1259\,eV$. The corresponding TFG SE spectra have been calculated via the DW-Redfield theory (Fig. 6.4a, $\eta = 0.1$) and the present approach (Fig. 6.4b, $\nu_e = 0.03\Omega$) at $T = 300$ K. For that system, the equilibrium population of the donor state is negligibly small even at a room temperature. It is quite surprising therefore that both the DW-Redfield and the present theory coincide semiquantitatively in a case for which vibrational damping is quite important. Indeed, the TFG SE spectra vanish on a time scale of $\sim 1ps$ (Fig. 6.4). The shape of the spectra differs markedly from that for the bath-free system, since the bath-free donor-state population at $t \sim 1ps$ is still substantial [56], and vibrational relaxation in the excited state is not finished yet. Of course, for higher dampings, the predictions of the DW-Redfield theory and the present approach start to deviate, in the manner described for the TFG SE spectra in the normal regime, that is, the present model exaggerates the contribution of free WP motion. Moreover, since the "relaxed" contribution to the TFG SE turns out to be negligibly small for this system, the RFs become just the "free" ones multiplied by an exponential decay factor (6.15-6.18), so that one recovers the optical dephasing model [2,122,126]. On the other hand, the validity of the Redfield theory itself is questionable for higher dampings.

To conclude, the phenomenological dissipation model describes the evolution of the TFG SE spectrum towards the relaxed fluorescence spectrum. For electronically adiabatic systems, one gets a semiquantitative agreement between the TFG SE spectra calculated within the present approach and the standard damped harmonic oscillator [1]. If the system under study possesses pronounced nonadiabatic couplings and undergoes, therefore, a rapid interconversion between diabatic electronic states, the equilibrium diabatic donor state population may be very small. In such a situation

the difference between the predictions of the phenomenological model and Redfield theory become apparent, since the relaxed contribution to the RFs disappears. Even in this case, the two approaches give rise to quite similar results for weak dissipation (see Fig. 6.4a and 6.4b). In general, for nonadiabatic systems, the predictions of the phenomenological model may deviate quantitatively from those of Redfield theory for intermediate-strength dampings and small temperatures. The present approach exaggerates contributions due to free WP dynamics as compared with the DW-Redfield theory, which predicts a more monotonous transformation of the TFG SE spectra. In any case, the short-time (at times of the order of several vibrational periods) and long-time (at times greater than a characteristic vibrational relaxation time) behaviors for the TFG SE spectra are correctly reproduced by our model. In addition, it allows one to easily treat rapid vibrational relaxation, when the nuclear mode(s) under study are overdamped.

6.6 Summary

In order to treat the time-dependent optical response of a (nonadiabatic) system coupled to a heat bath, a simple phenomenological model has been proposed, which describes the major bath-induced relaxation processes. These are the excited-state electronic population decay, electronic coherence dephasing, and vibrational relaxation. The model allows one to express the nonlinear RFs for a dissipative material system through those of the corresponding bath-free system. We have restricted ourselves to the consideration of the nonlinear RFs, although higher order RFs can be evaluated in much the same manner. To facilitate the calculation of nonlinear RFs in the framework of the present theory, we have considered two important situations, for which evaluation of the nonlinear RFs simplifies considerably. These are the eigenstate representation for (i) both ground and excited state Hamiltonians and for (ii) the ground state Hamiltonian only, while the excited state is treated in a representation-free manner. For these particular cases, simple and readily numerically tractable formulas have been derived for the nonlinear RFs.

To illustrate the computation of optical responses via our theory and various standard methods, we have compared the TFG SE spectra calculated within the present approach with those obtained for a damped harmonic oscillator (Chapter 3) and the DW-Redfield theory of the nonadiabatic ET (Chapter 4). The phenomenological model has been shown to semiquantitatively reproduce the TFG SE spectra for electronically adiabatic systems. For nonadiabatic systems, the phenomenological approach correlates well with Redfield theory in the case of underdamped nuclear relaxation, when TFG SE signal reflects essential signatures of the free motion. With increasing the strength of the bath-induced dissipation, the phenomenological model may deviate from Redfield theory. On the other hand, the model allows one to correctly describe the case of rapid vibrational relaxation, when the vibrational mode(s) of the system can be regarded as overdamped. In this limit of strong system-bath coupling, Redfield theory is not applicable.

The model is very efficient numerically since the computational cost is determined by the propagation of dissipation-free Hamiltonians, as distinct from, e.g., Redfield

theory.

It is hoped that the alternative model developed in this chapter may prove useful as an efficient tool for the qualitative calculation of optical responses and, therefore, the interpretation of observed time-resolved spectra. In particular, it can be applied for the complex systems with many degrees of freedom, part of which are treated in a quantum-mechanical description and the rest of the modes in a classical approximation. Furthermore, the model allows the consideration of the overdamped motion in contrast to models which are limited to weak dissipation.

Chapter 7

Conclusions

The theory of time- and frequency-gated spontaneous emission spectra has been elaborated. The present formulation generalizes previous derivations, clarifies the interrelations between different existing expressions, and establishes the validity of certain commonly assumed approximations. Various explicit expressions for the time- and frequency-gated spontaneous emission signals have been derived, which are suitable for performing actual calculations for nontrivial systems.

A number of generic (that is, model independent) properties of time-resolved spectra has been established. The time- and frequency-gated spontaneous emission is shown to be equivalent to the stimulated-emission contribution to the integral pump-probe spectrum in the case of non-overlapping pulses. In this case, the time-gate function plays the role of the envelope of the probe pulse, and the spectral filter function determines its carrier frequency. The validity of the commonly employed slowly varying envelope approximation is discussed and generalized expressions are derived for the time- and frequency-gated spontaneous emission in terms of Wigner spectrograms beyond this approximation.

The doorway-window picture of temporally and spectrally resolved spectra has been further developed. This casts the description of the time-resolved fluorescence into an intuitively appealing form in terms of wave-packet dynamics in the excited state. Computationally, this method requires the doorway and window operators to be calculated only once, so that propagation of the doorway operator over a certain time interval according to the chosen (dissipative) model and its subsequent averaging together with the window operator yields the time- and frequency-gated spontaneous emission spectrum. If the doorway and window operators are expanded over the complete set of eigenfunctions of the bath-free Hamiltonian and if one assumes an exponential time-gate function, the doorway and window functions can be evaluated analytically beyond the snapshot limit.

The theory has been illustrated for the example of an electronic two-level system with a single Condon-active harmonic vibrational mode which is coupled to a thermal bath. The effect of imperfect time and frequency resolution is studied. The specific features of the wave-packet dynamics in the excited state are shown to survive the time- and frequency-gated mapping procedure, and manifest themselves in the fluorescence spectra. This underlines that the time-resolved fluorescence clearly reflects the wave-packet dynamics in the excited state, provided a good compromise is found between

temporal and spectral resolution. In this case, the information about the material dynamics can be extracted from the time-resolved fluorescence signals by an appropriate theoretical analysis. In particular, the time- and frequency-gated spontaneous emission spectrum carries information not only on the strength of the system-bath coupling, but also on the relative magnitude of the bath correlation time.

Time-resolved fluorescence signals have been calculated for representative models of electron-transfer systems. The electron-transfer dynamics is modeled in terms of two diabatic electronic states which are electronically coupled as well as strongly coupled to a reaction mode, which in turn is weakly coupled to a dissipative environment. The bath degrees of freedom are integrated out in the framework of Redfield theory. The reduced density matrix is obtained by the numerical solution of the Redfield equations of motion. For suitably chosen parameters, the model describes interesting features of ultrafast electron-transfer dynamics such as electronic beatings (due to electronic coherence) and step-like electronic population decay (due to vibrational coherence).

To elucidate the effect of various coherences on the fluorescence signal, a number of simulations has been performed for electron-transfer models in which either electronic coherence or vibrational coherence effects are dominant. It is demonstrated that the time resolution of the gate must be of the order of or shorter than the electronic beating period in order to detect electronic quantum beats. It is shown that step structures in the electronic population probability due to vibrationally coherent electron transfer can be experimentally detected, provided the duration of the pump and gate pulses is of the order of a vibrational period or shorter. This prediction is not limited to the case of weak system-bath coupling. When the duration of the pulses significantly exceeds the vibrational period, the mode-specific features are shown to be averaged out, resulting in exponential electronic population decay corresponding to the electron-transfer rate.

It has been demonstrated that the effect of optical preparation by pump pulses of finite duration is qualitatively similar to that of the temporal resolution of the gate pulse. To monitor the mode-specific features of the electron transfer dynamics in a time-resolved fluorescence experiment, one must employ sufficiently short pump pulses to excite coherently a significant part of vibrational levels. To detect the characteristic step-like structure in ultrafast spectroscopic signals, the pump-pulse duration as well as the gate-pulse duration must be shorter than the vibrational period.

Time- and frequency-gated spontaneous emission spectra have been calculated for various durations of the pump and gate pulses. For suitably chosen parameters of the pump and gate pulses, these spectra are demonstrated to map the vibrational wave-packet dynamics of the electron transfer systems, so that both types of coherences can show up in measured time-resolved fluorescence signals. It is argued that the time- and frequency-gated spontaneous emission spectrum, as a function of time, qualitatively reflects the electronic population dynamics. At small times, the spectrum represents the spontaneous emission of the initially prepared nonequilibrium excited state. Later on, it gives the development of this fluorescence spectrum towards equilibrium one. Since the time-resolved fluorescence signal maps directly the periodic vibrational wave-packet motion in the excited state, time- and frequency-gated spectra provide us with more information on the system dynamics than frequency-averaged time-resolved signals or the conventional stationary fluorescence spectrum.

It is concluded that the influence of the measuring devices (the pump pulse for

preparation and the gate pulse for detection) is significant and must be accurately taken into account. The present formulation clarifies the relation between the intrinsic system dynamics (e.g., the time-dependent electronic population dynamics) and "real" experimental observables.

The developed approach to the description of time- and frequency-gated spontaneous emission spectra has been applied to the interpretation of recent time-resolved fluorescence experiments of Yoshihara and coworkers, performed to study the ultrafast electron transfer in the donor-acceptor complex TCNE-HMB. A theoretical model consisting of the electronic ground state and two nonadiabatically coupled excited electronic states, which are strongly coupled to a single reaction mode, has been constructed. The system parameters are obtained from a fitting procedure and ab initio calculations [154]. It is demonstrated that the developed model correctly reproduces the general trends in various experimentally measured responses, which include cuts of time- and frequency-gated spectra at particular frequencies, peak-shifts of the fluorescence spectra, and frequency-integrated signals. Moreover, the relative shapes and intensities of the spectral cuts at different frequencies are correctly reproduced. A clear distinction between predictions of the standard harmonic oscillator models and nonadiabatic models of the ultrafast electron transfer is established. It is argued that the observed features in the signal behavior can be rationalized without introducing non-Condon effects. The methods developed in the present work have been shown to be useful for the interpretation of time-resolved fluorescence experiments on ultrafast electron-transfer systems exhibiting coherent responses.

An alternative model has been developed for the calculation of optical response functions for electronically nonadiabatic systems coupled to a heat bath. A phenomenological dissipation ansatz is suggested which describes the major bath-induced relaxation processes, namely excited-state population decay, optical dephasing, and vibrational relaxation. The model is constructed in such a way that it allows one to express the nonlinear response functions for a dissipative system in terms of those for the corresponding bath-free system. The explicit formulas for the third-order response functions are given.

To illustrate the performance and validity of the phenomenological model, time- and frequency-gated spontaneous emission spectra have been calculated. The time-dependent spectra derived from the model are compared with those calculated for the standard damped harmonic oscillator model and for a model nonadiabatic electron-transfer system with Redfield theory. It is concluded that the model provides qualitatively correct response functions and, therefore, may be useful for the interpretation of observed time-resolved spectra. In particular, it can be applied to large systems with nonadiabatic couplings and many degrees of freedom. The model is very efficient numerically, since the computational cost is determined by the propagation of dissipation-free Hamiltonians, in contrast to, e.g., Redfield theory.

Appendix A

Time- and frequency-gated spontaneous emission spectra in terms of Wigner spectrograms

Following Mukamel and coworkers [63, 64, 83–85], we adopt Wigner spectrograms for the description of the TFG SE. Let us introduce the new variables

$$\bar{t} = (t' + t'')/2, \;\; s = t' - t'' \tag{A.1}$$

and the bare TFG spectral function

$$S_0(\bar{t}, \omega) = \int_{-\infty}^{\infty} ds\, e^{is\omega} < P(\bar{t} + s/2) P(\bar{t} - s/2) > . \tag{A.2}$$

After the insertion of Eq. (A.2) into Eq. (2.12) one arrives at Eq. (2.10) in which

$$S_t(t_0, \omega_1) = \int_{-\infty}^{\infty} d\bar{t}\, d\omega\, \overline{W}(\bar{t}, \omega_1 - \omega, t_0)\, S_0(\bar{t}, \omega), \tag{A.3}$$

with

$$\overline{W}(\bar{t}, \omega, t_0) \equiv (\frac{1}{4}\partial_{\bar{t}}^2 + \omega^2) W(\bar{t}, \omega, t_0), \tag{A.4}$$

$$W(\bar{t}, \omega, t_0) = \int_{-\infty}^{\infty} ds\, e^{is\omega} E_t(\bar{t} + s/2; t_0) E_t^*(\bar{t} - s/2; t_0). \tag{A.5}$$

One sees that the explicit inclusion of the time derivatives of the transition dipole moments results in an additional contribution to the transformation function $\overline{W}$, which is given by the term in parentheses in Eq. (A.4). By using, e.g., the Gaussian gating function (2.2), one can evaluate $\overline{W}$ analytically:

$$W(\bar{t}, \omega, t_0) = \frac{\sqrt{2\pi}}{\Gamma} \exp(-\frac{\omega^2}{2\Gamma^2} - 2\Gamma^2(\bar{t} - t_0)^2), \tag{A.6}$$

$$\overline{W}(\bar{t}, \omega, t_0) \equiv \left\{ \left[\Gamma^2(4\Gamma^2(\bar{t} - t_0)^2 - 1) + \omega^2 \right]^2 - 2\Gamma^4(8\Gamma^2(\bar{t} - t_0)^2 - 1) \right\} W(\bar{t}, \omega, t_0). \tag{A.7}$$

If the material system under study possesses a narrow spectrum in the vicinity of the frequency ω_{eg} of the electron transition, and if $\Gamma \gg \gamma$ (a good filter), then $\overline{W} \approx \omega_0^4 W$. Otherwise, one should use the more general expression (A.4).

It is important that for the standard TFG functions (2.2)-(2.4) the transformation function $\overline{W}$ simplifies to $\overline{W}(\bar{t} - t_0, \omega)$. So, the bare TFG spectrum $S(t_0, \omega_0)$ and the ideal frequency filter spectrum $S_t(t_0, \omega_1)$ can be extracted from Eqs. (2.10) and (A.3) by performing the appropriate inverse Fourier transforms. This opens the way for getting direct information about the material system from measured TFG spectra (see also papers [18–20, 119]). The procedure requires, of course, the TFG SE spectra to be available with considerable accuracy, both with respect to time and frequency.

Appendix B

Nonperturbative treatment of the excitation process

In this Appendix, the basic idea of the nonperturbative calculation of the optical polarization is introduced and the steps leading to its practical implementation are outlined.

Formulation of the problem

As has been demonstrated in Chapters 2-6, the conventional perturbative approach to the nonlinear spectroscopy of dissipative systems is convenient and efficient, providing the system dynamics and/or DW functions can be evaluated analytically or in terms of the system Hamiltonian eigenfunctions. Otherwise, the implementation of the nonperturbative approach is more promising, as has been demonstrated in [123, 124] for the case of pump-probe spectroscopy. Here we would like to outline how the approach can be implemented for the calculation of the TFG SE signal (work in this direction is in progress). This will allow us

- to consider overlapping pulses
- to take into account the system-bath interaction during the excitation and gate pulses
- to study nonlinear (with respect to the excitation pulse) effects, i.e., saturation effects
- to explore (if necessary) chirped excitation pulses.

Starting expressions

As has been demonstrated in Chapter 2 (see Eq. (2.16)), the general TFG SE spectrum is defined as follows:

$$S_{st}(t_0,\omega_0) \sim Re \int_{-\infty}^{\infty} dt \int_{-\infty}^{t} dt'\, E_t(t-t_0)E_t(t'-t_0) \exp\left\{-(\gamma+i\omega_0)(t-t')\right\} C(t,t'). \tag{B.1}$$

Here

$$C(t,t') \equiv < P(t)P(t') > \tag{B.2}$$

is the CF of the polarization operators,

$$P(t) \equiv U^{+}(t,-\infty)VU(t,-\infty). \tag{B.3}$$

$U(t,t')$ is the Hamiltonian propagator for the equation

$$\partial_t \rho(t) = -i[(H + H_I(t), \rho(t)].$$

H is the total (system+bath) Hamiltonian of a (nonadiabatic) system, and

$$H_I(t) \equiv -\lambda V E_L(t) \left(\exp\{-i(\varphi_L + \omega_L t)\} + cc\right)$$

describes the interaction of the system with the excitation pulse. The latter is characterized by the frequency ω_L, phase $\varphi_L \equiv \overrightarrow{k}\,\overrightarrow{r}$, and the envelope $E_L(t)$. $\lambda \equiv \mu E/\hbar$ is the dimensionless parameter determining the strength of the system-field interaction. Hereafter, $\hbar = 1$. The dipole moment operator is determined as follows:

$$V = \chi_{e1}(|\Psi_g >< \Psi_{e1}| + |\Psi_{e1} >< \Psi_g|) + \chi_{e2}(|\Psi_g >< \Psi_{e2}| + |\Psi_{e2} >< \Psi_g|)$$

and χ_{ei}^2 are the corresponding oscillator strengths.

If one is interested in the integral signal,

$$S_t(t_0) = \int_{-\infty}^{\infty} d\omega_0 \, S_{st}(t_0, \omega_0), \tag{B.4}$$

the resulting equation is much simpler:

$$S_t(t_0) \sim Re \int_{-\infty}^{\infty} dt \, E_t^2(t - t_0) C(t,t) = Re \int_{-\infty}^{\infty} dt \, E_t^2(t - t_0) < P^2(t) > \tag{B.5}$$

Our goal is to evaluate the CF (B.2) nonperturbatively.

Calculation scheme

Phase dependence of $P(t)$

When one calculates $P(t)$ nonperturbatively, one should take care of its dependence on the phase angle φ_L. Since we have not yet adapted the RDM description, we can use the results obtained in [124]. Therefore, by invoking the rotating wave approximation (RWA), one can state that

$$P(t) \sim \overline{p}(t) e^{-i\varphi_L} + \overline{p}(t)^* e^{i\varphi_L} + p_0(t)$$

to *any* order in the perturbation expansion. Since an actual signal is a result of many uncorrelated laser shots, one has to average $C(t,t')$ over φ_L. This can easily be achieved by calculating $C(t,t')$ at $\varphi_L = 0$, π, and $\pi/2$, so that

$$< C(t,t') >_{\varphi_L} = \frac{1}{2} \{(C(t,t';\varphi_L = 0) + C(t,t';\varphi_L = \pi/2) + C(t,t';\varphi_L = \pi)\}.$$

RDM description

According to, e.g., [168], one can evaluate Eq. (B.2) as follows:

$$< P(t+\tau)P(t) >=< VG(\tau,t)VG(t,-\infty)\rho_{eq} >, \tag{B.6}$$

$$< P^2(t) >=< V^2G(t,-\infty)\rho_{eq} > . \tag{B.7}$$

On the right hand side of these equations, the averaging is assumed over the system space only, and $G(\tau,t)$ is the Liouville-space propagator for the RDM equation

$$\partial_t\rho(t) = -i[(H_S + H_I(t), \rho(t)] + \widehat{R}\rho(t). \tag{B.8}$$

$\widehat{R}$ is the Redfield operator. One should start from a time moment, for which $E_L(t)$ is still nearly zero.

RWA and the Redfield equation

We write the system Hamiltonian as

$$H^S = \begin{pmatrix} H_g^S & 0 \\ 0 & E_{00} + H_e^S \end{pmatrix}. \tag{B.9}$$

Here H_α^S are the system vibrational Hamiltonians in the ground state ($\alpha = g$) and the excited nonadiabatic electronic state ($\alpha = e$), and E_{00} is the energy of the 0-0 transition. For the sake of mathematical convenience, we prefer to evaluate Eq. (B.8) in the complete $g \oplus e$ space. To this goal, we introduce the eigenvalue representation for the Hamiltonian

$$\widetilde{H}^S = \begin{pmatrix} H_g^S & 0 \\ 0 & H_e^S \end{pmatrix}, \tag{B.10}$$

so that

$$\widetilde{H}^S|\alpha >= E_\alpha|\alpha > . \tag{B.11}$$

Evidently,

$$H^S|\alpha >= (E_\alpha + \delta_{\alpha e}E_{00})|\alpha > . \tag{B.12}$$

Here the Kronecker δ is introduced, which symbolically means, that the excited state eigenvalues (α belongs to e) for $\widetilde{H}^S$ differ from those for H^S by E_{00}. In terms of the eigenvalues (B.12) the RDM Eq. (B.8) reads:

$$\partial_t\rho_{\alpha\beta}(t) = -i(\omega_{\alpha\beta} + (\delta_{\alpha e} - \delta_{\beta e})E_{00})\rho_{\alpha\beta}(t) + \widehat{R}_{\alpha\beta ab}\rho_{ab}(t) \tag{B.13}$$

$$+\lambda[V_{\alpha b}\rho_{b\beta}(t) - \rho_{\alpha b}(t)V_{b\beta}(t)]E_L(t)\left(\exp\{-i(\varphi_L + \omega_L t)\} + cc\right).$$

Hereafter, the repeated dummy Latin indexes are to be summed over, and

$$\omega_{\alpha\beta} = E_\alpha - E_\beta. \tag{B.14}$$

If one explicitly expresses the eigenvalues $|\alpha>$ in terms of the direct product of the suitable harmonic oscillator basis $|h_a>$ and the electronic state basis $|\Psi_i>$ ($i = g, e1, e2$)

$$|\alpha>=\xi^{\alpha}_{ai}|h_a>|\Psi_i>,$$

then

$$V_{\alpha\beta}=\chi_{e1}(\xi^{\alpha}_{ag}\xi^{\beta}_{ae1}+\xi^{\alpha}_{ae1}\xi^{\beta}_{ag})+\chi_{e2}(\xi^{\alpha}_{ag}\xi^{\beta}_{ae2}+\xi^{\alpha}_{ae2}\xi^{\beta}_{ag}).$$

By introducing

$$\rho_{\alpha\beta}(t)=exp\{-i(\omega_{\alpha\beta}+(\delta_{\alpha e}-\delta_{\beta e})E_{00})t\}\sigma_{\alpha\beta}(t) \tag{B.15}$$

and adopting RWA, one transforms Eq. (B.13) as follows:

$$\begin{aligned}\partial_t\sigma_{\alpha\beta}(t)&=exp\{i(\omega_{\alpha\beta}-\omega_{ab})t\}\widehat{R}_{\alpha\beta ab}\sigma_{ab}(t) \qquad \text{(B.16)}\\ -\lambda E_L(t)V_{\alpha b}\sigma_{b\beta}(t)[\delta_{\alpha e}\delta_{bg}\exp\{-i(\varphi_L+\overline{\omega}_L t)\}&+\delta_{\alpha g}\delta_{be}\exp\{i(\varphi_L+\overline{\omega}_L t)\}]\\ +\lambda E_L(t)\sigma_{\alpha b}(t)V_{b\beta}[\delta_{\beta e}\delta_{bg}\exp\{i(\varphi_L+\overline{\omega}_L t)\}&+\delta_{\beta g}\delta_{be}\exp\{-i(\varphi_L+\overline{\omega}_L t)\}].\end{aligned}$$

Here

$$\overline{\omega}_L\equiv\omega_L-\omega_{00}.$$

While deriving Eq. (B.16), we have assumed that the Redfield-induced relaxation proceeds independently in the e and g states, i.e., the Redfield tensor does not couple these states. Therefore, the Eq. (B.16) contains no rapidly oscillating terms.

Calculation of spectra

In general, the evaluation of $C(t,t')$ is very time consuming, since one has to perform N full-time propagations, where N is the number of grid points on a discretized time scale. Indeed, let τ_0 be the timescale of interest for the evolution of the TFG SE spectrum. Then the total propagation timescale τ_{pr} must be $\simeq 3/\Gamma_L+\tau_0+3/\Gamma$. Since the Redfield equation is ill-defined for $t<0$, it is logical to surmise that the pump pulse is peaked, e.g., at $t\approx 3/\Gamma_L$ and start the propagation from $t=0$. So, one has to make the propagation $G(t,0)$ first and then perform $G(\tau_{pr},t)$, for any $0\geq t\geq\tau_{pr}$ (N propagations). If, however, one is interested in the integral fluorescence signal (B.5), one has to perform only one propagation $G(\tau_{pr},0)$ which presents no difficulties.

Appendix C

Pump-probe signal in the framework of the phenomenological relaxation model

In Chapter 5, we have introduced the phenomenological relaxation model for the calculation of TFG SE spectra. We emphasized that all other spectroscopic signals can be expressed through the nonlinear RFs in much the same manner. Taking into account the mentioned similarity between TFG SE and pump-probe (PP) signal, it is natural, therefore, to extend the description to time and frequency resolved pump-probe PP signals [1, 169]. The details will be given elsewhere [170]. Here we give explicit analytical expressions for the integral PP signals. It is hoped that these simple formulas may be useful for a (at least) qualitative interpretation of observed PP spectra. The present contribution may be considered as an extension of the formulation of paper [169] towards nonadiabatic systems.

For our aims, we write the system Hamiltonian H as a sum of the Hamiltonians in the ground ($|g>$) and excited ($|e>$) electronic states, $H = |g> h_g < g| + |e> h_e < e|$. Furthermore, we assume that $|e>$ consists of several coupled electronic substates $|\psi_q>$, i.e. $|e>= |\psi_1> \bigotimes |\psi_2> ... \bigotimes |\psi_N>$, $h_e = \sum_{p,q} |\psi_p> h_e^{pq} < \psi_q|$. The system-field interaction is then given by

$$H_{int}(t) = -E(t) \sum_q \xi_q |g>< \psi_q| + H.c. \tag{C.1}$$

Here $E(t)$ is a sum of the pump and probe pulses, and ξ_q^2 is the oscillator strength for the transition between the ground ($|g>$) and excited ($|\psi_q>$) electronic states.

We have further made the following three explicit assumptions, which are discussed in detail in Chapters 2 and 5: (i) the pump and probe laser pulses are well separated in time, so that the DW formalism is applicable; (ii) the pump and probe pulses of the frequency Ω_1 and Ω_2 are adequately described by exponential envelopes $E_i(t) = \exp(-\Gamma_i|t|)$ $(i = 1, 2)$; (iii) the eigenvalue representation for the ground and excited state Hamiltonians is feasible.

These assumptions are sufficient to derive analytical formulas for the PP signals.

Let us introduce the functions ($i = D,\ W$)

$$X^i_{\alpha\beta}(\Omega,\Gamma,\overline{\Gamma}) = \sum_{n;p} V^\alpha_{np} V^\beta_{np} Q^i_n \left\{ \frac{1}{\overline{\Gamma} - i\overline{\omega}_{\alpha n}} \frac{1}{\overline{\Gamma} - i\overline{\omega}_{\beta n}} \right. \tag{C.2}$$

$$\left. + \frac{1}{2\Gamma - i\omega_{\alpha\beta}} \frac{1}{\overline{\Gamma} - i\overline{\omega}_{\beta n}} + \frac{1}{2\Gamma + i\omega_{\alpha\beta}} \frac{1}{\overline{\Gamma} - i\overline{\omega}_{\alpha n}} \right\} + c.c.,$$

$$X^{i;pq}_{nm}(\Omega,\Gamma,\overline{\Gamma}) = \sum_{\alpha} V^\alpha_{np} V^\alpha_{mq} Q^i_m \left\{ \frac{1}{\overline{\Gamma} - i\overline{\omega}_{\alpha m}} \frac{1}{\overline{\Gamma} - i\overline{\omega}_{\alpha n}} \right. \tag{C.3}$$

$$\left. + \frac{1}{2\Gamma - i\omega_{nm}} \frac{1}{\overline{\Gamma} - i\overline{\omega}_{\alpha n}} + \frac{1}{2\Gamma + i\omega_{nm}} \frac{1}{\overline{\Gamma} - i\overline{\omega}_{\alpha m}} \right\} + c.c.,$$

$$X_g(\Omega,\Gamma,\overline{\Gamma}) = \sum_{n,p;\alpha} \frac{(V^\alpha_{np})^2 \rho^B_g(n)}{\overline{\Gamma} - i\overline{\omega}_{\alpha n}} \left\{ \frac{1}{\overline{\Gamma} - i\overline{\omega}_{\alpha n}} + \frac{1}{\Gamma} \right\} + c.c., \tag{C.4}$$

$$X_e(\Omega,\Gamma,\overline{\Gamma}) = \sum_{n,p;\alpha} \frac{(V^\alpha_{np})^2 \rho^B_g(\alpha)}{\overline{\Gamma} - i\overline{\omega}_{\alpha n}} \left\{ \frac{1}{\overline{\Gamma} - i\overline{\omega}_{\alpha n}} + \frac{1}{\Gamma} \right\} + c.c. \tag{C.5}$$

Here $V^\alpha_{nq} \equiv C^\alpha_{nq}\xi_q$, where C^α_{nq} are the expansion coefficients of the excited state eigenvectors in terms of the ground state vibrational eigenvectors ($|\alpha> \equiv \sum_{n,q} C^\alpha_{nq}|n>|\psi_q>$) and

$$Q^i_n = \left[\begin{array}{ll} \rho^B_g(n), & i = D \\ 1, & i = W \end{array} \right. , \quad \overline{\omega}_{\alpha n} \equiv \Omega - \omega_{\alpha n}, \ \ \overline{\Gamma}_k \equiv \Gamma_k + \xi_{eg} \ (k = 1, 2). \tag{C.6}$$

Then the integral PP signal [1], which consists of a sum of the ground and excited state contributions $S(t,\Omega_1,\Omega_2) = S_g(t,\Omega_1,\Omega_2) + S_e(t,\Omega_1,\Omega_2)$, is described by the following expressions

$$S_e(t,\Omega_1,\Omega_2) = \sum_{\alpha,\beta} \left\{ X^W_{\alpha\beta}(\Omega_2,\Gamma_2,\overline{\Gamma}_2) e^{-(i\omega_{\alpha\beta}+\nu_e+\xi_e)t} X^D_{\beta\alpha}(\Omega_1,\Gamma_1,\overline{\Gamma}_1) \right\} + \tag{C.7}$$

$$(1 - e^{-\nu_e t}) e^{-\xi_e t} X_e(\Omega_2,\Gamma_2,\overline{\Gamma}_2) X_g(\Omega_1,\Gamma_1,\overline{\Gamma}_1)$$

$$S_g(t,\Omega_1,\Omega_2) = \sum_{n,m;p,q} \left\{ X^{W;pq}_{nm}(\Omega_2,\Gamma_2,\overline{\Gamma}_2) e^{-(i\omega_{nm}+\nu_g)t} X^{D;qp}_{mn}(\Omega_1,\Gamma_1,\overline{\Gamma}_1) \right\} + \tag{C.8}$$

$$(1 - e^{-\nu_g t}) X_g(\Omega_2,\Gamma_2,\overline{\Gamma}_2) X_g(\Omega_1,\Gamma_1,\overline{\Gamma}_1)$$

When there is a single bright excited electronic state $|\psi_p>$, the summation over p and q disappears.

The expressions for the dispersed PP signal are obtained similarly.

Bibliography

[1] S. Mukamel, *Principles of Nonlinear Optical Spectroscopy* (Oxford University Press, New York, 1995).

[2] W. Domcke and G. Stock, Adv. Chem. Phys. **100**, 1 (1997).

[3] L. W. Ungar and J. A. Cina, Adv. Chem. Phys. **100,** 171 (1997).

[4] G. Steinmeyer, D. H. Sutter, L. Gallmann, N. Matuschek, and U. Kelleret, Science **286**, 1507 (1999).

[5] A. Shirakawa, I. Sakane, M. Takasaka, and T. Kobayashi, Appl. Phys. Lett. **74**, 2268 (1999).

[6] D. H. Song, P. Kambhampati, T. W. Kee, and P. F. Barbara, J. Phys. Chem. A **106**, 4591 (2002).

[7] I. Rubtsov and K. Yoshihara, in *Femtochemistry*, edited by F. C. DeSchryver, S. D. Feyter, and G. Schweiteret (Wiley, Berlin, 2001), p. 367.

[8] S. Engleitner, M. Seel, and W. Zinth, J. Phys. Chem. **103**, 3013 (1999).

[9] K. B. Moeller, N. L. Henriksen, and A. H. Zewail, J. Chem. Phys. **113**, 10477 (2000).

[10] K. Wynne and R. M. Hochstrasser, Adv. Chem. Phys. **106**, 263 (1999).

[11] *Femtochemistry and Femtobiology: Ultrafast Dynamics in Molecular Science*, edited by A. Douhal and J. Santamaria (World Scientific, Singapore, 2002).

[12] M. J. Rosker, F. W. Wise, and C. L. Tang, Phys. Rev. Lett. **57**, 321 (1986).

[13] M. J. Rosker and C. L. Tang, J. Chem. Phys. **86**, 2827 (1987).

[14] J. Chesnoy and A. Mokhtari, Phys. Rev. A **38**, 3566 (1988).

[15] H. L. Fragnito, J. Y. Bigot, P. C. Becker, and C. V. Shank, Chem. Phys. Lett. **160**, 101 (1989).

[16] L. R. Khundkar and H. Z. A, Ann. Rev. Phys. Chem. **41**, 15 (1990).

[17] T. J. Dunn, J. N. Sweetser, I. A. Walmsley, and C. Radzewicz, Phys. Rev. Lett. **70**, 3388 (1993).

[18] T. J. Dunn, I. A. Walmsley, and S. Mukamel, Phys. Rev. Lett. **74,** 884 (1995).

[19] L. J. Waxer, I. A. Walmsley, and W. Vogel, Phys. Rev. A **56,** R2491 (1997).

[20] I. A. Walmsley and Waxer, J. Phys. B **31,** 1825 (1998).

[21] I. V. Rubtsov and K. Yoshihara, J. Phys. Chem. A **103,** 10202 (1999).

[22] I. V. Rubtsov, H. Shirota, and K. Yoshihara, J. Phys. Chem. A **103,** 1801 (1999).

[23] R. Jimenez, G. R. Fleming, P. V. Kumar, and M. Maroncelli, Nature **369**, 471 (1994).

[24] H. Wang, J. Shah, T. C. Damen, and L. Pfeiffer, Phys. Rev. Lett. **74**, 3065 (1995).

[25] R. J. Stanley and S. G. Boxer, J. Phys. Chem. **99**, 859 (1995).

[26] S. Akimoto, I. Yamazaki, T. Sakawa, and M. Mimuro, J. Phys. Chem. A **106**, 2237 (2002).

[27] H. Kano and T. Kobayashi, J. Chem. Phys. **116**, 184 (2002).

[28] N. Mataga, H. Chosrowjan, Y. Shibata, Y. Imamoto, M. Kataoka, and F. Tokunaga, Chem. Phys. Lett. **352**, 220 (2002).

[29] H. Mahr and M. Hirsch, Opt. Commun. **13**, 96 (1975).

[30] A. Mokhtari, A. Chebira, and J. Chesnoy, J. Opt. Soc. Am. B **7**, 1551 (1990).

[31] M. Du, S. J. Rosental, X. L. Xie, T. J. Diamagno, M. Schmidt, D. K. Hanson, M. Schiffer, J. R. Norris, and G. R. Fleming, Proc. Natl. Acad. Sci. USA **89**, 8517 (1992).

[32] A. E. Johnson, W. Jarzeba, G. C. Walker, and P. F. Barbara, Israel J. Chem. **33**, 199 (1993).

[33] W. P. de Boeij, M. S. Pschenichnikov, and D. A. Wiersma, Chem. Phys. Lett. **238**, 1 (1995).

[34] F. Bloch and A. Siegert, Phys. Rev. **57,** 522 (1940).

[35] M. Mitsunaga and C. L. Tang, Phys. Rev. A **35,** 1720 (1986).

[36] I. A. Walmsley, M. Mitsunaga, and C. L. Tang, Phys. Rev. A **38,** 4681 (1988).

[37] V. Chernyak and S. Mukamel, J. Chem. Phys. **108,** 5812 (1998).

[38] J. Sung and M. Cho, J. Chem. Phys. **113,** 7072 (2000).

[39] M. Cho, J. Chem. Phys. **115,** 4424 (2001).

[40] Y. Tanimura and K. Okumura, J. Chem. Phys. **106,** 2078 (1996).

[41] Y. Tanimura and K. Okumura, J. Chem. Phys. **107,** 2267 (1997).

[42] J. Wu and J. Cao, J. Chem. Phys. **115,** 5831 (2001).

[43] Y. Suzuki and K. Okumura, J. Chem. Phys. **115,** 2267 (2001).

[44] M. Toutounji, G. J. Small, and S. Mukamel, J. Chem. Phys. **109,** 7949 (1998).

[45] M. Toutounji, G. J. Small, and S. Mukamel, J. Chem. Phys. **110,** 1017 (1999).

[46] M. Yang and G. R. Fleming, J. Chem. Phys. **111,** 27 (1999).

[47] M. Yang and G. R. Fleming, J. Chem. Phys. **113,** 2823 (2000).

[48] M. Ovchinnikov, V. A. Apkarian, and G. A. Voth, J. Chem. Phys. **114,** 7130 (2001).

[49] A. T. N. Kumar, F. Rosca, A. Widom, and P. M. Champion, J. Chem. Phys. **114,** 701 (2001).

[50] V. May and M. Schreiber, Phys. Rev. A **45,** 2868 (1992).

[51] O. Kühn, V. May, and M. Schreiber, J. Chem. Phys. **101**, 10404 (1994).

[52] J. M. Jean, J. Chem. Phys. **101**, 10464 (1994).

[53] J. M. Jean, J. Phys. Chem. A **102,** 7549 (1998).

[54] L. W. Ungar and J. A. Cina, J. Phys. Chem. A **102,** 7382 (1998).

[55] A. Kühl and W. Domcke, Chem. Phys. **259,** 227 (2000).

[56] D. Egorova, A. Kühl, and W. Domcke, Chem. Phys. **268**, 105 (2001).

[57] A. Kühl and W. Domcke, J. Chem. Phys. **116,** 263 (2002).

[58] U. Kleinekathöfer, I. Kondov, and M. Schreiber, Chem. Phys. **268,** 121 (2001).

[59] I. Kondov, U. Kleinekathöfer, and M. Schreiber, Chem. Phys. **114,** 1497 (2001).

[60] C. Kalyanaraman and D.G. Evans, J. Chem. Phys. **115,** 7076 (2001).

[61] S. Hahn and G. Stock, J. Chem. Phys. **116,** 1085 (2002).

[62] W. T. Pollard, A. K. Felts, and R. A. Friesner, Adv. Chem. Phys. **93**, 77 (1996).

[63] V. Chernyak, T. Minami, and S. Mukamel, J. Chem. Phys. **112**, 7953 (2000).

[64] J. Kirkwood, C. Scheurer, V. Chernyak, and S. Mukamel, J. Chem. Phys. **114**, 2419 (2001).

[65] Y. Tanimura and S. Mukamel, J. Chem. Phys. **101,** 3049 (1994).

[66] Y. Tanimura and S. Mukamel, Chem. Phys. **107,** 1779 (1997).

[67] F. Shuang, C. Yang, and Y. Yan, J. Chem. Phys. **114,** 3868 (2001).

[68] H. Lin, B. Fain, N. Hamer, and C. Y. Yeh, Chem. Phys. Lett. **162,** 73 (1989).

[69] S. H. Lin, B. Fain, and C. Y. Yeh, Phys. Rev. A **41,** 2718 (1990).

[70] B. Fain, S. H. Lin, and V. Khidekel, Phys. Rev. A **47,** 3222 (1993).

[71] M. Hayashi, T. S. Yang, J. Yu, A. Mebel, S. H. Lin, I. V. Rubtsov, and K. Yoshihara, J. Phys. Chem. A **102**, 4256 (1998).

[72] M. Hayashi, T.-S. Yang, C. H. Chang, R. Chang, K. K. Liang, and S. H. Lin, J. Korean Phys. Soc. **32,** 217 (1998).

[73] M. Hayashi, T.-S. Yang, K. K. Liang, C. H. Chang, and S. H. Lin, J. Chin. Chem. Soc. **47,** 741 (2000).

[74] R. Chang, M. Hayashi, S. H. Lin, J.-H. Hsu, and W. S. Fann, J. Chem. Phys. **115,** 4939 (2001).

[75] S. Hahn and G. Stock, J. Phys. Chem. A **105,** 2626 (2001).

[76] S. Hahn and G. Stock, Chem. Phys. Lett. **296,** 137 (1998).

[77] S. Hahn and G. Stock, Chem. Phys. **259,** 297 (2000).

[78] F. Santoro, C. Petrongolo, and A. Lami, J. Chem. Phys. **113**, 4073 (2000).

[79] P. Kowalczyk, C. Radzewicz, J. Mostowski, and I. A. Walmsley, Phys. Rev. A **42**, 5622 (1990).

[80] L. Seidner and W. Domcke, Chem. Phys. **186,** 27 (1994).

[81] L. Seidner, G. Stock, and W. Domcke, J. Chem. Phys. **103,** 3998 (1995).

[82] B. Wolfseder, L. Seidner, G. Stock, and W. Domcke, Chem. Phys. **217,** 275 (1997).

[83] S. Mukamel, C. Ciordas-Ciurdariu, and V. Khidekel, IEEE J. Quant. Electr. **32,** 1278 (1996).

[84] S. Mukamel, C. Ciordas-Ciurdariu, and V. Khidekel, Adv. Chem. Phys. **101,** 345 (1997).

[85] S. Mukamel, J. Chem. Phys. **107**, 4165 (1997).

[86] J. Cao, J. Chem. Phys. **107,** 3204 (1997).

[87] Y. Yan, Phys. Rev. A **58,** 2721 (1998).

[88] C. Meier and D. J. Tannor, J. Chem. Phys. **111,** 3365 (1999).

[89] O. Kuhn, Y. Zhao, F. Shuang, and Y. Yan, J. Chem. Phys. **112,** 6104 (2000).

[90] Y. Yan, F. Shuang, R. Xu, J. Cheng, X. Li, C. Yang, and H. Zhang, J. Chem. Phys. **113,** 2068 (2000).

[91] T. Mancal and V. May, J. Chem. Phys. **114,** 1510 (2001).

[92] D. Kilin and M. Schreiber, J. Lumin. **92,** 13 (2001).

[93] P. Hamm, M. Lim, and R. M. Hochstrasser, Phys. Rev. Lett. **81,** 5326 (1988).

[94] B. Wolfseder L. Seidner, W. Domcke, G. Stock, M. Seel, S. Engleitner, and W. Zinth, Chem. Phys. **233**, 323 (1998).

[95] A. Matro and J. A. Cina, J. Phys. Chem. **99**, 2568 (1995).

[96] S. H. Lin, M. Hayashi, S. Suzuki, X. Gu, W. Xiao, and M. Sugawara, Chem. Phys. **197**, 435 (1995).

[97] M. Sugawara, M. Hayashi, S. Suzuki, and S. H. Lin, Mol. Phys. **87**, 637 (1996).

[98] M. Hayashi, T. S. Yang, A. Mebel, C. H. Chang, S. H. Lin, and N. F. Scherer, Chem. Phys. **217**, 259 (1997).

[99] J. Jean, R. Friesner, and G. Fleming, J. Chem. Phys. 5827 (1992).

[100] J. M. Jean, J. Chem. Phys. **104**, 5638 (1996).

[101] M. Bixon and J. Jortner, J. Chem. Phys. **107**, 1470 (1997).

[102] J. Tang and S. H. Lin, Chem. Phys. Lett. **254**, 6 (1996).

[103] T. O. Cheche and S. H. Lin, Phys. Rev. E **64**, 061103 (2001).

[104] A. Lucke, C. H. Mak, R. Egger, J. Ankerhold, J. Stockburger, and H. Grabert, J. Chem. Phys. **107**, 8397 (1997).

[105] J. Casado-Pascual, C. Denk, M. Morillo, and R. I. Cukier, J. Chem. Phys. **113**, 11176 (2000).

[106] P. J. Reid, C. Silva, P. F. Barbara, L. Karki, and J. T. Hupp, J. Phys. Chem. **99**, 2609 (1995).

[107] M. H. Vos, M. R. Jones, and J.-L. Martin, Chem. Phys **233**, 179 (1998).

[108] M. H. Vos, J. C. Lambry, S. J. Robles, D. C. Youvan, J. Breton, and J.-L. Martin, Proc. Natl. Acad. Sci. USA **88**, 8885 (1991).

[109] C. Zimmermann, F. Willig, S. Ramakrishna, B. Burfeindt, B. Pettinger, R. Eichberger, and W. Storck, J. Phys. Chem. B **105**, 9245 (2001).

[110] I. V. Rubtsov and K. Yoshihara, J. Phys. Chem. A **101**, 6138 (1997).

[111] M. F. Gelin, A. V. Pisliakov, and W. Domcke, Phys. Rev. A **65**, 062507 (2002).

[112] A. V. Pisliakov, M. F. Gelin, and W. Domcke, J. Phys. Chem. A **107**, 2657 (2003).

[113] M. F. Gelin, A. V. Pisliakov, D. Egorova, and W. Domcke, J. Chem. Phys. **118**, 5287 (2003).

[114] G. Stock, R. Schneider, and W. Domcke, J. Chem. Phys. **90**, 7184 (1989).

[115] Y. Zhao and R. S. Knox, J. Phys. Chem. A **104,** 7751 (2000).

[116] J. Lu, F. Shao, K. Fan, and S. Du, J. Chem. Phys. **114,** 3373 (2001).

[117] J. H. Eberly and K. Wodkiewicz, J. Opt. Soc. Am. **67**, 1253 (1977).

[118] V. Wong and I. A. Walmsley, J. Opt. Soc. Am. B **12,** 1491 (1995).

[119] A. Zucchetti, W. Vogel, D.-G. Welsch, and I. A. Walmsley, Phys. Rev. A **60,** 2716 (1999).

[120] G. S. Agrawal, *Quantum Statistical Theories of Spontaneous Emission and Their Relation to Other Approaches*, Vol. 70 of *Springer Tracts in Modern Physics* (Springer-Verlag, Berlin, 1984).

[121] W. Louisell, in *Proceedings of the International School of Physics - Enrico Fermi*, edited by R. Glauber (Academic Press, New York, 1969), Vol. XLII, p. 680.

[122] G. Stock and W. Domcke, J. Chem. Phys. **93,** 5496 (1990).

[123] B. Wolfseder, L. Seidner, G. Stock, and W. Domcke, Chem. Phys. **217**, 275 (1997).

[124] L. Seidner, G. Stock, and W. Domcke, J. Chem. Phys. **103**, 3998 (1995).

[125] W. T. Pollard and R. A. Mathies, Annu. Rev. Phys. Chem. **43,** 497 (1992).

[126] G. Stock and W. Domcke, J. Opt. Soc. Am. **7,** 1970 (1990).

[127] Y. Gu, A. Widom, and P. M. Champion, J. Chem. Phys. **100,** 2547 (1994).

[128] R. Karrlein and H. Grabert, Phys. Rev. E **55,** 153 (1997).

[129] Y. Yan and S. Mukamel, J. Chem. Phys. **89,** 5160 (1988).

[130] U. Weiss, *Quantum Dissipative Systems* (World Scientific, Singapore, 1993).

[131] R. F. Loring, Y. Yan, and S. Mukamel, J. Chem. Phys. **87,** 5840 (1987).

[132] Y. Georgievskii, C. Hsu and R. A. Marcus, J. Chem. Phys. **108,** 7356 (1998).

[133] L. Allen and J. Eberly, *Optical Resonance and Two-Level Atoms* (Dover, New York, 1987).

[134] R. A. Marcus, J. Chem. Phys. **24**, 966 (1956).

[135] T. Takagahara, E. Hanamura, and R. Kubo, J. Phys. Soc. Jpn. **44**, 728 (1978).

[136] A. J. Leggett, S. Chakravarty, A. T. Dorsey, M. P. A. Fisher, A. Garg, and W. Zwerger, Rev. Mod. Phys. **59**, 1 (1987).

[137] A. G. Redfield, Adv. Magn. Reson. **1**, 1 (1965).

[138] K. Blum, *Density Matrix Theory and Applications* (Plenum Press, New York, 1981).

[139] W. H. Press, B. P. Flannery, S. A. Teukolsky, and W. T. Vetterling, *Numerical Recipes* (Cambridge University Press, Cambridge, 1986).

[140] H. Koeppel and H.-D. Meyer, Chem. Phys. Lett. **107**, 149 (1984).

[141] G. Stock and W. Domcke, Chem. Phys. **124**, 227 (1988).

[142] B. D. Fainberg, Opt. Spectrosc. **65**, 722 (1988).

[143] D. G. Evans and R. D. Coalson, J. Chem. Phys. **104**, 3598 (1996).

[144] M. Ben-Nun, R. D. Levine, and G. R. Fleming, J. Chem. Phys. **105**, 3035 (1996).

[145] A. Lucke and J. Ankerhold, J. Chem. Phys. **115**, 4696 (2001).

[146] L. D. Zusman, Chem. Phys. **49**, 295 (1980).

[147] M. Thoss and H. B. Wang, Chem. Phys. Lett. **358,** 298 (2002).

[148] H. B. Wang and M. Thoss, J. Phys. Chem. A **107,** 2126 (2003).

[149] S. E. Bradforth, R. Jimenez, F. van Mourik, R. van Grondelle, and G. R. Fleming, J. Phys. Chem. **99**, 16179 (1995).

[150] R. S. Mulliken and W. B. Person, *Molecular Complexes* (Wiley, New York, 1969).

[151] R. Foster, *Organic Charge-Transfer Complexes* (Academic Press, London, 1969).

[152] B. M. Britt, J. L. McHale, and D. M. Friedrich, J. Phys. Chem. **99**, 6347 (1995).

[153] B. M. Britt and J. L. McHale, Chem. Phys. Lett. **270**, 551 (1997).

[154] M. Hayashi, T.-S. Yang, J. Yu, A. Mebel, and S. H. Lin, J. Phys. Chem. A **101**, 4156 (1997).

[155] F. Markel, N. S. Ferris, I. R. Gould, and A. B. Myers, J. Am. Chem. Soc. **114**, 6208 (1992).

[156] K. Kulinowski, I. R. Gould, and A. B. Myers, J. Phys. Chem. **99**, 9017 (1995).

[157] K. Wynne, C. Galli, and R. M. Hochstrasser, J. Chem. Phys. **100**, 4797 (1994).

[158] K. Wynne, G. Reid, and R. M. Hochstrasser, J. Chem. Phys. **105**, 2287 (1996).

[159] Prof. K. Yoshihara, personal communication.

[160] D. Chandler, J. Chem. Phys. **60,** 3500 (1974).

[161] D. N. Zubarev, V. Morozov, and G. Röpke, *Statistical Mechanics of Nonequilibrium Processes, vol. 2, Relaxation and Hydrodynamic Processes* (Akademie, Berlin, 1997).

[162] P. Hänggi, P. Talkner, and M. Borkovec, Rev. Mod. Phys. **62,** 251 (1990).

[163] P. Resibois and M. De Leener, *Classical Kinetic Theory of Fluids* (John Wiley & Sons, 1977).

[164] D. Kohen, D. J. Tannor, J. Chem. Phys. **107,** 5141 (1997).

[165] H. Spohn, Rev. Mod. Phys. **53,** 569 (1980).

[166] S. Dilthey, S. Hahn and G. Stock, J. Chem. Phys. **112,** 4910 (2000).

[167] P. Pechukas, J. Ankerhold, H. Grabert, Ann. Phys. (Leipzig) **9,** 794 (2000).

[168] C. V. Gardiner, *Handbook of Statistic Methods* (Springer-Verlag, Berlin, 1990).

[169] Y. Yan and S. Mukamel, Phys. Rev. A **41**, 6485 (1990).

[170] M. F. Gelin, A. V. Pisliakov, and W. Domcke, to be published.

Acknowledgments

First of all, I would like to thank my research advisor, Prof. Dr. Wolfgang Domcke, who supported me tremendously during the time I was working on this thesis. He always was a great source of ideas and new perspectives. He taught me to see the physical picture behind complicated mathematical expressions. It has been a unique and most pleasant experience working with him.

I would like to express my warmest thanks to Dr. Maxim Gelin. Writing this work would not have been possible without his help. He has supported me on this journey from the beginning and encouraged continuously over the years. Thanks to Maxim for being a great friend. Minsk, Munich, Florence, Dresden, Greece, Paris ... See you in California?

I also thank all former and current group members for the wonderful environment in which I have performed my studies. In particular, I thank Dr. Michael Thoss for fruitful discussions and valuable comments.

I thank all visitors of our group with whom I shared my room, Dr. Vladimir Ermoshin, Prof. Andrei Kazansky, Dr. Susanta Mahapatra, Prof. Andrzei Sobolewski, who have broadened my scientific horizon in different directions.

I would like to thank all the teachers I had over the years, especially my past advisor in Minsk, Prof. Dr. A. P. Blokhin, who introduced me to this field.

My sincere thanks to my parents who patiently supported me during the whole process of my education and believed in me.

Last, and certainly not least, I have to acknowledge the presence of my wife, Ludmila, and my daughter, Masha, in my life. Their love has been boundless, their support selfless. I am tremendously grateful for the sacrifices they have made for me. To them I dedicate this thesis.